DISSERTATION

for obtaining the doctoral degree of the

combined Faculty of Mathematics, Engineering and Natural Sciences

of the

Ruprecht - Karls - University Heidelberg

Presented by

Pia Hempelmann, M. Sc.

born in Herford, Germany

Oral examination: 19th July 2022

STARD3: A Sphingolipid Transporter at Lysosome-ER Contact Sites

Referees:

Prof. Dr. Britta Brügger

Dr. Doris Höglinger

This work was carried out under the supervision of Dr. Doris Höglinger at the Biochemistry Center of Heidelberg University (BZH), Germany, from January 2019 to May 2022. Bachelor and Master students, as well as collaboration partners, have contributed to this work and are specifically named in the respective chapters.

“No amount of experimentation can ever prove me right;

A single experiment can prove me wrong.”

Albert Einstein

Contents

Abstract

Sphingolipid transport between organelles has been increasingly studied during the last years, and a large body of evidence points to protein-mediated sphingolipid transfer at organelle contact sites. This is well characterized for sphingolipid transfer along the biosynthetic pathway from the endoplasmic reticulum (ER) towards the plasma membrane. However, the catabolic pathway is far less well studied. Here, a crucial but unexplored step is the recycling of the sphingosine backbone upon lysosomal sphingolipid degradation and its reintegration into the biosynthetic pathway at the ER. In this study, I propose that the lysosomal cholesterol transporter STARD3 acts as a sphingosine transfer protein at lysosome-ER contact sites to facilitate sphingosine entry into the recycling pathway.

STARD3 has been previously described to tether lysosomes to the ER via its FFAT motif that binds to ER-resident proteins. At this contact, its START-domain transfers cholesterol from the ER to lysosomes to support endosome maturation and to maintain cholesterol levels at the ER. I employed functionalized, photocrosslinkable sphingosine in intact cells to show that STARD3 also binds to sphingosine. Functionally, I could show that overexpression of STARD3 drives the sphingosine metabolism towards biogenesis of higher sphingolipid species, such as sphingomyelin, while depleting cellular STARD3 levels results in a delayed sphingosine metabolism, which indicates STARD3 as a lysosomal sphingosine exporter. This transfer is dependent on a functional FFAT motif, consistent with sphingosine transfer taking place at the lysosome-ER contact site. STARD3 FFAT mutation or drug-induced prevention of sphingosine entry into the recycling pathway switches the sphingolipid metabolism towards the degradation pathway. Finally, molecular simulations, mutational analyses, and cholesterol competition studies revealed the START domain as a sphingosine transfer domain that can either transfer cholesterol or sphingosine at lysosome-ER contact sites.

Overall, I hypothesize that STARD3 transfers sphingosine from the lysosome towards the ER along a subcellular lipid gradient, potentially in exchange for the transfer of cholesterol. As such, STARD3 is the first protein able to facilitate sphingosine exit from lysosomes towards other organelles. This represents an important connection between the catabolic and anabolic sphingolipid pathways and has wide-ranging implications for future studies relating to lysosomal lipid efflux and sphingolipid-mediated processes in health and disease.

Zusammenfassung

Der Sphingolipid-Transport zwischen Organellen wurde in den letzten Jahren zunehmend untersucht, und eine Vielzahl von Beweisen weist auf einen Protein-vermittelten Sphingolipid-Transfer an Organellen-Kontaktstellen hin. Dies ist für den Transfer von Sphingolipiden entlang des Biosynthesewegs vom Endoplasmatischen Retikulum (ER) zur Plasmamembran gut charakterisiert. Der katabole Weg ist jedoch weitaus weniger bekannt. Ein entscheidender, aber unerforschter Schritt ist hier das Recycling des Sphingosin-Rückgrats beim lysosomalen Sphingolipid-Abbau und seine Wiedereingliederung in den Biosyntheseweg am ER. In dieser Dissertation zeige ich, dass der lysosomale Cholesterintransporter STARD3 als Sphingosin-Transferprotein an Lysosom-ER-Kontaktstellen fungiert, um den Eintritt von Sphingosin in den Recyclingweg zu erleichtern.

STARD3 wurde zuvor beschrieben, um Lysosomen, über sein FFAT-Motiv, das an ER-residente Proteine bindet, an das ER zu knüpfen. Bei diesem Kontakt überträgt seine START-Domäne Cholesterin vom ER zu den Lysosomen, um die Endosomenreifung zu unterstützen und den niedrigen Cholesterinspiegel des ER aufrechtzuerhalten. Ich verwendete funktionalisiertes, photovernetzbares Sphingosin in intakten Zellen, um zu zeigen, dass STARD3 auch an Sphingosin bindet. Funktionell konnte ich zeigen, dass die Überexpression von STARD3 den Sphingosin-Metabolismus in Richtung Biogenese höherer Sphingolipid-Spezies wie Sphingomyelin treibt, während ein Abbau der zellulären STARD3-Spiegel zu einem verzögerten Sphingosin-Metabolismus führt, was darauf hindeutet, dass STARD3 ein lysosomaler Sphingosin-Exporter ist. Dieser Transfer hängt von einem funktionellen FFAT-Motiv ab, was mit dem Sphingosin-Transfer übereinstimmt, der an der Lysosom-ER-Kontaktstelle stattfindet. FFAT-Mutation oder medikamenteninduzierte Verhinderung des Eintritts von Sphingosin in den Recyclingweg schaltet den Sphingolipidstoffwechsel auf den Abbauweg um. Schließlich zeigten molekulare Simulationen, Mutationsanalysen und Cholesterin-Kompetitionsstudien die START-Domäne als Sphingosin-Transferdomäne, die entweder Cholesterin oder Sphingosin an Lysosom-ER-Kontaktstellen übertragen kann.

Insgesamt gehe ich davon aus, dass STARD3 Sphingosin vom Lysosom entlang eines subzellulären Lipidgradienten zum ER transportiert, möglicherweise im Austausch für den Transfer von Cholesterol. Als solches ist STARD3 das erste Protein, das in der Lage ist, den Austritt von Sphingosin aus den Lysosomen zu anderen Organellen zu erleichtern. Dies stellt eine wichtige Verbindung zwischen den katabolen und anabolen Sphingolipidwegen dar und hat weitreichende Auswirkungen auf zukünftige Studien in Bezug auf lysosomalen Lipidflux und Sphingolipid-vermittelte Prozesse in Gesundheit und Krankheit.

List of Figures

All illustrations were created with Biorender.com, if not explicitly stated otherwise.

Chapter I – Introduction

1.1 Cells, organelles, and the secretory pathway

Cells are the smallest units of life that can live autonomously. They can either exist as single-cell organisms such as yeast or bacteria or build multicellular structures to form tissues, organs, and as the supreme authority, entire organisms[1]. Since these multicellular structures fulfill a wide range of functions, different cell types have evolved. For example, brain tissue mainly consists of neurons that characteristically communicate via electrical and chemical signals to ensure a rapid transfer of biological signals[2]. In contrast, adipose tissue is mainly built of adipocytes that primarily store and mobilize lipids, such as triglycerides, to control energy homeostasis[3]. Consequently, the shape, size, and metabolic behaviour of specialized cell types differ according to their function. For example, neurons form long, slender, and highly branched cell shapes to reach other neurons for forming synapses[4], whereas adipocytes exhibit round shapes that can expand during overnutrition to 100 µm in diameter for storing lipid excess[5].

However, most eukaryotic cell types share basic cellular organelle structures, including the nucleus, the endoplasmic reticulum (ER), ribosomes, the Golgi apparatus, and mitochondria. Every organelle has characteristic tasks that are highly adaptable to environmental changes such as nutrition state or stress[6,7]. Hence, an exchange of nutrients and other cellular components, such as lipids, is indispensable to respond to these changes in a highly dynamic way. This exchange happens via organelle interaction either through vesicular trafficking or through membrane contact site formation where membranes of different organelles come in close apposition[8].

The ER is a well-understood system for organelle adaptability and interaction. Noteworthy, it is the largest membrane-bound organelle in the cell, comprising tubules

and sheet-like cisternae extending from the nuclear envelop to the cellular periphery[9,10]. Unsurprisingly, it interacts with all membrane-bound organelles of the cell, including the plasma membrane[9,11], lysosomes[12–14], and the Golgi apparatus[15–17]. Besides this direct interaction via membrane contact sites, the ER plays a crucial role in the secretory pathway. A large number of lipids are synthesized in the ER[18], and approximately 30 % of all cellular proteins are directly recruited to the ER after their ribosome-mediated synthesis[19]. If they do not stay in the ER membrane or lumen, they need to be supplied to target organelles mainly facilitated by the secretory pathway[20]. The first step in the secretory pathway is the recruitment of chaperones to the ER, which catalyze the folding of proteins into tertiary and quaternary structures[19]. Afterwards, protein-coated carriers, such as the coat protein complex II (COPII) vesicles, transfer the processed proteins from the ER to the Golgi apparatus. This transfer is mediated via an ER-Golgi intermediate compartment (ERGIC), defined as an independent structure which is not continuous with the ER or the Golgi apparatus[21]. The opposite transport route is mediated by COPI vesicles to return the cargo from the Golgi to the ER. This vesicle-mediated transport between the ER and the Golgi is known as the early secretory pathway (Figure 1.1a) [22].

In contrast, cargo secretion proceeding from the Golgi to target organelles such as lysosomes and the plasma membrane is described as the late secretory pathway (Fig. 1.1b). The Golgi apparatus comprises *cis*, *medial*, and *trans* compartments, each containing a specific composition of enzymes[23]. ER-derived vesicles deliver the proteins to the *cis* face. There, the vesicles fuse via the soluble NSF-attachment protein receptor (SNARE)-complex formation with the *cis* Golgi membrane to release the cargo into the Golgi lumen[24]. Inside, released proteins pass through the Golgi towards the *trans* face while undergoing processing via glycosylation and other modifications[25]. Once arrived at the *trans* compartment of the Golgi, also named *trans* Golgi network (TGN), the cargo proteins are recognized by the luminal domains of specific transmembrane receptors recruited to the TGN. The cytosolic site of these receptors is often associated with cargo adaptors which recruit clathrin, a class of proteins involved in many mechanisms of membrane movement[26]. Accordingly, clathrin-coated vesicles (CCV), containing the highly modified cargo, derive from the TGN. Subsequently, the cargo is transferred in a

vesicle-dependent manner to target organelles such as lysosomes and endosomes. Moreover, the plasma membrane is one of the final acceptors of delivered cargo since approximately 11-15 % of all human proteins are secreted to the extracellular space and around 10 % localize to the plasma membrane. However, unlike other pathways such as CCV-mediated cargo transfer from the TGN to lysosomes, there is still no universal molecular machinery found that drives the formation, translocation, and fusion of TGN to plasma membrane carriers[27]. However, a few TGN-derived transfer vesicles, such as Arf1-positive[28], Lamp1-RUSH[29], and Rab6-positive[30,31] carriers, have been identified.

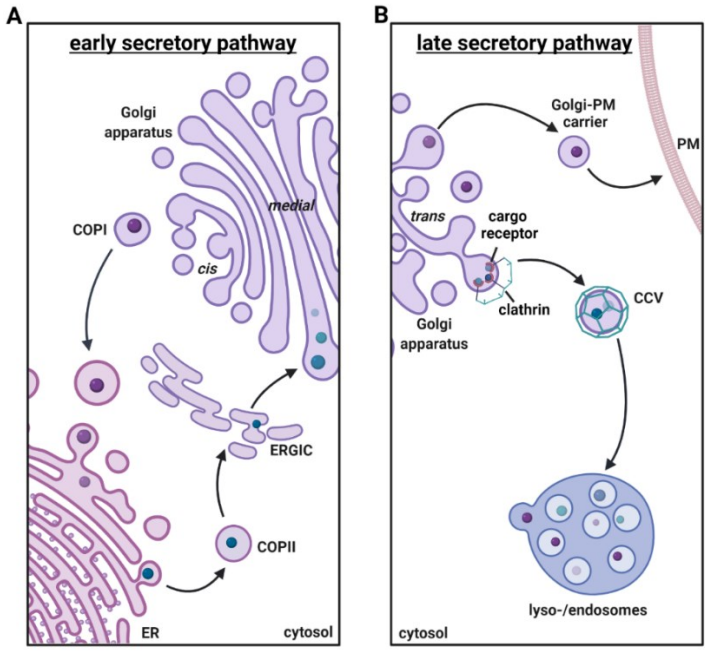

Figure 1.1: The secretory pathway. A| Early secretory pathway - Vesicular transfer between ER and Golgi apparatus. B| Late secretory pathway - clathrin-dependent and clathrin-independent vesicular transfer from Golgi apparatus to lyso-/endosomes or the PM, respectively.

Not only proteins are secreted via the secretory pathway, but also lipids need to be supplied from the ER to target organelles. In contrast to well-studied protein secretion, lipid sorting into vesicles is only poorly understood so far[32]. Besides vesicle-mediated lipid transfer, lipid sorting has been suggested to also happen at membrane contact sites.

However, single lipid species have also been shown to regulate vesicle-mediated cargo transfer. In particular, sphingomyelin (SM) 18:0 has been shown to interact with p24, a protein involved in COPI vesicle biogenesis, to regulate COPI vesicle budding and retrograde transport from the Golgi to the ER[33]. In the late secretory pathway, a few specific lipid carriers have been identified so far[27]. One example are the SM carriers. SM is a complex sphingolipid that is a major component of the plasma membrane. It has been either found in lipid rafts, microdomains densely packed with lipids such as cholesterol and SM[34,35], or as a precursor for ceramide (Cer), a bioactive sphingolipid species involved in many signaling processes[36,37]. However, SM is synthesized at the Golgi apparatus[38], and, in consequence, it needs to be transported to the plasma membrane. To this end, a specific class of TGN-derived vesicles has been identified to transfer SM to the plasma membrane in a highly efficient manner[27]. These SM-rich carriers have a high abundance of Cab45 (calcium-binding protein 45), a calcium-sensing protein which localizes to the luminal side of the TGN[39]. Cab45 oligomerization is triggered by a luminal calcium flux originated from SPCA1 (secretory pathway calcium ATPase 1) that leads to sorting of SM into secretory carriers and its transfer to the plasma membrane[40]. Taken together, a highly regulated protein sorting machinery is required to ensure accurately packaging of the right cargo into the correct carrier and its transfer towards the correct organelle[23].

In summary, the secretory pathway is a major transfer route for cellular building blocks to transport them in a highly dynamic manner to their target destination for incorporation into cellular structures, specific pathways, or signaling cascades. To maintain cellular homeostasis and ensure intracellular exchange of lipids, proteins, carbohydrates, and other molecules such as vitamins, a tremendously specific functioning of cells and organelles is required.

1.2 Lysosomes

Lysosomes are membrane-bound organelles that were discovered in 1955 by Christian de Duve[41]. A mammalian cell contains 50 to 1000 lysosomes distributed in the entire cytoplasm, although they have a higher concentration in the perinuclear region[42]. It has been found that lysosomes are exceedingly dynamic structures that can move from the cellular periphery to the perinuclear region and vice versa along microtubule tracks[42,43]. Their movement depends on several factors, such as immobilization through interaction with perinuclear ER[44] and the Golgi apparatus[45] or mobilization by interaction with microtubule motors[46,47]. Interestingly, the nutrient state of the cell also affects lysosomal positioning and also the number of lysosomes per cell. Furthermore, lysosomal lipid and protein compositions are actively controlled by the cell to respond to environmental changes[42]. This highly regulated adaption to the cellular environmental state suggests lysosomes as complex organelles having multiple functions.

1.2.1 Lysosome maturation and properties

Lysosomes comprise two major protein classes: soluble hydrolases for degrading specific substrates and integral lysosomal membrane proteins (LMPs), which mainly reside in the limiting membrane of lysosomes. In mammalian cells, around 25 LMPs with diverse functions have been identified so far[48]. Their functions range from substrate im- and export from the cytosol to the lysosomal lumen (and vice versa), acidification of the lysosome, and tethering organelle membranes[49].

These proteins, since not synthesized in lysosomes, need to be recruited to lysosomes during lysosome biogenesis. Therefore, they can either be directly transported from the TGN to lysosomes or indirectly through an intermediate transfer from the TGN to the plasma membrane, followed by subsequent endocytosis[50].

Incoming material from endocytosis enters the endocytic pathway starting with early endosomes (EEs) that are considered as the initiation point in endosome maturation. How EEs receive the cargo is not fully understood yet, but it is anticipated that their membrane structures and luminal composition derive from the fusion of endocytic

vesicles[51]. EEs receive incoming vesicles and recycle the vesicular membrane and cargo rapidly. Sometimes the entire vesicle, including its membrane and cargo, is retained inside the endosomal lumen and stays there over the entire maturation process[52]. EEs can mature to 'recycling' endosomes which represents the first and most crucial step in cargo sorting and its recycling circuit with the plasma membrane. There, exocytic vesicles are fused with the plasma membrane and release their cargo to the extracellular space via exocytosis (Fig. 1.2)[53].

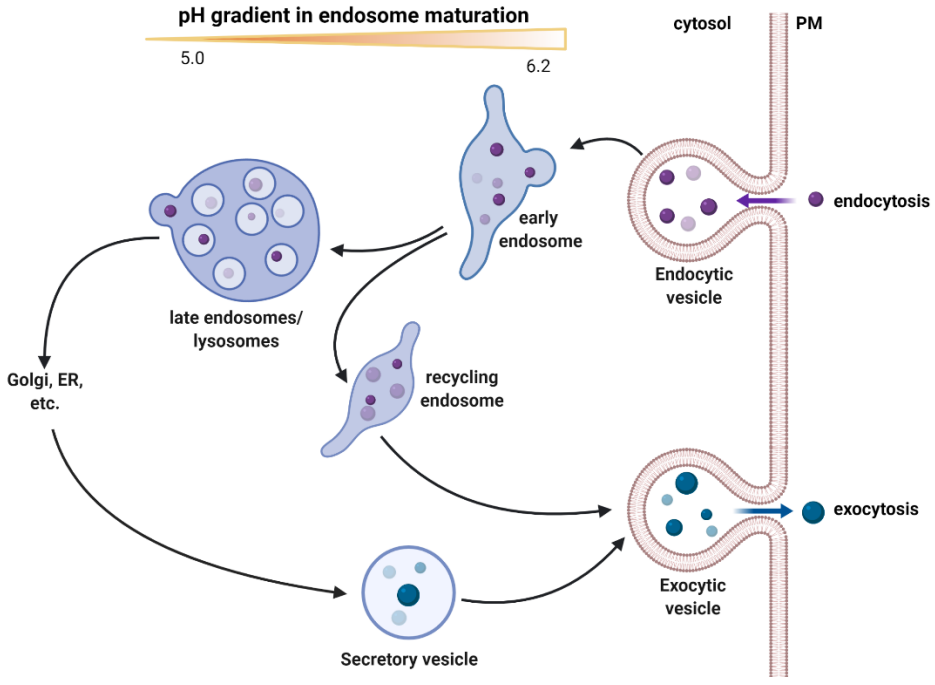

Figure 1.2: Lysosomal maturation including endo- and exocytosis. Endocytic vesicles take up incoming material and further process it during endosome maturation or recycle it via exocytic vesicles.

If EEs are not converted to recycling endosomes, they mature into late endosomes (LEs). This process is initiated by the recruitment of the cytosolic protein Rab5[54]. Endosomal maturation is regulated by sequential recruitment of different Rab GTPases such as Rab7, which is a key component of LEs. This sequential shift of Rab proteins is referred to as Rab conversion[55,56]. However, not only protein recruitment defines endosome

maturation, but the pH decrease of the endosomal lumen is also relevant. Prominently, the V-ATPase, a multi-subunit proton pump, is involved in the acidification of endosomes. The pH values range from 6.2 to 5.5/5.0 in EEs and LEs/lysosomes, respectively[57].

The pH also plays an important role in the main function of lysosomes: the digestion of macromolecules. Lysosomes contain over 50 different soluble hydrolases that degrade all kinds of nutrients, such as proteins, carbohydrates, lipids, as well as DNA and RNA[58]. Therefore, lysosomes are often referred to as the trashcan of the cell. Many lysosomal hydrolytic enzymes are activated by the low pH values inside the lysosomal lumen, indicating the pH gradient from EEs to LEs as a control point for the lysosomal macromolecular digestion[59]. Notably, the pH-dependent activation of lysosomal degradative enzymes also serves as a cellular protective system; even if lysosomal membranes are defective so that lysosomal hydrolases are released into the cytosol, they cannot digest cytosolic nutrients due to the neutral pH prevailing there[60]. However, deficiencies or mutations in lysosomal hydrolases or membrane proteins are often associated with severe neurodegenerative and metabolic diseases summarized as lysosomal storage disorders[50].

1.2.2 Lysosomal involvement in cellular processes

Even if macromolecular digestion is still assumed as the main lysosomal function, it has been discovered that lysosomes are also involved in many other cellular processes, including metabolic signaling, gene regulation, cell adhesion, and migration[61].

A prominent example is the lysosomal interaction with the mechanistic target of rapamycin complex 1 (mTORC1), a protein kinase that serves as a master regulator of cellular growth[62]. In its active state, mTOR associates with the lysosomal surface and senses amino acid[63], glucose[64], and insulin[65] levels to promote the biogenesis of proteins, lipids, and organelles[66]. In starvation conditions, when nutrient levels are low, mTORC1 is inactive and dissociates from lysosomes[67]. When this happens, mTORC1 can no longer phosphorylate downstream targets, such as the transcription factor EB (TFEB), which

induces its subsequent translocation to the nucleus[66]. There, TFEB regulates the transcription of genes involved in autophagy and lysosomal biogenesis and thereby initiates the fusion of lysosomes and autophagosomes, which promotes cargo degradation[68]. Additionally, TFEB influences lysosome-mediated exocytosis[69].

In summary, lysosomes have crucial and highly controlled functions in the degradation and recycling of macromolecules but also play critical roles in many other cellular processes, such as cellular nutrient sensing. All these observations lead to the assumption that lysosomes are more than a hub for macromolecular digestion.

1.3 Lipids are essential cellular building blocks

Lipids are a very heterogeneous group of natural substances. They are important for energy storage on the physiological level as well as for signaling processes and as structural components on the cellular level. One mammalian cell is estimated to contain approximately 1,000 lipid species[70], but more than 37,000 different lipids, varying in their backbone, chain length, saturation, or headgroups, have been identified so far[71]. These lipids can be allocated to three major lipid classes: glycerolipids, sphingolipids, and sterols (Fig. 1.3).

Glycerol lipids are composed of a glycerol-3-phosphate backbone that can be mono-, bi, or tri-substituted with long-chain acyl or alkyl groups and/or an additional polar alcohol headgroup[72,73]. The most common glycerolipid species are the triacylglycerols (TAGs) containing tri-substituted fatty acid esters. TAGs are mainly involved in tissue fat storage and are therefore often found in adipocytes[74]. Another example of glycerolipids is phosphatidylcholine (PC). PC is the most abundant glycerolipid species in mammalian cells and represents over 30 % of the total cellular lipid content. Structurally, it has a choline headgroup attached at *sn*-3 and two fatty acid chains at *sn*-1 and *sn*-2 to the glycerol backbone[75].

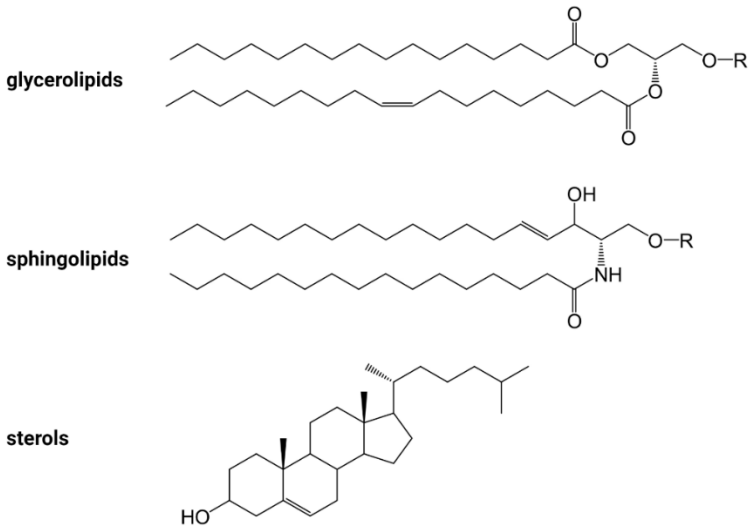

Figure 1.3: Major groups of mammalian lipids. Depicted are a 1,2-Diacylglyceride species, a Cer species, and cholesterol as an example for the glycerolipids, sphingolipids, and sterols, respectively. The R signifies variable headgroups.

Sterols share a conspicuous four-ring backbone often substituted with an alcohol group at position 3 of ring A. The best-known sterol species of mammalian cells is cholesterol. Cholesterol is a 27-carbon molecule containing the typical four-ring system, a hydroxy group, and a hydrocarbon tail[76]. It maintains membrane fluidity and serves as a precursor for steroid hormones, bile acid, and vitamin D6[77]. Cholesterol can be either *de novo* synthesized from acetyl-CoA in the ER lumen or derived from dietary resources[78].

Sphingolipids are constructed of a sphingoid base backbone. In mammalian cells, this sphingoid base is sphingosine (Sph). Sph is an 18-carbon amino alcohol with an unsaturated hydrocarbon chain. It can be amide linked to distinct fatty acids and substituted with various headgroups and serves therefore as the precursor for all complex mammalian sphingolipids such as ceramide (Cer) or sphingomyelin (SM)[79].

1.3.1 The sphingolipid network

Sphingolipids are essential in many different cellular processes due to their structural diversity. For example, they serve as membrane building blocks and bioactive lipids in many signaling cascades[79].

On the cellular level, sphingolipids are *de novo* synthesized at the cytosolic leaflet of the ER. Several enzymes, including the serine palmitoyltransferase (SPT) convert cytosolic serine and palmitoyl CoA molecules into 3-ketohydrosphingosine (kdhSph)[80]. Next, its ketone group is reduced to a hydroxyl group by the 3-ketodihydrosphingosine reductase (KDSR) in an NADPH-dependent manner[79]. The resulting dihydrosphingosine (dhSph) is further acylated by six related (dihydro-) ceramide synthases (CerS) referred to as CerS1-6 to form dihydroceramide (dhCer)[81]. The subsequent induction of a double bond by the action of a sphingolipid desaturase (DES) releases Cer, the precursor for all complex sphingolipids[79].

Cer is a highly hydrophobic molecule that tends to reside in membranes, for instance, in the ER membrane, which is also the organelle it is synthesized in[82]. On the one hand, if Cer is not directly transferred to the Golgi, ceramide galactosyltransferases can attach UDP-galactose to the 1-hydroxyl moiety of Cer to produce galactosylceramide (GalCer), which is a precursor for sulfatides[83]. On the other hand, Cer mobilization from the ER to the Golgi membrane follows two different trafficking routes, either through vesicular transport[84] or by direct transfer at ER-Golgi contact sites using the Cer transfer protein (CERT)[85]. Upon Cer arrival at the Golgi apparatus, complex sphingolipids such as glycosphingolipids (GSLs) and SM are made. Notably, simple GSLs, such as glucosylceramide, are synthesized at the cytosolic surface of the Golgi apparatus, while SM is synthesized in the Golgi lumen[79]. This suggests a distinct ER to Golgi Cer transfer dependent on its target destination.

The first step in GSL production happens at the *cis*-Golgi complex, where UDP-glucose is attached to the 1-hydroxyl group of Cer. This first glycosylation step is catalyzed by the glucosylceramide synthase (GCS) and results in GlcCer, the simplest GSL, having only one sugar residue headgroup[86]. Multiple sugar residues can attach to this first glucose

resulting in complex GSLs. GSLs are exported to the extracellular leaflet of the plasma membrane, having crucial functions in cell-cell recognition processes[87].

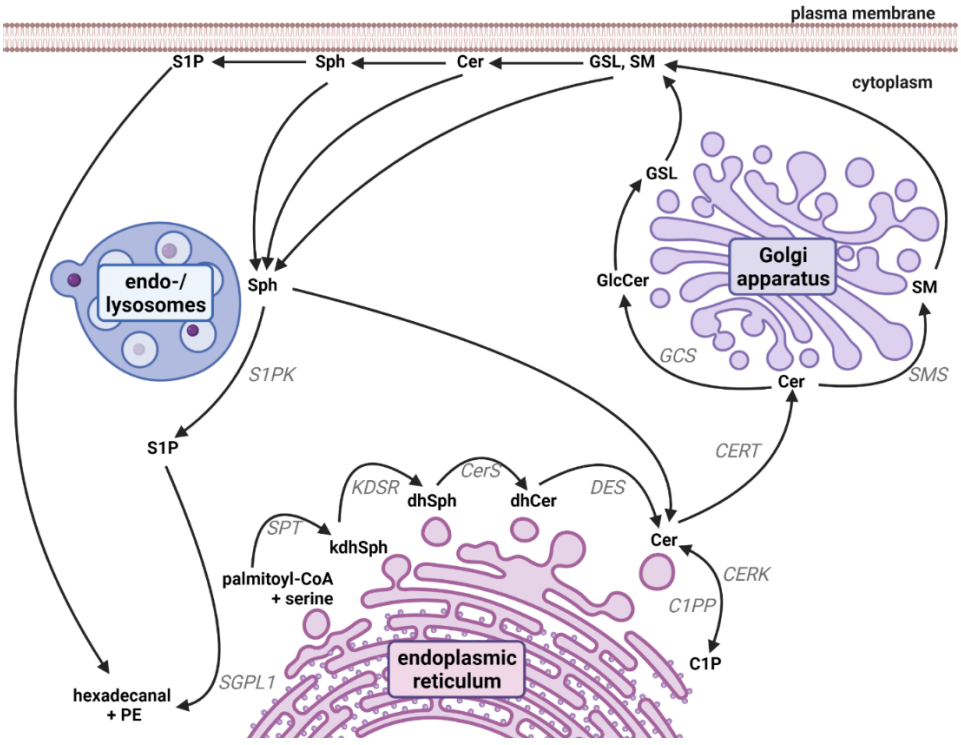

Figure 1.4: The sphingolipid network. From sphingolipid de novo synthesis at the ER, to the biosynthesis of complex sphingolipids at Golgi, ER, and PM, to sphingolipid catabolism in lysosomes and their breakdown to non-sphingolipids.

SM is the most abundant sphingolipid in mammalian cells. Cer is transported to the *trans*-Golgi complex, where sphingomyelin synthase (SMS) 1 and 2 are located. However, SMS2 is also known to reside in the plasma membrane[79]. SMSs are anchored in the Golgi or plasma membrane via six transmembrane domains, facing the catalytic domain towards the Golgi lumen or the extracellular space, respectively. There, SMSs catalyze the reaction of phosphocholine (originated from PC molecules) and Cer to SM and diacylglycerol (DAG). Since SMSs regulate the levels of PC, Cer, SM, and DAG (four

important bioactive lipids), at the same time, it has been proposed to have an essential role in regulating cellular fate[88].

Even though Cer is preferentially incorporated into complex sphingolipids, it can also be phosphorylated at its hydroxyl group resulting in ceramide-1-phosphate (C1P). Ceramide kinases (CERK) activate this reaction at the *trans*-Golgi complex, favoring Cers having a chain length greater than C12[89]. It has been shown that C1P transfer to the plasma membrane happens in a vesicular-dependent manner through the secretory pathway. The exact role of C1P is still unclear, but it has been reported that C1P phosphatases potentially dephosphorylate C1P back to Cer at the plasma membrane[90].

Sphingolipid homeostasis requires a carefully regulated degradation process. SM degradation is catalyzed by sphingomyelinases (SMases) that are categorized into three main classes based on their pH optimum: acid SMases, alkaline SMases, and neutral SMases[79]. Acid SMases have a low pH optimum and are therefore predominantly located in lysosomes[91]. Neutral SMases, which can be subclassified in SMase 1 and 2, are found in several organelles, including the plasma membrane, Golgi complex, ER, nucleus, mitochondria, and recycling compartments[37,92–94]. Acid and neutral SMases are found in most mammalian tissues, while alkaline SMases are exclusively expressed in intestines and liver tissues[95]. Yet, all SMases promote the hydrolysis of the phosphocholine headgroup resulting in Cer.

Similar to SMases, the degradation of Cer is performed by three different ceramidases: acid, neutral, and alkaline ceramidases. Following the previous argumentation, acid ceramidases mainly reside in lysosomes and neutral ceramidases in the plasma membrane. Alkaline ceramidases differ in their subcellular localization[79]. They cleave off the fatty acid and release the free Sph backbone.

Sph can either follow a sphingolipid recycling process, termed the salvage pathway, or it can be degraded to non-sphingolipid molecules. Prior to degradation, Sph is phosphorylated to sphingosine-1-phosphate (S1P) by the action of sphingosine kinase 1 (SphK1). However, the exact mechanism of how SphKs phosphorylate Sph is not fully

understood yet, but it is known that cellular S1P levels are kept low by spatio-temporal regulation[96]. Two SphK isoforms have been identified so far: SphK1 and 2. Both kinases work in a contrary fashion. On the one hand, stimulation of SphK1 results in S1P production, which has been implicated in mitotic and anti-apoptotic effects[97,98]. On the other hand, stimulation of SphK2 has been connected to suppressed growth and enhanced apoptosis[99,100]. Additionally, SphK2 overexpression has been reported to regulate Sph entry into the recycling pathway by increasing palmitate, which serves as substrate for CerS[100]. These different functions can be potentially connected to their different subcellular localization. While SphK1 predominantly remains in the cytosol, SphK2 was reported to partly co-localize with the ER[100], the nucleus, and the perinuclear region[79].

To introduce Sph into the salvage pathway, it has been reported that Sph phosphorylation and dephosphorylation by a concerted activation of SphK2 and S1P phosphohydrolase 1 (SPP-1) regulate the recycling of Sph into Cer[96]. Notably, SphK2 was reported to have an enhanced ability to recycle Sph for Cer production compared to SphK1[100]. Besides regulation via phosphorylation, Sph needs to be transported to the ER where CerS is located. How this transport from lysosomes to the ER is managed is still unclear, but incorporating recycled Sph into Cer and complex sphingolipids such as SM is tremendously important to maintain cellular sphingolipid levels[101].

As already mentioned, Sph phosphorylation is also crucial in the Sph breakdown pathway. S1P is recruited to the ER, where the sphingosine-1-phosphate lyase (S1PL) is exclusively located. It has a single transmembrane domain and a catalytic site facing the ER's cytosolic leaflet. There, it receives S1P and cleaves the sphingoid backbone irreversibly, resulting in hexadecenal and phosphoethanolamine (PE)[102]. This reaction is the final step in sphingolipid degradation and the only exit from the sphingolipid metabolism (Fig. 1.4).

1.3.2 Lysosomal lipid storage diseases

Lipid storage diseases, often termed lipidoses, are inherited metabolic disorders where distinct lipid species accumulate in cells or tissues[103]. These accumulations stem from dysfunctions in metabolic enzymes involved in lipid degradation or transport. Typically, the affected lipids end up in the lyso-/endosomal compartment of the cell leading to the disease being referred to as lysosomal storage disorders. Around 50 different genetic disorders have been characterized so far. Many of them affect various organs leading to severe symptoms and premature death[104].

Lipidoses can be grouped into two major classes: sphingolipidoses and lipidoses in which other lipids than sphingolipids accumulate. Sphingolipidoses are always related to a defect in sphingolipid metabolism, while the others affect the lipid metabolism of non-sphingolipids, such as cholesterol[105]. Some of the initially discovered sphingolipidoses, such as Gaucher disease, Farber disease, Niemann-Pick (type A and B) disease, Krabbe disease, and Fabry disease, are characterized by defects in enzymes from the sphingolipid catabolism and store unnatural amounts of sphingolipids in lysosomes (Fig. 1.5) [106]. Gaucher disease is caused by a deficiency of glucocerebrosidase, a lysosomal enzyme needed for GlcCer degradation. As a result, GlcCer accumulates in lysosomes[107]. Patients of Farber's disease have defects in lysosomal acid ceramidases, which leads to Cer accumulation[108]. Niemann-Pick disease occurs in three different phenotypes. Type A and B affect the acid SMase resulting in SM storage, while Niemann-Pick type C disease does not belong to the sphingolipidoses[109]. Both, Krabbe and Fabry disease have deficiencies in enzymes of the galactosphingolipid pathway. Krabbe disease is characterized by a defect in the galactocerebrosidase, resulting in the accumulation of galactosylsphingosine (GalSph), a lyso-derivative of GalCer[110]. Patients of Fabry disease have a deficiency in alpha-galactosidase, forcing the accumulation of globotriaosylceramide, a complex glycosphingolipid, based on GalCer[111].

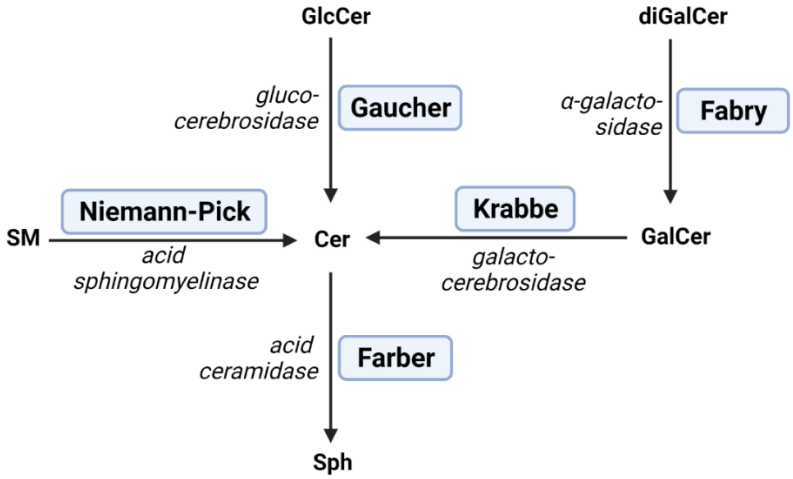

Figure 1.5: Important sphingolipidoses. Lysosomal storage disorders, their enzyme deficiencies, and integration into the sphingolipid metabolism.

Lysosomal storage diseases belonging to non-sphingolipid storage disorders are Wolman's disease and Niemann-Pick type C disease. In these diseases, cholesterol esters and cholesterol are stored in lysosomes[112–114]. Moreover, mucopolysaccharidoses (MPSs) also belong to the class of non-sphingolipid storage disorders. These patients have deficiencies or malfunctions in enzymes necessary for carbohydrate breakdown, leading to storage of incompletely degraded substrates[115].

Nowadays, many of those lipidoses can be treated with therapeutical approaches such as enzyme replacement therapy (ERT), cell-mediated therapy (CMT), gene therapy, enzyme enhancement therapy, or substrate reduction therapy (SRT)[105].

1.4 Cellular lipid transfer

As already mentioned in chapter 1.1, lipids can be transported via the secretory pathway. However, this vesicle-mediated lipid transfer is relatively slow, and furthermore, organelles that are not connected to the secretory pathway, such as mitochondria, need

an alternative lipid transfer route. Therefore, lipids can be rapidly transported from organelle to organelle by lipid transfer proteins (LTPs). This transfer is much faster and more efficient than transfer through the secretory pathway[116].

1.4.1 Lipid transfer at membrane contact sites

LTPs primarily act at membrane contact sites (MCSs), regions where membranes of two different organelles come in close proximity to accelerate lipid transfer over a short distance[117]. The first LTPs have been described in the late 1970s[118,119], but the understanding of their physiological functions and regulations has only deepened in the last 20 years[120]. Besides lipid transfer via LTPs, other lipid transfer mechanisms have been observed at biological membranes: spontaneous monomeric lipid exchange, lateral diffusion, and trans bilayer flip-flop mechanisms[121]. Yet, lipid transfer via LTPs is the most directed transfer that can even happen against the subcellular lipid concentration gradient[122,123]. More than 125 genes encode for at least ten families of LTPs[124]. They are characterized by the structure of their lipid-binding domain that differs according to the lipid species they bind to. For example, the MD-2-related lipid recognition (ML) domain is mainly composed of β-strands[125], while the pocket of the oxysterol-binding protein (OSBP), StAR-related lipid-transfer (START), and Niemann-Pick C1 consist of both β-strands and α-helices[126–128]. All lipid-binding domains are equipped with a hydrophobic cavity that stabilizes the lipid in the gap between the two membranes [116]. Besides the flexible lipid-binding domain, some LTPs are anchored in the donor or acceptor membrane via several transmembrane domains. Others are soluble proteins that need to be recruited to target organelles. However, many LTPs bind MCS-localized proteins that serve as a tether to stabilize the contact between the two membranes[117].

One highly conserved protein family that serves as a tether at many contact sites is the vesicle-associated membrane protein (VAMP)-associated protein (VAP) family. They are located in the ER membrane via a single transmembrane domain. Notably, the ER is involved in a majority of contacts due to its characteristical distribution throughout the entire cell[129]. Two different VAP proteins have been identified so far, VAPA and VAPB. They share a 63 % sequence similarity and are discovered to form homo- or

heterodimers[130]. Besides their C-terminal transmembrane domain, they consist of an N-terminal motile sperm protein (MSP) domain, facing towards the cytosol and a central coiled-coil region. It has been shown that a GXXXG motif present in the transmembrane domain and the coiled-coil region mediate VAP oligomerization[130–132], while the MSP domain is essential for protein-protein interaction[133]. It binds to the FFAT (two phenylalanines in an acidic tract) peptide motif that is highly conserved in many LTPs. Recently, it has been shown that the phosphorylation of some residues within the FFAT motif is involved in MCS formation and lipid transfer[134].

One example of LTPs interacting with VAPs is CERT (also named STARD11). CERT is a soluble protein that transfers Cer at ER-Golgi contact sites. CERT has several functional domains and motifs, including a START domain for lipid-binding, a pleckstrin homology (PH) domain that targets the Golgi apparatus via phosphatidylinositol phosphates (PIPs), a serine repeat motif that is involved in regulating CERT activity, and an FFAT motif that binds to VAPs at the ER surface[135].

VAPs are not the only proteins able to interact with FFAT or FFAT-like motifs. More recently, the MSP domain-containing proteins (MOSPD) 1, 2, and 3 have been identified as ER-resident proteins also interacting with different variants of the FFAT motif. While MOSPD2 seems to interact with similar FFAT motifs as the VAPs, MOSPD 1 and 3 prefer to contact FFNT (two phenylalanines in a neutral tract) motifs[136]. FFNT motifs belong to the category of FFAT-like domains that lack the acidic characteristics of a classical FFAT motif[137]. These minor changes open a door for novel, highly specific protein-protein interactions at MCSs.

Lysosome-ER contact sites have been extensively studied in context to lipid transfer in the past years. Several lysosomal proteins or proteins that are recruited to lysosomes have been identified to contribute to lysosome-ER contact site-mediated lipid transfer. All currently known lysosomal and lysosomal recruited lipid transfer proteins acting at lysosome-ER contact sites are shown in table 1.

Table 1: Lyso- and endosomal (recruited) lipid transporters acting at lysosome-ER contact sites in mammalian cells.

Name	Transported lipid	Lysosomal targeting	ER targeting	References
LIMP2 (SCARB2)	Cholesterol, PS, Sph	Anchored in the lysosomal membrane with 2 transmembrane domains, builds homodimers	unknown	[138–141]
ORP1	Cholesterol, PI(4)P	Recognizes PIPs and binds to Rab7	VAPs	[142]
ORP1L	Cholesterol	Recognizes PIPs and binds to Rab7	VAPs, MOSPD2	[14,143–145]
ORP6	Cholesterol	Recognizes PIPs	VAPs	[146]
ORP10	PI(4),PS	Recognizes PIPs	Dimerizes with ORP9, which binds to VAPs	[147,148]
OSBP	Cholesterol, PI(4)P	Recognizes PIPs	VAPs	[149]
STARD3 (MLN64)	Cholesterol, Sph?	Anchored in the lysosomal membrane with its MENTAL domain	VAPs, MOSPD2	[150–152]
NPC1	Cholesterol, Sph	Anchored in the lysosomal membrane with 13 transmembrane domains	GramD1b, ORP5	[112,140,153–155]
VPS13C	glycerolipids	WD40 module	VAPs	[156,157]

The fact that cholesterol transport at lysosome-ER contact sites has been broadly studied, but other lipids, such as sphingolipids, have been barely investigated is due to only recently upcoming tools that allow investigations of especially sphingolipid-protein interactions[140,158–160]. It is highly likely that gradually more lipid transfer proteins, besides the proteins shown in table 1, will be identified.

1.4.2 The lysosomal lipid transfer protein STARD3

The StAR-related lipid transfer protein 3 (STARD3) was originally discovered in the early 1990s. The study aimed to find new genes involved in breast cancer by screening several

unknown cDNAs isolated from a pool of metastatic lymph nodes (MLN) derived from breast cancers. Clone number 64 was identified as STARD3, which was originally named MLN64[161]. STARD3 was found to be overexpressed in all breast cancer tumors that are positive for the epidermal growth factor receptor 2 (HER2) oncogene, but only very low amounts were found in other tissues and cell lines[162]. In the late 1990s, it was found that STARD3 shares a functionally conserved domain with a steroidogenic acute regulatory (StAR) protein[163]. This finding established the StAR-related lipid transfer (START) protein family[164–168].

Notably, in the early 2000s, STARD3 was for the first time associated with lysosomal localization[169]. Alpy et al. (2013) established that STARD3 has an ER-lysosome tethering activity. Electron, as well as immunofluorescence microscopy experiments, showed that ER-lysosome contact sites are expanded in cells overexpressing STARD3. Furthermore, these contacts are dependent on STARD3-VAP interaction and mutating the residues K94D and M96D in the MSP domain of the VAPs abolished the binding to the FFAT motif of STARD3 and thereby impairing the lysosome-ER contact site formation[12].

Additionally to STARD3-VAP interaction, the FFAT motif of STARD3 has also been shown to interact with MOSPD2, but not MOSPD1 or 3[136]. This interaction has not been extensively studied yet, and it is still unclear if STARD3-MOSPD2 contact has different functions compared to STARD3-VAP interaction.

Structurally, STARD3 consists of three different domains or motifs: the MLN64-N-terminal (MENTAL) domain, an FFAT motif, and a START domain. The MENTAL domain comprises four transmembrane domains that anchor STARD3 in the limiting membrane of lysosomes. This domain is also found in STARD3 N-terminal-like (STARD3NL) proteins that have been shown to have similar functions as STARD3[170]. The START domain of STARD3 is, as already mentioned in chapter 1.4.1, an approximately 210 residue-sized domain facing towards the cytosol. It is folded in α-helices and β-strands that build a hydrophobic cavity inside the protein. Molecular simulation studies have shown that cholesterol perfectly fits in this hydrophobic tunnel, which suggests STARD3 as a cholesterol transfer protein[171].

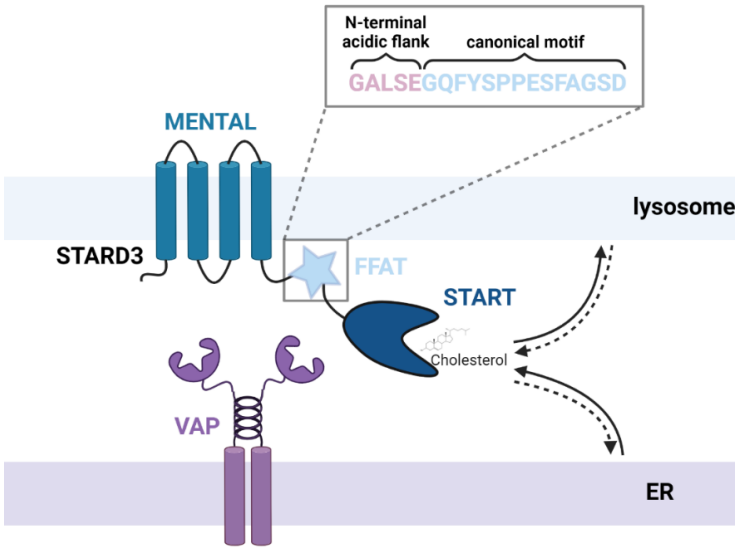

Figure 1.6: Structure of STARD3 and VAP. Stard3-dependent cholesterol transfer at lysosome-ER contact sites.

Indeed, STARD3 has been reported to transfer cholesterol at lysosome-ER contact sites. Wilhelm et al. (2017) used two different approaches to show that STARD3 was indeed a cholesterol transporter. On the one hand, they overexpressed the entire STARD3 protein in cell-based studies and characterized its impact on cellular cholesterol distribution. On the other hand, they used the purified START domain of STARD3 and VAPs to reconstitute lysosome- and ER-like liposomes, respectively, to visualize cholesterol transfer between those *in vitro*. In detail, for their cell-based studies, two different fluorescent probes to quantify free cholesterol inside cells showed that STARD3 overexpression promoted cholesterol accumulation inside lysosomes, indicating a STARD3-dependent cholesterol transfer from the ER towards the lysosome. This cholesterol accumulation inside lysosomes was not found in cells overexpressing three different STARD3 mutants. The first one, a truncated STARD3, completely abolishes the entire START domain, the second has only 2 residues of the START domain mutated, namely M307R and N311D (MR/ND), and the third one, contains two mutations in the FFAT motif, namely F206A and Y209A (FA/YA). These findings indicate that both the START domain, more detailed the highly

conserved M307/N311 residues inside the hydrophobic cavity and the lysosome-ER contact site formation, impaired in the FA/YA mutant, are essential for STARD3-dependent cholesterol transfer[150]. This mechanism is suggested to maintain consistent cholesterol levels at the ER and to support the formation of lysosomal membranes, such as intraluminal vesicles (ILVs)[172].

Interestingly, not only the START domain is able to bind cholesterol, but also the MENTAL domain. This binding is suggested to serve as a mechanism to maintain cholesterol levels in the limiting membrane of lysosomes prior to its transfer to cytosolic acceptors[152].

Notably, STARD3 has also been shown to transfer cholesterol from lysosomes towards the ER. Meneses-Salas et al. (2020) reported that an AnxA6 deficiency in NPC1 mutant cells triggers a STARD3-dependent cholesterol transfer from lysosomes to the ER. This demonstrates that STARD3 could act as a bidirectional cholesterol transporter at lysosome-ER contact sites[173].

Furthermore, STARD3 has been shown to mediate lysosome-mitochondria contacts that are enriched in NPC1 knock-out cells. This contact could serve as an alternative cholesterol transfer route to rescue the lysosomal cholesterol accumulating phenotype in NPC1 patients[112,174]. Therefore, STARD3 overexpression has been associated with a high cholesterol content in a number of distinct organelles such as the plasma membrane[175] and mitochondria[174].

Surprisingly, STARD3 has been also associated to interact with sphingolipids. Höglinger et al. (2017) performed a chemoproteomic profiling approach to investigate lipid-protein complexes. They screened for proteins interacting with sphingolipids, fatty acids, or DAGs. To this end, they used trifunctional lipids and revealed STARD3 to be uniquely identified with TFS. This screen suggests STARD3 not only as cholesterol-binding protein, but also to potentially interact with other lipids such as sphingolipids[159].

This finding leaves many open questions, such as which domain of STARD3 interacts with sphingolipids? Does STARD3 actively transports sphingolipids? Which sphingolipid species is transported by STARD3? And does this transfer occur at lysosome-ER contact

site, potentially in exchange for cholesterol? All these open questions lead us to investigate STARD3-sphingolipid interactions more closely.

1.5 Functionalized lipids as a tool to investigate intracellular signaling

Historically, it was difficult to study lipids in their natural environment for a very long time due to missing tools. Several strategies have been developed to overcome this challenge in the last few decades.

The fact that lipids are relatively small molecules compared to other naturally occurring substances, such as proteins, is one of the most challenging issues in studying lipids. Therefore, large modifications such as fluorescent peptide tags (as they are used in protein biochemistry), are not feasible since they would dramatically change the metabolic behavior and biophysical properties of lipids. Additional challenges are faced due to the high diversity among lipids. In consequence, universal tools to apply to all lipids are lacking. Moreover, lipids are rapidly metabolized, making it difficult to trace them through the cell in real-time.

To overcome these challenges, fluorescent lipids, that have a relatively small fluorescent group attached, have been developed. Fluorescent groups that were commonly used are fluorescein, rhodamine, coumarin, naphthalimid, cyanines, and BODIPY[176]. These developments fundamentally changed lipid biology research. Besides several other discoveries in many lipid species, a fluorescent analog of Cer, N-[7-(4-nitrobenzo-2-oxa-1,3-diazole)]-epsilon-aminocaproyl sphingosine (C6-NBD-Cer), was used to investigate sphingolipid metabolism in fibroblasts. This pioneer study, published in the early 1980s, revealed the transport of sphingolipids from the Golgi apparatus to the plasma membrane and thereby the conversion of Cer to SM and cerebroside, which marks one of the most important milestones in sphingolipid research[177].

Additionally, radiolabelled lipids, incorporating either ^{3}H or ^{14}C, have been used to study sphingolipid metabolism. This technique unraveled fundamental questions in sphingolipid biology, such as revealing the chain length and saturation of attached fatty acids in various sphingolipid species[178]. Nevertheless, it also has many disadvantages, such as its impracticality in real-time resolution assays such as live-cell microscopy. The fact that radiolabelled lipids are not suitable to answer complex questions in sphingolipid biology gave rise to other, more advanced methods.

Recently, in 2016, a new functionalized Sph probe was published. This Sph analog has been chemically modified by covalently attaching two extremely small functional features. On the one hand, it has a photoactivatable crosslinking group composed of a UV-sensitive (365 nm) diazirine ring attached to the sphingoid backbone[158]. This crosslinking group has previously been reported to be suitable for detecting protein-sphingolipid interactions[158]. On the other hand, it has a terminal alkyne handle for click-chemistry approaches. There, azide-modified fluorescent groups, or other reporter molecules such as 3-azido-7-hydroxycoumarin or biotin-azide, respectively, can be attached by copper(I)-catalyzed azide-alkyne cycloaddition (CuAAC) reactions. Besides lipid-protein interaction detection, this approach allows subcellular lipid tracing by either live-cell microscopy or pulse-chase experiments. Furthermore, since this photoactivatable and clickable Sph (pacSph) can be introduced into endogenous sphingolipid metabolism, its incorporation into other sphingolipid species such as Cer or SM, can be investigated by thin-layer chromatography (TLC). These approaches have been used in SGPL1 knock-out cells to prevent sphingolipid breakdown. These cells have been developed to be a tool to investigate sphingolipid metabolism in a very directed way[179]. Furthermore, functionalized groups have not only been introduced in Sph for sphingolipid studies but also for cholesterol investigations using a photoactivatable and clickable cholesterol (pacChol)[112,180].

These bifunctional lipid analogs have been refined in the past years. One additional feature is a coumarin cage. This cage is covalently linked to the amino group of the Sph backbone and prevents the lipid from being recognized by the cells as metabolic active

lipid species and thereby circumventing its rapid metabolism. It can be activated by a pulse of light (405 nm), which initiates the cleavage of the cage group and results in the release of active pacSph. This mechanism is commonly termed as 'uncaging'. These trifunctional Sph probes (TFS) are valuable tools to study comprehensive questions on single lipid species in living cells[159].

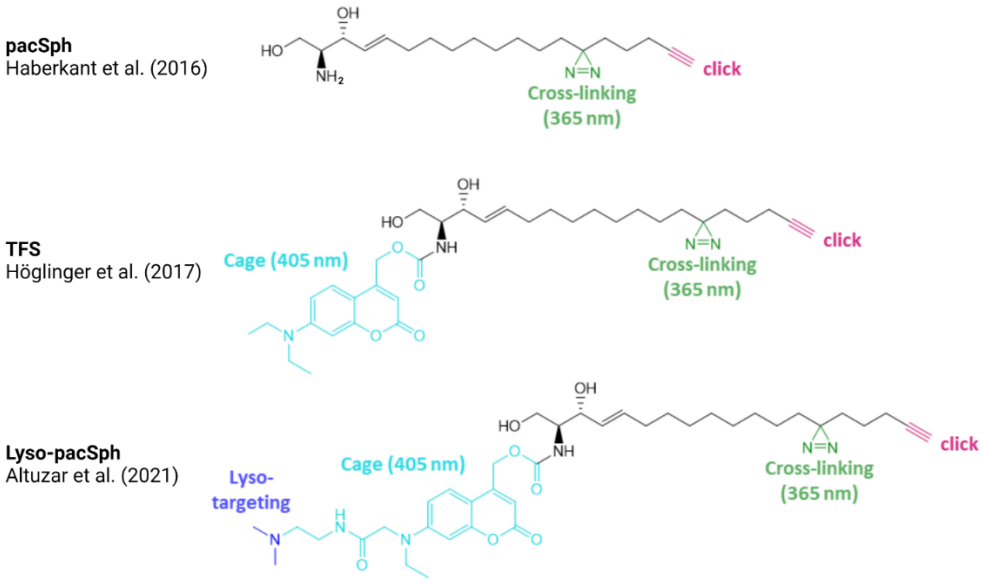

Figure 1.7: Development of functionalized Sph. Sph with attached functional groups for click chemistry (magenta), crosslinking (green), uncaging (cyan), and lysosome targeting (blue).

One disadvantage of this caged Sph analog is its non-selective association with all internal membranes and, in consequence, its distribution throughout the entire cell before uncaging. This issue has been overcome by attaching organelle targeting groups to the coumarin cage that pre-localizes the lipid to specific organelles such as lysosomes or the plasma membrane. Two different approaches have been developed so far. In 2018, the principle of a click cage was published. There, azide-modified plasma membrane, ER, mitochondria, and lysosome targeting moieties have been developed. CuAAC reactions can attach them to alkyne-modified coumarin cages, covalently coupled to a lipid of interest. This attachment pre-localizes the lipid to a target organelle where UV-

dependent uncaging can precisely activate it[181]. The second approach developed in 2021 directly couples a lysosome-targeting group to a coumarin cage. These functional tools have been attached to pacSph or pacChol. The resulting multifunctional lysosome-targeted pacSph and pacChol (lyso-pacSph/lyso-pacChol) have been used to study acute lysosomal lipid export by NPC1 and LIMP2[140].

All in all, many highly advanced tools have been developed in the last few years. They have successfully been applied to study complex cellular lipid processes and revealed new insights into organelle-specific lipid metabolism and transfer. Especially sphingolipid research has benefited from these tools since no other techniques were available to follow their interactions and localizations before[159,182].

Aim of the thesis

The role of STARD3 in context of cholesterol transfer has been extensively studied in the past years. Several studies identified STARD3 as an important cholesterol transporter at membrane contact sites under physiological conditions and in pathology such as NPC disease. However, little is known about the potential ability of STARD3 to transfer other lipids. Only one publication revealed STARD3 to exclusively bind to a trifunctional sphingolipid probe (TFS) but not to other lipids such as DAGs or fatty acids. This promising screen leads to the assumption that STARD3 does not only transfer cholesterol, but potentially also sphingolipids. However, the detailed mechanism of STARD3-mediated sphingolipid transfer has not been studied yet.

The aim of this thesis is to characterize and verify the ability of STARD3 to bind and transfer sphingolipids. Multifunctionalized lipids, such as pacSph or lyso-pacSph, provide an advanced opportunity to investigate lipid-protein interactions. Applying these probes to intact cells allows the characterization of STARD3-sphingolipid interaction using biochemical approaches, such as crosslinking immunoprecipitation, as well as probing for its biological functions by investigating downstream metabolism and localization. In the first part of the thesis, I will aim to investigate which sphingolipid species interacts with STARD3 by using inhibitors and knock-out conditions of enzymes involved in sphingolipid metabolism. Furthermore, I aim to investigate the effect of STARD3 on post-lysosomal sphingolipid metabolism.

In addition, this thesis aims to investigate if STARD3-dependent sphingolipid transfer occurs at lysosome-ER contacts. To this end, artificial contacts between the ER and lysosomes will be created by overexpressing ORP1LΔORD, a lysosomal protein that facilitates lysosome-ER contact site formation but cannot transfer lipids. In the next step,

the contribution of protein interactions between STARD3-VAP and STARD3-MOSPD2 on sphingolipid metabolism interactions will be investigated in order to delineate whether sphingolipid transport indeed occurs at the contact site, in analogy to cholesterol.

Finally, I seek to investigate the mechanism by which the lipid transfer domain of STARD3 binds to sphingolipids. I hypothesize that sphingolipids and cholesterol occupy the same hydrophobic cavity inside the transfer domain. Following insights obtained by molecular dynamic simulation studies will be performed in collaboration with the Nickel group at the BZH (experiments performed by Fabio Lolicato). Then, I will investigate how different START mutants, including already known cholesterol-binding mutants such as M307R/N311D, behave in STARD3-mediated sphingolipid transfer.

Altogether, the results obtained from this study will characterize a possible mechanism of how sphingolipids are exported from the lysosome to enter the recycling pathway, an important, yet still unclear step at the crossroads between sphingolipid catabolism and anabolism.

Chapter II – Results and Discussion

2.1 STARD3 transfers sphingosine

STARD3-dependent cholesterol transfer has been extensively studied in the past years. However, only one study has ever reported a possible ability of STARD3 to bind sphingolipids. In 2017, Höglinger et al. screened for proteins that exclusively bind to sphingolipids but not to other lipids such as fatty acids or DAGs, using trifunctionalized probes. This screen revealed STARD3 as a potential sphingolipid-binding protein but has not been followed up as of yet[159].

In this work, several functionalized lipids combined with cell biology and biochemistry approaches will be used to unravel the STARD3-dependent sphingolipid transfer at lysosome-ER contact sites.

2.1.1 Verification of STARD3-pacSph binding in cell lysates

The proteins involved in lysosomal sphingolipid export have not been identified so far, even though the Sph obtained from lysosomal recycling covers the need for sphingolipid backbones in the biosynthetic pathway to the high degrees of 50 - 90 %, depending on cell type[101,183,184]. Therefore, it is even more important to investigate promising candidates such as STARD3 concerning sphingolipid transfer at lysosomes.

In order to corroborate the lipid-protein interaction screen from Höglinger et al. (2017), I employed two commercially available functionalized lipids, namely pacSph and pacFA, to verify the exclusive binding of STARD3 to Sph but not to other lipids, such as fatty acids. To this end, HeLa 11ht WT cells stably overexpressing FLAG-STARD3 were lysed,

and 50 µM of either pacSph or pacFA were added to enable interactions between these lipids and their respective binding proteins. After 1 h, lipid-protein complexes were crosslinked using UV light (365 nm), followed by an attachment of biotin-azide, via click chemistry, in order to perform streptavidin-based immunoprecipitation (Fig. 2.1a).

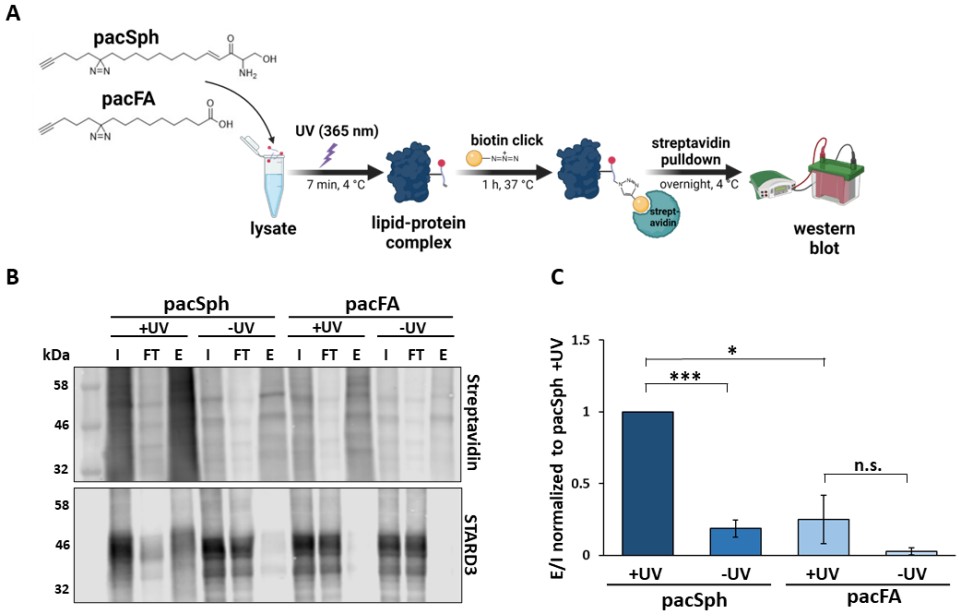

Figure 2.1: *In vitro* immunoprecipitation of STARD3 with pacSph or pacFA. A| Experimental workflow of *in vitro* immunoprecipitation. B| Western blots of immunoprecipitation assays using streptavidin visualization of biotinylated proteins or antibody staining of STARD3. C| Quantification of three independent immunoprecipitation experiments by calculating the ratio of eluate intensity over input intensity, normalized to pacSph (+UV). Error bars show the standard error of the mean and Welch two-sample t-tests were performed as indicated (n.s. *p*-value ≥ 0.05; * *p*-value < 0.05; ** *p*-value < 0.01, *** *p*-value < 0.001).

This biochemical approach to investigating protein-lipid interactions revealed a different pattern of proteins that bound to either pacSph or pacFA, which could be visualized by immunoblotting using streptavidin. Furthermore, the overall streptavidin intensity differed when comparing pacSph against pacFA, as well as +UV against -UV. It was stronger in +UV than -UV and much more pronounced in pacSph than pacFA samples

(Fig. 2.1b). This observation leads to the assumption that Sph and fatty acids specifically interact not only with different proteins but also with a different affinity. Additionally, the enrichment of streptavidin signal in +UV over -UV indicated that UV irradiation is essential to visualize protein-lipid complexes by immunoblotting. This difference confirmed that experimenting in the absence of UV irradiation is a helpful control to verify the proper functioning of this biochemical assay. However, several proteins were labelled with biotin in all conditions. Since streptavidin signal could also be detected in both -UV conditions, it is most likely that unspecific binding of biotin, as well as click-reaction artefacts, led to the precipitation of many proteins without a crosslinked lipid, revealing the limitations of this biochemical assay.

Interestingly, STARD3 was detectable in the elution fraction (E) of +UV pacSph labelled lysates but not in the respective -UV control. Additionally, the detected STARD3 in the eluate was shifted upwards compared to its respective input signal, indicating a change in size and charge when STARD3 is crosslinked to pacSph. Conversely, less STARD3 was detectable in the flow-through (FT) of +UV pacSph compared to -UV pacSph samples, indicating a successful immunoprecipitation of biotinylated STARD3. On the other hand, STARD3 could neither be detected in the eluates of +UV nor -UV of pacFA labelled lysates, although the same amount of protein was used in all conditions (Fig. 2.1b). By quantifying the intensity of the eluate bands over the respective inputs, STARD3 was detected in pacSph (+UV) conditions in a significantly higher ratio compared to pacFA (+UV) conditions (Fig. 2.1c). This outcome supports a specific binding of STARD3 to pacSph but not to other lipids, such as pacFA, in cellular lysates and thereby confirms the proteomic screen in which STARD3 was initially found to bind Sph[185].

In conclusion, sphingolipids and fatty acids interact with various but distinct proteins, which highlights the diversity and specificity of lipid-protein interactions. However, many lipid-binding proteins have been shown to bind several different lipid species. For example, NPC1 and LIMP2 are known cholesterol transporters that also bind Sph[140], or OSBP[186]. Osh6 counter exchanges cholesterol or phosphatidylserine (PS) for PI(4)P[187].

Therefore, it is not unusual for a cholesterol transfer protein, such as STARD3, to additionally interact with other lipids, such as Sph. Given the precedents mentioned above, it is tempting to propose a role of STARD3 as a sphingolipid-cholesterol co-transporter.

2.1.2 STARD3 interacts with sphingosine or sphingosine-1-phosphate *in cellulo*

In vitro STARD3-pacSph interaction shown in chapter 2.1.1 prompted me to investigate whether STARD3 also interacts with sphingolipids in living cells. Previously, it has been shown that pacSph is quickly taken up by cells, either through endocytosis or via direct uptake through the plasma membrane[182]. Using pulse-chase approaches, it has been visualized that pacSph is firstly accommodated in lysosomal structures. Afterwards, it is quickly released out of lysosomes and could be predominantly found in the ER after only 15 min of chase. After 30 min, pacSph metabolites were predominantly found in the Golgi apparatus and subsequently further transported to the plasma membrane. This study revealed that pacSph enters the sphingolipid recycling pathway and can be metabolized into complex sphingolipid species[182]. Besides this transfer towards the biosynthetic pathway, it has also been shown that a large proportion of pacSph quickly enters the degradative pathway measured by increased PC levels. SGPL1 knock-out cells have been identified as a valuable tool to prevent sphingolipid breakdown and thereby direct pacSph towards the biosynthetic pathway[179].

In order to investigate pacSph crosslinking in viable cells to ensure that the observed lipid-protein complexes result from functional interactions, I transiently transfected HeLa WT and SGPL1 knock-out cells with FLAG-STARD3 and labelled them for 1 h with 2 µM pacSph. Upon incorporation into the sphingolipid metabolism, protein-lipid complexes were crosslinked, cells were lysed, and biotin-azide was attached via click chemistry.

Then, streptavidin-based immunoprecipitation was performed, and protein-lipid complexes were analyzed by western blot (Fig. 2.2).

When analyzing the streptavidin signal in both, WT and SGPL1 knock-out cells, I detected an increase in streptavidin signal in the eluates (E) compared to their respective inputs (I), indicating effective immunoprecipitation. This increase was still present but less pronounced in the respective -UV controls. The protein bands found in the -UV controls correlated with the protein pattern found in +UV samples, indicating either unspecific biotinylation of several proteins independent of lipid crosslinking or unspecific crosslinking events without UV irradiation. Interestingly, streptavidin detectable proteins differed in WT compared to SGPL1 knock-out cells. Fewer protein bands were visible in SGPL1 knock-out cells compared to WT cells, implying that pacSph degradation products, such as glycerolipids, were also crosslinked to various proteins.

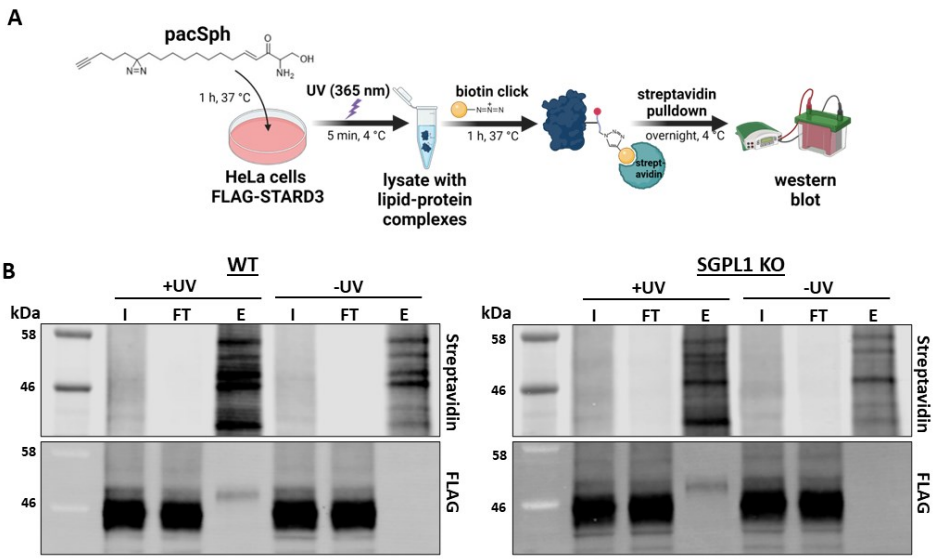

Figure 2.2: *In cellulo* immunoprecipitation of STARD3 in HeLa WT and SGPL1 knock-out cells. A| Experimental workflow of *in cellulo* immunoprecipitation. B| Western blots of immunoprecipitation assays showing streptavidin or FLAG-STARD3 detection in HeLa WT or SGPL1 knock-out cells.

When analyzing pacSph-STARD3 interaction using a specific FLAG antibody, I could detect STARD3 in minor but equal amounts in the +UV eluates of WT and SGPL1 knock-out cells but not in their respective -UV controls. Again, the crosslinked and immunoprecipitated STARD3 migrated at a higher molecular weight compared to its respective input and flow-through samples. This precipitation of STARD3-pacSph metabolite complexes in both WT and SGPL1 knock-out cells showed that, indeed, sphingolipids were able to interact with (an albeit small fraction of) overexpressed STARD3 in living cells.

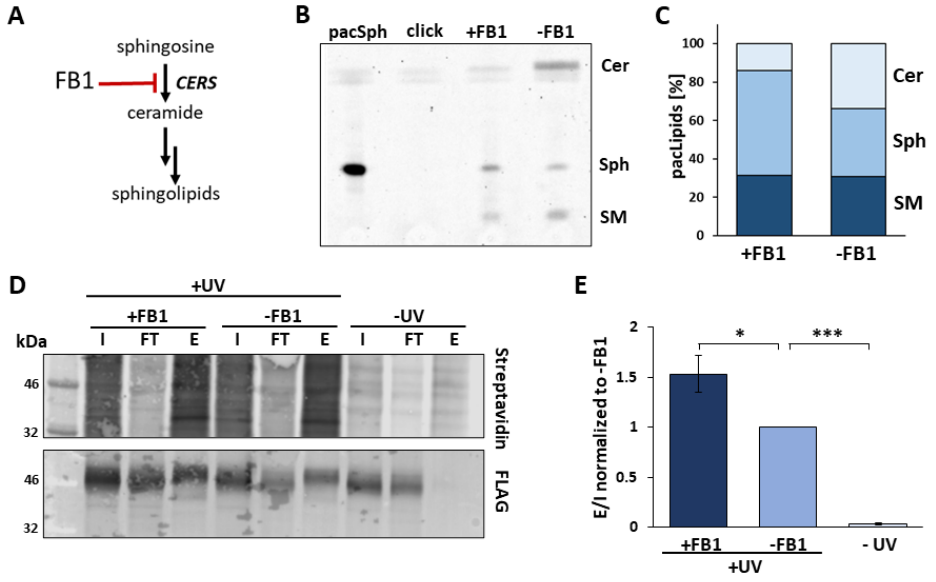

Figure 2.3: Fumonisin B1 (FB1) to manipulate sphingolipid biosynthesis in cells. A| Principle of FB1 inhibition on ceramide synthases (CerS). B| TLC of HeLa SGPL1 knock-out cells treated with 50 µM FB1 and labelled with 2 µM pacSph for 1 h. C| TLC quantification of SM, Sph and Cer as stacked bar graph of three independent experiments. D| Streptavidin-based immunoprecipitation of pacSph-STARD3 complexes in HeLa SGPL1 knock-out cells treated with 50 µM FB1. E| Quantification of three independent immunoprecipitation experiments showing eluates (E) over inputs (I) normalized to -FB1 sample. Error bars show the standard error of the mean and Welch two-sample *t*-tests were performed between -FB1 and +FB1 or -UV (n.s. *p*-value ≥ 0.05; * *p*-value < 0.05; ** *p*-value < 0.01, *** *p*-value < 0.001).

Having confirmed that STARD3 does interact with sphingolipids, I next asked which sphingolipid lipid species is the STARD3 interaction partner. To this end, I used the small

molecule Fumonisin B1 (FB1). FB1 is a mycotoxin that specifically inhibits ceramide synthases (CerS) responsible for the acylation of sphingoid bases using fatty acyl-CoA for Cer biosynthesis in the *de novo* or recycling pathway (Fig. 2.3a)[188]. The structural basis of FB1 is similar to long-chain (sphingoid) bases, such as Sph, which allows them to be recognized as substrate analogs for CerSs[189].

To confirm FB1-dependent Cer inhibition, SGPL1 knock-out cells were treated with 50 µM FB1 overnight and labelled with 2 µM pacSph for 1 h. Subsequently, lipids were extracted, and pacSph metabolites were visualized by attaching a UV-sensitive coumarin via click-chemistry and separated by thin-layer chromatography (TLC). TLC analysis verified the functionality of FB1 by showing a reduced biosynthesis of Cer, but an accumulation of Sph in FB1 treated (+FB1) compared to non-treated (-FB1) cells (Fig. 2.3b and c).

In order to investigate whether STARD3 interacts with pacSph as indicated from the lysate crosslinking experiments as opposed to higher pacSph metabolites, HeLa SGPL1 knock-out cells were transiently transfected with FLAG-STARD3 and treated with 50 µM FB1 to diminish Sph turnover to Cer. Afterwards, the same pacSph immunoprecipitation assay (as described in Fig. 2.2a) was performed. As a result, the pattern of streptavidin detectable proteins was similar in FB1-treated (+FB1) and non-treated (-FB1) cells. However, STARD3, detected by a specific FLAG-antibody, was enriched in the eluate of +FB1 compared to -FB1 and not detected in the -UV control (Fig. 2.3.d). Significant 1.5-fold enrichment of FB1-treated compared to non-treated cells was calculated (Fig. 2.3e). This outcome indicates a predominant interaction of STARD3 with lower sphingolipids such as Sph or S1P.

Sph and S1P are bioactive sphingolipid species that can regulate critical biological functions, such as cell growth and survival, differentiation, angiogenesis, autophagy, and cell migration[190]. They have been extensively studied in the past years and many pathologies, such as cardiovascular, immunological, neurological, and inflammatory diseases, could be connected to dysfunctions in their metabolism[191]. However, their

subcellular transfer is still not fully understood. Especially, Sph transfer out of the lysosome towards the recycling pathway has not been clarified so far. The results discussed in chapters 2.1.1 and 2.1.2 assume STARD3 to facilitate lysosomal Sph import or export. *In vitro* lipid-protein interaction assays showed specific binding of STARD3 and Sph, which could be confirmed in intact cells.

Nevertheless, *in cellulo* immunoprecipitation assays could not exclude S1P as potential STARD3 interacting lipid. It is tempting to speculate that the charged properties of S1P render it unable to fit in the highly hydrophobic cavity of the START domain of STARD3, which is the suggested interaction site. Altogether, I presume Sph as the most likely interaction partner of STARD3.

2.1.3 STARD3 boosts Sph towards the biosynthetic sphingolipid pathway

Under physiological conditions, STARD3 has been reported to transfer cholesterol from the ER towards lysosomes in order to maintain low cholesterol levels at the ER[150]. Additionally, it has been shown that STARD3 is able to change the cholesterol transfer direction from the lysosome towards the ER[173] or mitochondria[174] in NPC deficient cells.

Previous results verified the binding ability of STARD3 to Sph under physiological conditions. These results motivated further research on STARD3-mediated Sph transport, focusing on lysosomal import or export.

To this end, I performed TLC-based assays in order to trace the metabolites of exogenously added pacSph through HeLa 11ht WT (ctrl) and FLAG-STARD3 overexpressing (STARD3 OX) cells to investigate if STARD3 has an impact on sphingolipid metabolism. To this end, HeLa 11ht WT and stably expressing FLAG-STARD3 cells were labelled with 2 µM pacSph for 5 min and chased for either 0 or 30 min (Fig. 2.4a). This

pulse-chase approach allowed a more precise analysis of cellular pacSph fate than a continuous pulse.

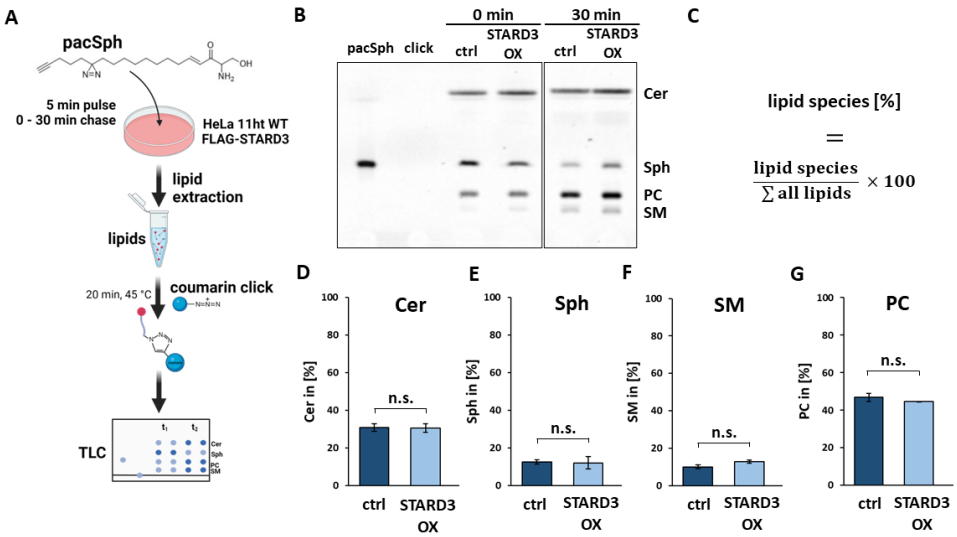

Figure 2.4: Thin-layer chromatography (TLC) using a pacSph pulse-chase approach. A| Workflow of TLC-based assay using a pacSph pulse-chase approach. B| TLC of HeLa 11ht WT (ctrl) and stably STARD3 overexpressing cells (STARD3 OX), labelled with 2 µM pacSph for 5 min and chased for 0-30 min without pacSph. C| Equation for lipid quantification calculation. D| Quantification of pacSph fate after 30 min shown as Cer, E| Sph, F| PC, and G| SM. Error bars show the standard error of the mean.

Thin-layer chromatographic analysis showed that pacSph had been taken up by cells visualized by the appearance of several bands that were identified as various lipid species, including Cer, Sph, PC, and SM. This incorporation of pacSph into different lipid species confirmed the entry of pacSph into cellular sphingolipid metabolism. A shift in lipid intensities was detectable when comparing both chase timepoints (0 and 30 min). While Sph had a higher intensity in 0 min samples, PC and SM were enriched after 30 min of chase. Cer levels did not change between 0 and 30 min (Fig. 2.4b). This shift corroborated that pacSph is able to enter the recycling sphingolipid pathway at the ER and the Golgi apparatus, where Cer and SM originate from. Higher sphingolipids, such as SM, were only enriched after 30 min chase, suggesting a temporal control of sphingolipid

metabolism. However, Sph release out of the lysosome could also be related to sphingolipid degradation, as indicated by PC, the main product of the degradation pathway, representing the dominant metabolite after 30 min.

To analyze the impact of STARD3 on sphingolipid metabolism, I quantified single lipid species from three independent TLCs and compared them between control and STARD3 overexpressing cells. To this end, the mean of one lipid species was divided by the mean of the total number of lipids from the same sample and plotted as percentages (Fig. 2.4c). The later timepoint (30 min) investigated whether STARD3 affected either pacSph incorporation into higher sphingolipids, such as Cer or SM, or its degradation. After 30 min, 30 % of pacSph was incorporated into Cer (Fig. 2.4d), and only 10 % stayed as Sph (Fig. 2.4e). However, their levels did not change when overexpressing STARD3. Interestingly, higher sphingolipids such as SM showed a minimal but non-significant increase in cells overexpressing STARD3 compared to control cells (Fig. 2.4f). Correspondingly, less pacSph entered the degradative pathway in STARD3 overexpressing cells which was visualized by a minimal diminishment in PC levels. Notably, almost 50 % of pacSph was degraded when taken up by cells (Fig. 2.4g).

The pacSph pulse-chase experiments did not give significant information about a STARD3-mediated Sph transfer. However, a STARD3-mediated Sph transfer towards the biosynthetic pathway of higher sphingolipids could be speculated since a minor shift towards SM in STARD3 overexpression conditions could be measured. However, this effect was barely detectable since a tremendous amount of pacSph was directly degraded to non-sphingolipids, such as PC. Since elevated cellular Sph levels are toxic and induce apoptosis[192,193], it is not surprising that cells taking up unnatural amounts of Sph try to further incorporate it into other, non-toxic metabolites, such as PC. STARD3 could be overexpressed in an SGPL1 knock-out background to overcome this major incorporation into glycerolipids. However, SGPL1 knock-out cells have been reported to manifest in a lysosomal storage disorder, shown by increased endogenous levels of Sph and S1P[179], which would confound interpretations when investigating lysosomal Sph exit.

Since Sph phosphorylation prior to its degradation could potentially already occur at the plasma membrane, directly after pacSph uptake before it reaches the lysosome, a lysosomal pre-localization of an inactive pacSph probe could potentially prevent its initial degradation.

To this end, a newly synthesized sphingolipid probe from our lab was applied to cells to overcome this drawback. This multifunctional lyso-pacSph allows, besides the well-established click and crosslink approaches, its lysosomal pre-localization and precise activation to investigate the acute effect of lysosomal Sph export[140]. Therefore, cells do not recognize lyso-pacSph as toxic Sph, which could potentially prevent its subsequent degradation. HeLa 11ht WT (ctrl), STARD3 overexpressing (STARD3 OX), and STARD3 knock-out (STARD3 KO) cells were labelled with 5 µM lyso-pacSph for 1 h and cultured overnight without the lipid to allow lyso-pacSph trapping inside lysosomes. The next day, the probe was activated and chased for 30 min to force its incorporation into sphingolipid metabolism (Fig. 2.5a). Afterwards lipids were examined by TLC as described above.

STARD3-dependent Sph transfer was investigated by comparing lipid metabolism in control cells, harboring endogenous STARD3 levels, to STARD3 overexpressing and STARD3 deficient cells. TLC analysis showed a different pattern of lipid species in all three cell lines. When examining total PC levels, it was immediately noticeable that less of the probe (20 % compared to 50 % when using exogenous pacSph) entered the degradative pathway. Consequently, the majority of the activated lyso-pacSph probe was incorporated into the biosynthetic pathway (Fig. 2.5b). Again, Cer abundance levels remained unchanged in overexpressed or depleted STARD3 conditions (Fig. 2.5c). Interestingly, Sph levels were elevated in STARD3 knock-out cells, indicating a delay of lysosomal Sph export (Fig. 2.5d). The SM enrichment trend in STARD3 overexpressing cells, already found in pacSph pulse-chase assays, was even more pronounced when applying lyso-pacSph as a reporter molecule. STARD3 overexpressing cells incorporated up to 60 % of the liberated lyso-pacSph into SM, whereas this value only reached 35 % in control cells (Fig. 2.5e). The incorporation of the probe towards the biosynthetic pathway

in STARD3 overexpression cells seemed to be at the expense of degradative products. PC levels in STARD3 overexpressed cells were significantly lower than in control cells, supporting the idea of a STARD3-dependent preference for lyso-pacSph incorporation into higher sphingolipid species, such as SM (Fig. 2.5f).

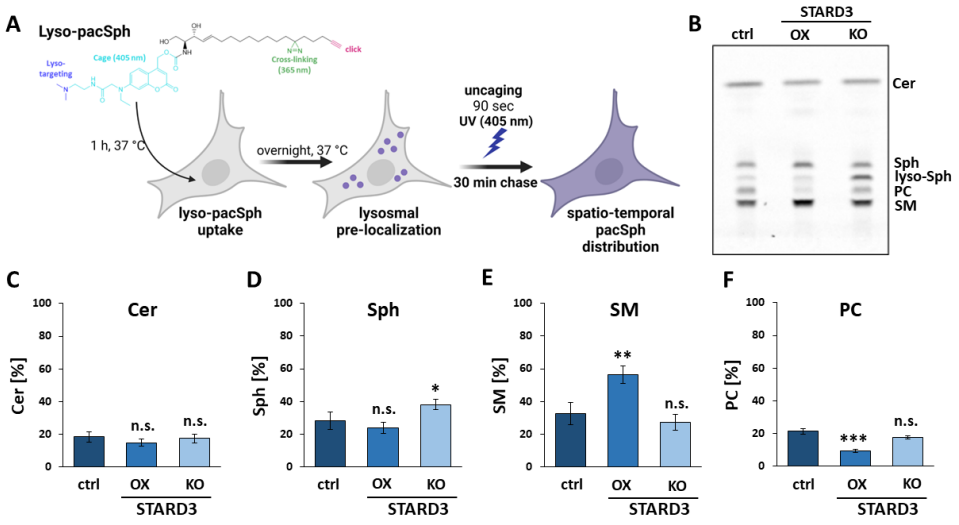

Figure 2.5: Thin-layer chromatography (TLC) using a lyso-pacSph approach. A| Principle of lyso-pacSph labelling, uncaging, and activation. B| TLC of HeLa 11ht WT (ctrl), stably overexpressing STARD3 (STARD3 OX) and STARD3 knock-out (STARD3 KO) cells, labelled with 5 µM lyso-pacSph and chased after probe activation for 30 min. C| Quantification of lyso-pacSph fate after 30 min shown as Cer, D| Sph, E| SM, and F| PC. Error bars show the standard error of the mean and Welch two-sample *t*-tests were performed between ctrl and STARD3 OX or STARD3 KO cells (n.s. *p*-value ≥ 0.05; * *p*-value < 0.05; ** *p*-value < 0.01, *** *p*-value < 0.001).

Interestingly, SM but not Cer levels were increased in STARD3 overexpression conditions. This outcome seems counterintuitive since Cer, which is biosynthesized at the ER, should be directly affected by increased lysosome to ER Sph transfer. I speculate that ER-to-Golgi transfer is much more efficient than lysosome-to-ER transport, which supposes that under out-of-equilibrium conditions, every Cer molecule made at the ER is subsequently transported to the Golgi for incorporation into higher sphingolipids, such as SM. Moreover, ER Cer levels are highly controlled due to the fact that minor changes can

affect various cellular functions including proliferation, differentiation and cell death[194,195] . Therefore, I hypothesize that most activated lyso-pacSph is either degraded (to PC) or incorporated into higher sphingolipids such as SM. In summary, the STARD3-dependend increase of SM levels could indeed be a hint for enhanced Sph transport at lysosome-ER contact sites.

To further investigate whether STARD3 deficiency diminishes lysosomal Sph export, the subcellular distribution of activated the lyso-pacSph probe was investigated in STARD3 knock-out and control cells by microscopy. Short timepoints, ranging from 0 to 15 min, were chosen to examine lysosomal Sph release precisely. After lyso-pacSph labelling (10 µM), uncaging, and chasing, lyso-pacSph metabolites were crosslinked to cellular material in close proximity. Next, cells were fixed, and the lipid excess was removed. Crosslinked lipids were clicked to an Alexa fluorophore and lysosomes were visualized by an immunofluorescence staining against LAMP1.

Confocal microscopy images revealed lysosomal staining of Sph in both control and STARD3-deficient cells immediately upon uncaging as dictated by the lysosomotropic properties of lyso-pacSph (Fig. 2.6a). At longer timepoints, control cells exhibited loss of vesicular staining and the appearance of subcellular structures that are most likely ER (10 min) and Golgi (15 min) organelles in control cells. However, the probe predominantly localized to lysosomal structures during the entire time course in STARD3 deficient cells (Fig. 2.6a). By quantifying the Persons' correlation coefficient of lyso-pacSph and LAMP1 a significant delay in lysosomal Sph export was calculated in STARD3 deficient compared to control cells after 10 and 15 min (Fig. 2.6b). This lysosomal sphingolipid accumulation in STARD3 deficient cells, in accordance with increased Sph levels as observed by TLC, further strengthens the important role for STARD3 as crucial Sph transporter.

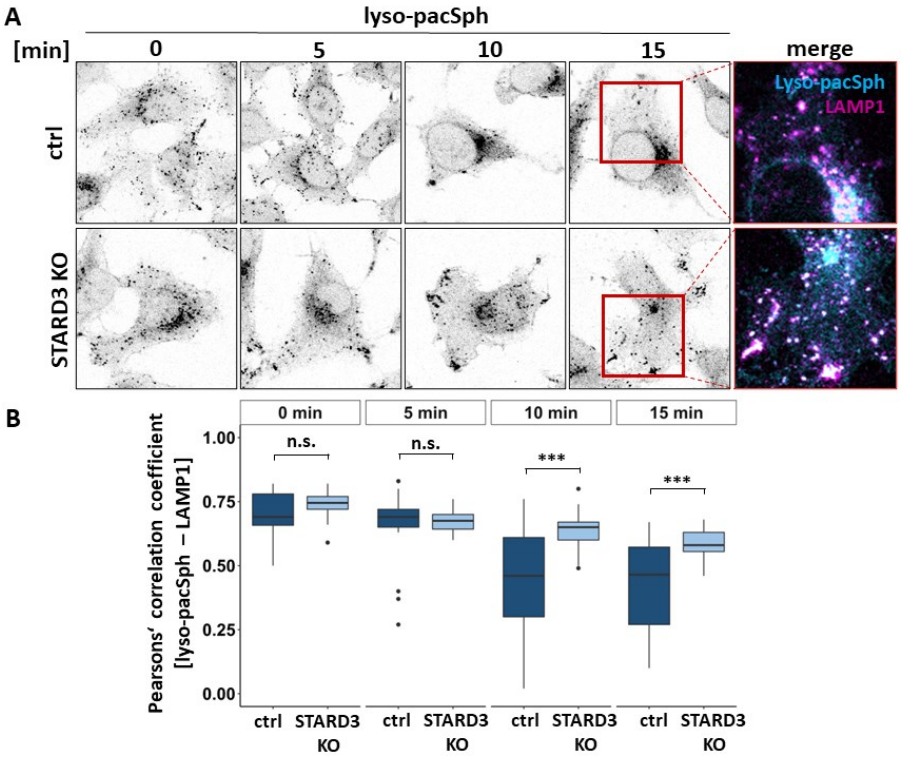

Figure 2.6: Visualization of lysosomal lyso-pacSph export in STARD3 knock-out cells. A| Confocal microscopy of 10 µM lyso-pacSph labelled and 0 to 15 min chased HeLa 11ht WT (ctrl) and STARD3 knock-out (STARD3 KO) cells. Single microscopy images represent subcellular lyso-pacSph distribution, while merge images show lyso-pacSph (cyan) and LAMP1 (magenta). B| Quantification of lyso-pacSph - lysosome colocalization. Pearsons' correlation coefficient between lyso-pacSph metabolites and LAMP1 stained organelles was extracted for each timepoint ($n \geq 20$) and presented as boxplots. Centerlines show the median, box limits indicate first (Q1) and third (Q3) quartiles, whiskers extend to a maximum distance of 1.5*IQR (interquartile range) from Q1 and Q3, respectively, or to the most extreme data point within the range. Welch two-sample t-tests were performed between ctrl and STARD3 KO cells for each timepoint (n.s. p-value ≥ 0.05; * p-value < 0.05; ** p-value < 0.01, *** p-value < 0.001).

In conclusion, STARD3 overexpression revealed a STARD3-dependent Sph transfer proceeding from the lysosome, leading to enhanced Sph incorporation into higher sphingolipids, such as SM. In STARD3 deficient conditions, a delay in lysosomal Sph export could be shown in TLC-based assays, as well as single-cell confocal microscopy.

These observations indicate a STARD3-dependent Sph transfer directed from the lysosomal lumen towards other subcellular structures. Interestingly, confocal microscopy images revealed a widespread sphingolipid distribution after lysosomal Sph release, which could be considered as predominant ER localization. STARD3 has been reported to interact with ER surface proteins, such as VAPA and VAPB[12]. Therefore, it is tempting to speculate that lysosomal Sph release occurs at lysosome-ER contact sites and that Sph transfer directs towards the ER. This direction is opposing to STARD3-dependent cholesterol transfer, which has been shown to point towards the lysosomal lumen under physiological conditions[196]. This lipid transfer in a bidirectional fashion hypothesizes a STARD3-dependent cholesterol-Sph counter transport. Consequently, STARD3-dependent lysosomal Sph export presents a novel mechanism for sphingolipids to enter the recycling pathway that has been unravelled so far.

However, STARD3 cannot serve as the only lysosomal sphingolipid exporter given that Sph could still be incorporated into higher sphingolipids in STARD3 deficient cells. In fact, the effect of Sph storage in STARD3-deficient conditions could only be observed in early timepoints. As such, STARD3 likely only contributes to a certain extent to Sph trafficking. This is in accordance with its relatively low expression levels that are 2-fold lower than other lysosomal lipid transporters, such as NPC1[197]. This STARD3-independent sphingolipid entry into the recycling pathway could be facilitated by other lipid transporters. It is tempting to speculate that other cholesterol transporters, such as ORP1L or NPC1, act similarly as STARD3 does and facilitate Sph exit out of the lysosome. Supportingly, a recent study unraveled NPC1 as Sph-binding protein[140]. However, further investigation is needed to figure out whether lysosome-ER contact site formation is essential for STARD3-dependent lysosomal Sph export.

2.2 STARD3-dependent lysosomal sphingosine export appears at lysosome-ER contact sites

Lipid transport at membrane contact sites has been extensively studied in the past few years. Several lipid-binding proteins, such as ORP1L[198], CERT[17], and STARD3[170], have been discovered to act in the narrow intermediate area of two different organelles. Most of them comprise different structural features that tether the contact to ensure lipid transfer. In particular, STARD3 harbors a highly conserved FFAT motif that has been reported to tether ER surface proteins, such as VAPA and VAPB[12] or MOSPD2[145], to safeguard cholesterol transfer between the ER and lysosomes. However, whether STARD3-dependent Sph transfer occurs at lysosome-ER contact sites has only been hypothesized so far. Here, I investigate the impact of the STARD3 FFAT motif on lysosomal Sph export, as well as several ER-resident surface proteins that potentially tether the lysosome-ER contact site.

2.2.1 Artificial lysosome-ER contacts do not induce sphingolipid transfer towards the ER

STARD3-dependent Sph transfer has been described in chapter 2.1. However, it has not been shown whether STARD3 directly transfers Sph or if the ability of STARD3 to tether lysosome-ER contacts is enough to induce Sph transfer from lysosomes to the ER by other mechanisms.

The oxysterol-binding protein-related protein 1 (ORP1L) has been reported to transfer cholesterol at lysosome-ER contact sites[144]. Therefore, it binds to lysosomal recruited Rab7 via its ankyrin repeat (ANK) region and forms a tether with VAP proteins at the ER surface, similar to STARD3. Additionally, ORP1L comprises a pleckstrin homology (PH) domain for binding phosphoinositides (PIPs) and an OSBP-related ligand-binding domain

(ORD) for cholesterol transfer (Fig. 2.7a)[143]. A truncated ORP1L construct (ORP1LΔORD), missing its ORD domain, has previously been reported to artificially tether lysosome-ER contacts without transporting lipids, such as cholesterol, between those organelles (Fig. 2.7b)[112]. Based on these findings, ORP1LΔORD is an optimal tool to investigate whether artificially increased lysosome-ER contacts are sufficient to induce lysosomal Sph export by other LTPs than STARD3 or if an active transport mediated by STARD3 is crucial. Moreover, increasing lysosome-ER contacts using ORP1LΔORD allows for investigating whether Sph, a relatively hydrophilic lipid, can diffuse between membranes when they come close enough together.

For that reason, I created a cell line stably overexpressing ORP1LΔORD. I applied the previously established lyso-pacSph TLC-based assay to these cells and investigated whether these artificially created contact sites induce the same lipid shift towards the sphingolipid biosynthetic pathway as STARD3 overexpressing cells did.

TLC analysis revealed that lyso-pacSph was incorporated into various lipid species 30 min post uncaging (Fig. 2.7c). To examine the relative amounts of lyso-pacSph metabolites in control (ctrl), STARD3, and ORP1LΔORD overexpressing cells, I quantified all lipids as previously described. ORP1LΔORD expressing cells showed minimally but not significantly increased Cer levels (Fig. 2.7d) accompanied by corresponding decreased Sph levels to the same amount (Fig. 2.7e). When investigating the incorporation of lyso-pacSph into the sphingolipid biosynthetic pathway by analyzing SM levels, the previously discovered significant increase in STARD3 overexpressing cells is again visible, but ORP1LΔORD overexpressing cells did not show preferred incorporation of lyso-pacSph into SM. Instead, their SM levels were comparable to control cells (Fig. 2.7f). Accordingly, the amount of PC was significantly decreased in STARD3 but not in ORP1LΔORD overexpressing cells (Fig. 2.7g).

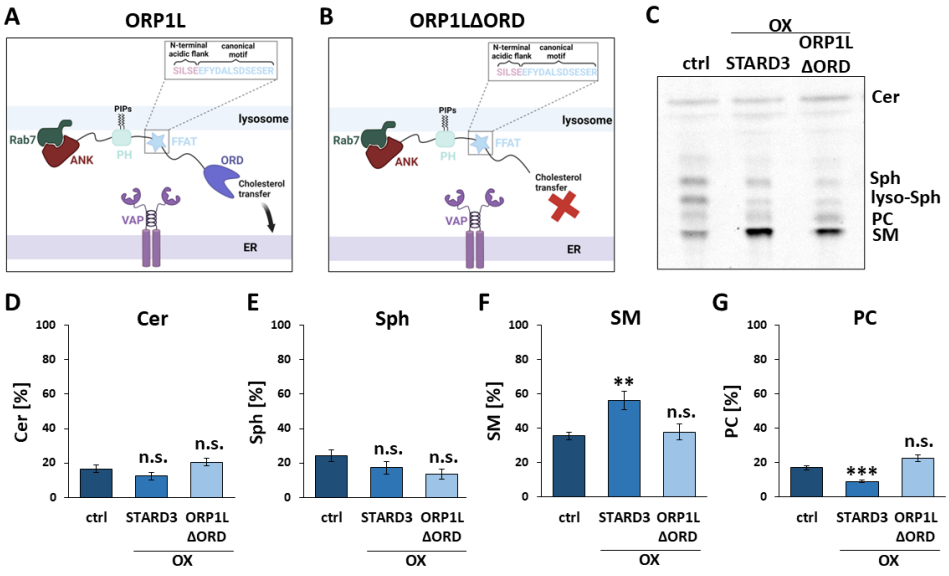

Figure 2.7: Sphingolipid metabolism at artificially induced lysosome-ER contacts. A| Functional ORP1L that can bind to VAP proteins at the ER surface to transfer cholesterol at lysosome-ER contact sites. B| ORP1LΔORD, a truncated version of ORP1L that misses the ORD domain for cholesterol transfer. C| TLC of HeLa 11ht WT (ctrl), stably overexpressing STARD3 (STARD3 OX) and ORP1LΔORD (ORP1LΔORD OX) cells, labelled with 5 µM lyso-pacSph and chased after probe activation for 30 min. D| Quantification of lyso-pacSph fate after 30 min shown as Cer, E| Sph, F| SM, and G| PC. Error bars show the standard error of the mean and Welch two-sample *t*-tests were performed between ctrl and STARD3 OX or ORP1LΔORD OX cells (n.s. p-value ≥ 0.05; * p-value < 0.05; ** p-value < 0.01, *** p-value < 0.001).

In summary, artificially induced lysosome-ER contacts by overexpressing ORP1LΔORD did not facilitate lysosomal Sph export and a subsequent entry into the sphingolipid biosynthetic pathway, such as in STARD3 overexpressing cells. However, a slight increase in Cer levels in ORP1LΔORD cells could indicate a minor boost of Sph towards the ER. Notably, this increased Sph incorporation into higher sphingolipids was not to the same extent as STARD3 overexpression caused. This could be explained by the existence of endogenously expressed STARD3 and other potential lysosomal Sph exporters in ORP1LΔORD cells that were possibly activated by artificially increasing lysosome-ER contacts. Indeed, ORP1LΔORD expression has been reported to rescue the cholesterol

accumulating phenotype in NPC1 knock-out cells, indicating its ability to induce lysosomal lipid export[112].

In conclusion, STARD3-dependent lysosomal Sph export is not only caused by artificially increased lysosome-ER contacts but by an active STARD3 Sph transfer mechanism that is most likely mediated by a lipid transfer domain, such as the START domain. This further advances our hypothesis that STARD3 could play an active role in Sph entry into the sphingolipid recycling pathway.

2.2.2 Impairment of STARD3-dependent contact site formation activates sphingolipid degradation

The membrane contact site tethering feature of many lipid transfer proteins is highly important for safeguarding subcellular lipid trafficking. A short linear motif, called "two phenylalanines (FF) in an acidic tract" (FFAT), is widely conserved in mammalian cells[199]. This small feature binds ER surface-resident proteins harboring an MSP domain, such as the VAPs do[200]. The core element of the FFAT motif contains seven amino acids, namely E_1-**F_2-F_3**-D_4-A_5-X_6-E_7, which are preceded by an adjacent acidic flanking region[201]. In fact, variations in all seven residues could be observed, resulting in FFAT-like motifs[202]. Moreover, a recent study reported that specific phosphorylation at FFAT regions controls the formation of membrane contacts as well as according lipid transfer[134].

As mentioned in chapter 1.4.2, STARD3 comprises an FFAT motif for tethering lysosomes to the ER. Its core element is constituted of Q_1-F_2-Y_3-S_4-P_5-P_6-E_7, which interacts with the MSP domain of VAPs[12] and MOSPD2[136]. STARD3-mediated cholesterol transfer at lysosome-ER contact sites is dependent on a functional FFAT motif[150]. However, whether the lysosome-ER contact site formation is essential for STARD3-mediated Sph transfer needs to be investigated.

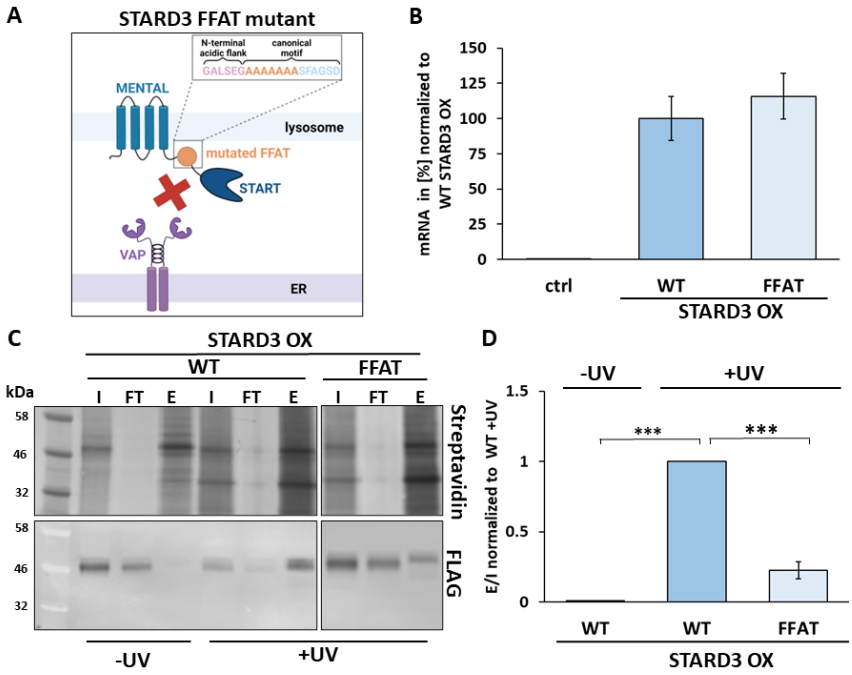

Figure 2.8: Immunoprecipitation of pacSph and STARD3 FFAT mutant. A| STARD3 FFAT mutant cannot bind to VAP proteins at the ER surface and thereby impairs lysosome-ER contacts. B| qPCR of ctrl, STARD3 OX, and STARD3 FFAT mutant OX expressing cells. mRNA levels are normalized to STARD3 OX and error bars show the standard deviation of the mean. C| Streptavidin-based immunoprecipitation of pacSph-STARD3 complexes in HeLa 11ht WT cells overexpressing either functional STARD3 (WT) or an FFAT mutant STARD3 (FFAT). D| Quantification of three independent immunoprecipitation experiments showing eluates (E) over inputs (I) normalized to functional STARD3 (WT) +UV sample. Error bars show the standard error of the mean and Welch two-sample *t*-tests were performed between -FB1 and +FB1 or -UV (n.s. *p*-value ≥ 0.05; * *p*-value < 0.05; ** *p*-value < 0.01, *** *p*-value < 0.001).

For that reason, I created a cell line stably overexpressing STARD3 that harbors a mutated FFAT motif (FFAT). The created core element of the FFAT mutant comprises seven alanine (A) residues to impair lysosome-ER contact site formation (Fig. 2.8a). Expression levels were analyzed by qPCR and a similar expression compared to the WT STARD3 was observed (Fig. 2.8b). First, the ability of STARD3, harboring the FFAT mutation, to bind Sph was examined by *in cellulo* immunoprecipitation as described in chapter 2.1.2. To this end, both cell lines were labelled with 2 µM pacSph for 1 h, and interacting proteins

were crosslinked to pacSph metabolites in cells. Afterwards, lysates were clicked to biotin-azide and immunoprecipitation was performed. Immunoprecipitation (Fig. 2.8c) and its quantification (Fig. 2.8d) showed a significantly reduced binding of pacSph to the STARD3 FFAT mutant (FFAT +UV) compared to functional STARD3 (WT +UV). This indicates that functional lysosome-ER contacts are crucial for STARD3-dependent Sph-binding and could also possibly regulate STARD3 mediated sphingolipid transfer. Alternatively, the FFAT motif could be the potential Sph-binding site. Accordingly, its mutation would lead to decreased co-immunoprecipitation of STARD3 and pacSph.

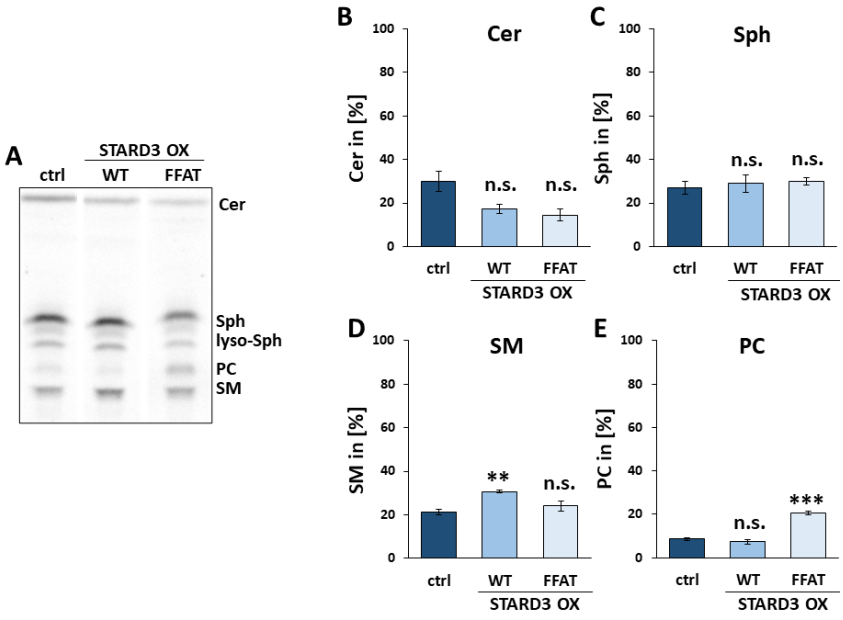

Figure 2.9: Sphingolipid metabolism in STARD3 FFAT mutant overexpressing cells. A| TLC of HeLa 11ht WT (ctrl), stably overexpressing wild type STARD3 (STARD3 OX WT) and FFAT mutant (STARD3 OX FFAT) cells, labelled with 5 µM lyso-pacSph and chased after probe activation for 30 min. B| Quantification of lyso-pacSph fate after 30 min shown as Cer, C| Sph, D| SM, and E| PC. Error bars show the standard error of the mean and Welch two- sample *t*-tests were performed between ctrl and STARD3 OX WT or STARD3 OX FFAT cells (n.s. *p*-value ≥ 0.05; * *p*-value < 0.05; ** *p*-value < 0.01, *** *p*-value < 0.001).

To investigate whether FFAT induced lysosome-ER contact impairment impacts lysosomal Sph export, I applied the established lyso-pacSph TLC-based assay with 30 min

chase (Fig. 2.9a). The quantification of all single sphingolipid species revealed less turnover of lyso-pacSph into Cer (Fig. 2.9b). Sph (Fig. 2.9c) and SM (Fig. 2.9d) levels did not change in the mutant compared to control cells. Interestingly, PC levels were dramatically increased when lysosome-ER contacts are impaired (Fig. 2.9e). This indicates an activation of the sphingolipid degradation pathway when lysosome-ER contacts are defective. The details of sphingolipid breakdown have not been completely understood so far. However, it is known that lysosomal recruitment of sphingosine kinase 1 (SphK1) is needed to phosphorylate Sph to S1P[203]. S1PL can then irreversibly cleave the Sph backbone at the ER[79], and parts of these backbones are recycled and incorporated into phospholipids such as PC[204,205].

Lysosomes have been reported to localize to different subcellular regions dependent on cellular nutrition state or stress[61]. Two spatially distinct subsets of lysosomes have been characterized: on the one hand, an immobile pool of lysosomes that localize to the perinuclear region close to the microtubule-organizing center, and on the other hand, a highly dynamic subset of lysosomes that localizes in the cellular periphery[44]. These different positions reflect distinct lysosomal characteristics and tasks. For example, peripheral lysosomes contribute to plasma membrane repair[206], while perinuclear lysosomes are associated with the generation of autolysosomes, indicating the activation of macromolecular digestion pathways[207].

To examine if the sphingolipid breakdown activation in STARD3 FFAT mutant cells is connected to a shift in lysosomal positioning towards the perinuclear region, the localization of functional STARD3 (STARD3 OX WT) and FFAT mutant (STARD3 OX FFAT) positive lysosomes was visualized by immunofluorescence microscopy using a specific FLAG antibody. An immediate difference between WT and FFAT mutant STARD3 overexpressing cells was discernible. While lysosomes containing functional STARD3 proteins were isolated from each other and distributed throughout the cells ranging from the perinuclear to the peripheral region, lysosomes containing FFAT mutant STARD3 formed clusters that accumulate at the perinuclear region (Fig. 2.10a). Additionally, live-

cell microscopy confirmed highly dynamic lysosomal movement in functional STARD3 overexpressing cells but immobile and clustered lysosomes when expressing the FFAT mutant (data shown at DOI 10.17632/768hbxwt9j.1)[208].

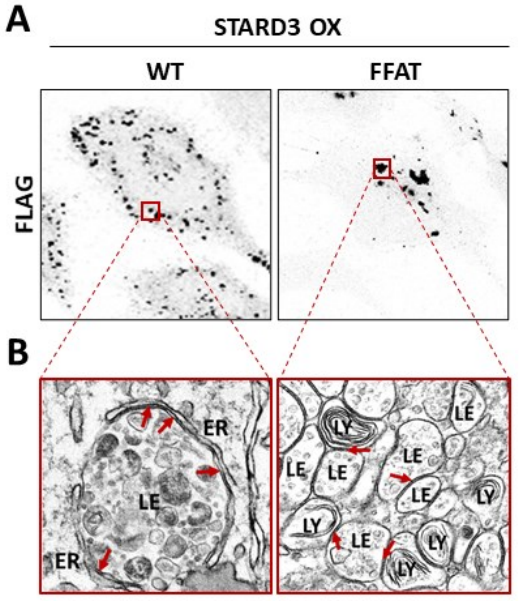

Figure 2.10: Microscopy of functional STARD3 and FFAT mutant STARD3 expressing cells. A| Visualization of cells overexpressing either functional STARD3 (STARD3 OX WT) or FFAT mutant STARD3 (STARD3 OX FFAT) by immunofluorescence microscopy using a FLAG antibody. B| Electron microscopy of lysosomes from WT or FFAT mutant STARD3 expressing cells prepared and imaged by Emily Eden (UCL, Oxford). Red arrows illustrate organelle contact sites.

To obtain a better resolution of lysosomal positioning with respect to membrane contact site formation, functional STARD3 and FFAT mutant expressing cells were examined by electron microscopy. I provided Emily Eden (UCL, Oxford) with fixed cells, and she visualized lysosomal contacts in both cell lines. Interestingly, she found extended lysosome-ER contacts in functional STARD3 overexpressing cells. This phenomenon has previously been reported to occur in STARD3 overexpression studies due to the unnatural enrichment of STARD3 proteins that are able to contact the VAPs at the ER surface[12]. However, FFAT motif mutation in STARD3 overexpression conditions led to

endo-/lysosomal tethering (Fig. 2.10b). This clustering at the perinuclear region was in accordance with the activation of the sphingolipid degradation pathway which most likely occurs in the immobile subset of lysosomes in this region, that is specialized for fusing with autophagosomes for starting macromolecular digestion[207]. However, the endo-/lysosomal tethering phenotype has not been described for STARD3 mutants so far. It could also derive from the artificially altered FFAT sequence, where potentially the Ala-rich region induces unnatural protein-protein interactions and thereby facilitates lysosomal tethering events.

In summary, mutating the FFAT motif of STARD3 resulted in a reduced STARD3 Sph-binding efficiency, the activation of the sphingolipid degradation pathway, and lysosomal tethering at the perinuclear region. Combining these outcomes, it is tempting to speculate that STARD3 does not only function as a lysosomal Sph exporter but that it could also serve as a regulator for cellular sphingolipid fate. This potential STARD3-mediated switch could shift from inducing Sph transfer towards the ER for the biosynthesis of higher sphingolipids, when lysosome-ER contacts are functional, to activation of the sphingolipid degradation pathway, when lysosome-ER contacts are impaired, and a toxic amount of Sph is stored back in lysosomes. However, this hypothesis needs further proof since the impairment of lysosome-ER contacts is artificially induced by an FFAT mutant that does not exist under physiological conditions. It has been reported that FFAT motif phosphorylation, in particular pS203, pS209, and pS213 residues, controls lysosome-ER tethering events[134]. Accordingly, to overcome potential unnatural protein-protein interactions resulting from Ala-rich regions in FFAT mutant cells used in this study, single mutations in S203, S209, and S213 preventing their phosphorylation would be an interesting tool to investigate the observed phenotype.

2.2.3 Inhibition of the sphingolipid biosynthetic pathway by FB1 leads to activation of the sphingolipid degradation pathway

To further investigate whether lysosomal Sph storage activates the sphingolipid degradation pathway, cellular sphingolipid biosynthesis was obstructed by FB1. As introduced in chapter 2.1.2, FB1 is a potent CerS inhibitor that increases cellular Sph levels in SGPL1 knock-out cells (Fig. 2.3b). To investigate the impact of FB1 on the activation of the sphingolipid degradation pathway, I treated HeLa 11ht control and STARD3 overexpressing cells with 50 µM FB1 overnight and analyzed lyso-pacSph fate by TLC after 30 min of chase (Fig. 2.11a).

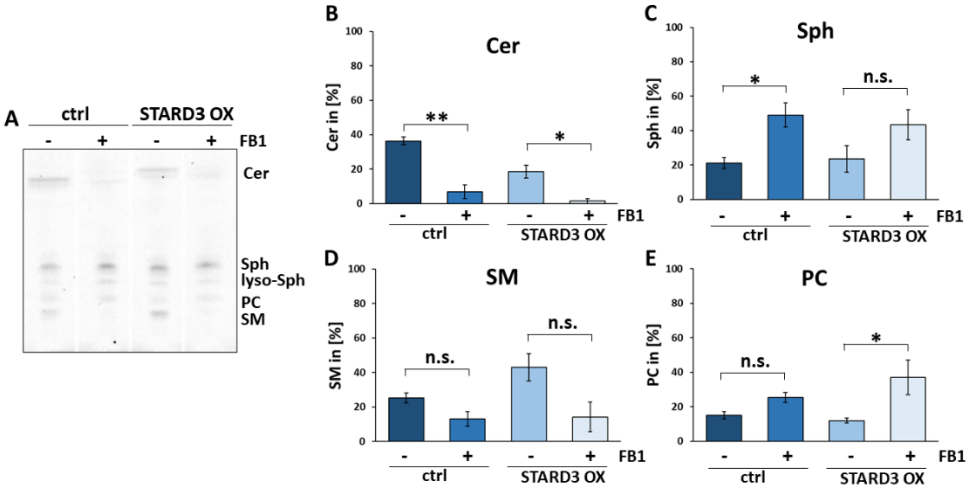

Figure 2.11: Sphingolipid metabolism in FB1 treated cells. A| TLC of HeLa 11ht WT (ctrl) and stably overexpressing functional STARD3 (STARD3 OX), treated with 50 µM FB1 overnight, labelled with 5 µM lyso-pacSph and chased after probe activation for 30 min. B| Quantification of lyso-pacSph fate after 30 min shown as Cer, C| Sph, D| SM, and E| PC. Error bars show the standard error of the mean and Welch two-sample *t*-tests were performed between ctrl and STARD3 OX WT or STARD3 OX FFAT cells (n.s. *p*-value ≥ 0.05; * *p*-value < 0.05; ** *p*-value < 0.01, *** *p*-value < 0.001).

The analysis revealed a significant decrease in Cer (Fig. 2.11b) and SM (Fig. 2.11d) levels in both control and STARD3 overexpression conditions when treated with FB1,

confirming ceramidase synthase inhibition. As already seen in SGPL1 knock-out cells (Fig. 2.3b and c), Sph levels were higher upon FB1 treatment in WT cells either with or without STARD3 overexpression (Fig. 2.11c). Interestingly, PC levels severely increased significantly in FB1 treated STARD3 overexpressing cells but only slightly in control cells (Fig. 2.11e). This implies a STARD3-dependent activation of the degradation pathway when lysosomal Sph cannot be incorporated into the biosynthesis of higher sphingolipids. This supports the hypothesis of STARD3 as a molecular switch, either activating sphingolipid biosynthesis or degradation.

Next, I investigated whether inhibition of sphingolipid biosynthesis correlates with endo-/lysosomal tethering events as observed in FFAT mutant expressing cells. To this end, STARD3 overexpressing cells were treated with 50 µM FB1 overnight, fixed, and overexpressed STARD3 was visualized by immunofluorescence staining using a specific FLAG-antibody. The microscopy images did not support this hypothesis by revealing widely distributed lysosomes from the perinuclear region to the cellular periphery without lysosomal clustering in FB1 treated cells (Fig. 2.12). As such, the increased incorporation into PC as seen from TLC under FB1 inhibition conditions is not accompanied by perinuclear clustering as observed in the FFAT mutant.

In summary, FB1 experiments confirmed a STARD3-dependent activation of the sphingolipid degradation pathway when Sph cannot enter the biosynthetic pathway. It is tempting to speculate that STARD3 thereby prevents lysosomal accumulation of Sph, which would lead to cytotoxicity. However, activation of the degradation pathway does not necessarily associate with lysosomal clustering in the perinuclear region.

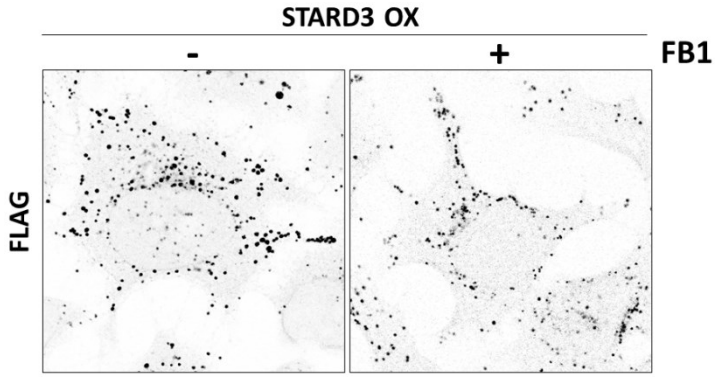

Figure 2.12: Immunofluorescence microscopy of STARD3 overexpressing cells treated with FB1. Visualization of cells overexpressing STARD3, treated with or without 50 µM FB1 overnight. STARD3-positive structures were visualized using a specific FLAG antibody.

Sph degradation starts with its phosphorylation at the C1-hydroxy group, which has been shown to be facilitated by SphKs[79]. To investigate whether Sph is phosphorylated prior to sphingolipid degradation in FFAT mutant and FB1 treated cells, SphK1 levels were analyzed by western blot (Fig. 2.13a).

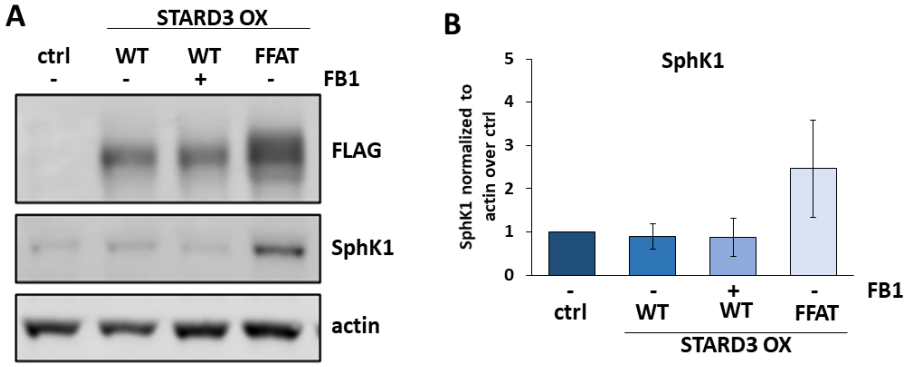

Figure 2.13: Western blot of SphK1 in FFAT mutant and FB1 treated cells. A| STARD3 (FLAG) and SphK1 expression were analyzed in control (ctrl), STARD3 overexpressing (STARD3 OX), FB1 treated STARD3 OX, and FFAT mutant cells. B| Quantification of SphK1 levels in three independent western blots by normalizing SphK1 mean intensity to actin and comparing to control cells. Error bars show the standard error of the mean.

Interestingly, only FFAT mutant cells showed 2.5-fold enriched levels of SphK1 compared to control cells (Fig. 2.13b). This enrichment of SphK1 levels in FFAT mutant expressing cell indicates SphK1-mediated phosphorylation of Sph to S1P prior to degradation. Moreover, the FFAT mutant showed an elevated STARD3 expression compared to functional STARD3 expressing cells, even if the mRNA levels analyzed by qPCR were equal. Notably, FB1-treated cells did not show any increase in SphK1 levels, even if TLC analysis already confirmed activation of the sphingolipid degradation pathway. This suggests that increased protein levels are not always accompanied by increased catalytic activity. However, SphK1 activity has been reported to be reduced in NPC diseased cells, where Sph and sphingolipids accumulate in lysosomes[209]. This indicates a role for SphK1 as the major kinase to phosphorylate Sph prior to its degradation.

2.2.4 VAPA and B are essential for functional sphingolipid metabolism

As already mentioned in chapter 1.4.1, two different VAP isomers, namely VAPA and VAPB, are located in the ER membrane. They build homo- and heterodimers that interact with various proteins such as STARD3[12], ORP1L[14], or CERT[135]. In particular, the FFAT motif of these proteins binds to the MSP domain of the VAPs and thereby tethers organelle contacts[201].

For cholesterol transfer, it has already been reported that STARD3 interacts with VAPs to ensure efficient sterol transfer at lysosome-ER contact sites[210]. Since STARD3-mediated Sph transfer has not been studied before, it is still unknown whether STARD3-VAP interaction is also a prerequisite for Sph transfer towards the ER. To further investigate this, I generated HeLa 11ht VAPA, VAPB, and VAPA/B knock-out cells (Fig. 2.14a) overexpressing functional STARD3 (STARD3 OX) and analyzed lysosomal Sph export using lyso-pacSph probe in a TLC-based 30 min chase assay (Fig.2.14b).

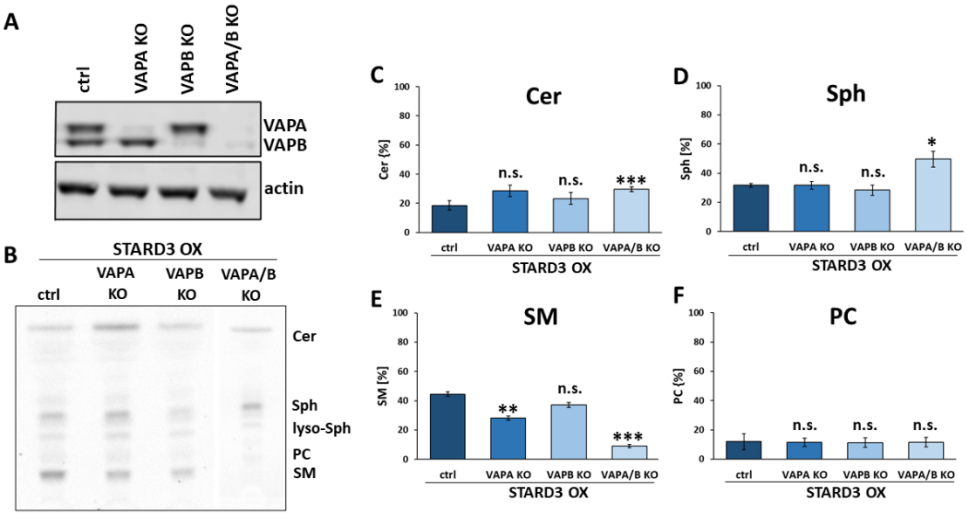

Figure 2.14: Protein and lipid analysis of VAPA, VAPB, and VAPA/B knock-out cells. A| Western blot of HeLa 11ht WT (ctrl), VAPA, VAPB, and VAPA/B knock-out cells for validating VAPA and VAPB protein levels. B| TLC of WT (ctrl), VAPA, VAPB, and VAPA/B knock-out cells stably overexpressing STARD3 (STARD3 OX). Cells were labelled with 5 µM lyso-pacSph and chased after probe activation for 30 min. C| Quantification of lyso-pacSph fate after 30 min shown as Cer, D| Sph, E| SM, and F| PC. Error bars show the standard error of the mean and Welch two-sample *t*-tests were performed between ctrl and STARD3 OX WT or STARD3 OX FFAT cells (n.s. p-value ≥ 0.05; * p-value < 0.05; ** p-value < 0.01, *** p-value < 0.001).

The analysis showed only minor changes in lipid levels in VAPA or VAPB single knock-outs compared to control cells overexpressing STARD3 (ctrl). Only SM levels were significantly decreased in VAPA knock-out cells, suggesting a role of VAPA in tethering STARD3 (Fig. 2.14e). Interestingly, VAPA/B double knock-out cells revealed a significant increase in both Cer (Fig. 2.14c) and Sph (Fig. 2.14d), accompanied by a dramatic decrease in SM levels (Fig. 2.14e). Moreover, PC levels stayed constant in all three cell lines (Fig.14f). Thereby, the VAPA/B knock-out cells displayed an impaired sphingolipid transfer towards the Golgi, where SM is synthesized, but an efficient Sph export out of the lysosome, which is manifested by the increase in Cer levels. The amount of lyso-pacSph that is not incorporated into SM is stored as Sph, most likely inside the lysosome. Surprisingly, none

of the Sph excess was degraded to PC, indicating that the degradation pathway is not automatically switched on when both VAPs are deficient.

To summarize, VAPA and to a greater extent VAPA/B deficient cells failed to transport Cer to the Golgi for incorporation into SM efficiently. This is not surprising since CERT, the LTP that mediates ER-Golgi sphingolipid transfer, binds to VAPs at the ER surface to tether Golgi-ER contacts. The amount of lyso-pacSph that could not enter the biosynthesis pathway for higher sphingolipids, such as SM in VAPA/B knock-out conditions, stayed as enriched Cer and Sph most likely inside the ER and lysosomes, respectively. Since VAPs are involved in many organelle contacts, it is difficult to detangle the contributions of the STARD3-VAP interaction by investigating lipid transport in VAP knock-out cells.

However, immunofluorescence microscopy of STARD3 in VAP knock-out cells revealed an unexpected phenotype. While VAPA and VAPB knock-out cells had the same peripheral distribution of STARD3-positive lysosomes as control cells, the VAPA/B double knock-out gave a phenotype similar to the FFAT mutant. There, lysosomes clustered in the perinuclear region (Fig. 2.15).

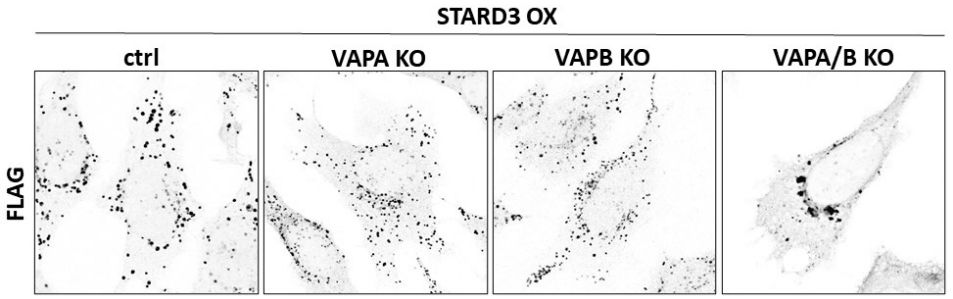

Figure 2.15: Immunofluorescence microscopy of STARD3 overexpressing control, VAPA, VAPB, and VAPA/B knock-out cells. STARD3-positive structures were visualized using a FLAG-specific antibody.

To investigate whether this VAPA/B phenotype is STARD3-dependent, I compared VAPA/B KO cells, either expressing endogenous (ctrl) or stably increased (STARD3 OX)

STARD3 levels. Lysosomes were visualized using a specific LAMP1 antibody, and to better define the perinuclear region, the Golgi was stained using a lectin dye (Fig. 2.16). Interestingly, lysosomal clustering and especially lysosomal positioning at the perinuclear region was more pronounced in STARD3 overexpressing cells compared to control cells. VAPA/B knock-out cells expressing endogenous STARD3 levels still showed some lysosomal clusters, but the number of tethered lysosomes was smaller, and their recruitment to the perinuclear region was less pronounced. This indicates a role for STARD3 in regulating intracellular lysosomal positioning. It also disproves the assumption that artificially altering the FFAT motif in STARD3 expressing cells lead to lysosomal clustering. Contrary, STARD3-dependent biological mechanisms resulting from organelle contact site impairment induce the observed phenotype.

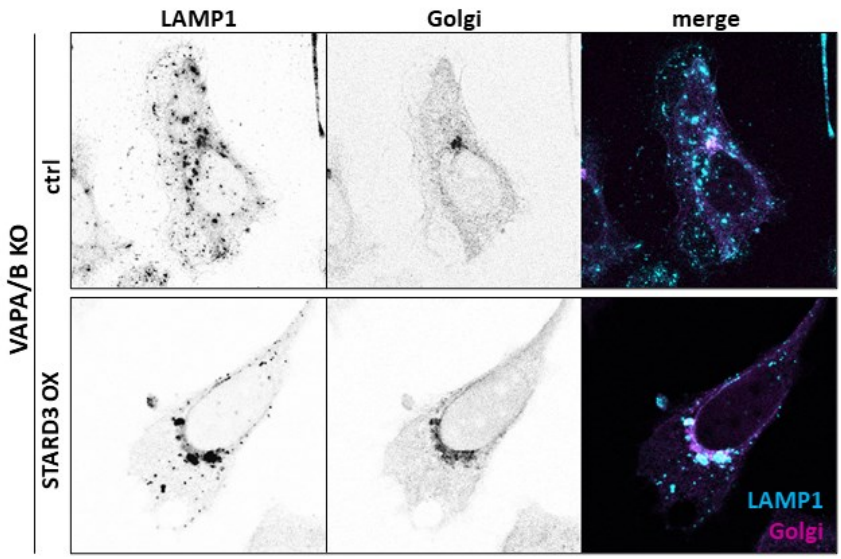

Figure 2.16: Immunofluorescence microscopy of VAPA/B knock-out cell either expressing endogenous STARD3 levels (ctrl) or stably increased STARD3 levels (STARD3 OX). Lysosomes were visualized using a specific LAMP1 antibody (cyan), and the Golgi apparatus was visualized using a specific lectin dye (magenta).

In conclusion, impairing membrane contact site formation either at the lysosome-ER (FFAT mutant) or Golgi-ER (VAPA/B KO STARD3 OX) interface leads to lysosomal clustering close to the Golgi apparatus. Lysosomal positioning is crucial for their functioning. Two already mentioned intracellular locations have been reported: peripheral lysosomes that move fast along microtubules and immobile perinuclear lysosomes that cluster around the microtubule-organizing center (MTOC)[44]. Since the MTOC and the Golgi apparatus are located in the same area of a cell, I cannot assuredly say which cellular structure is contacted by lysosomes either expressing STARD3 FFAT mutant in control cells or functional STARD3 in VAPAB knock-out cells. Lysosome-Golgi contacts have been reported to be important for regulating the mammalian target of rapamycin complex 1 (mTORC1), a master regulator for cell growth[211]. Lysosome-MTOC colocalization has been connected to the activation of autophagy by lysosomal fusion with autophagosomes for macromolecular digestion[207]. However, it has been reported that multiple lysosomes cluster around a single autophagosome before they fuse to autolysosomes[212]. Accordingly, it has been speculated that this prefusion "architecture" increases the efficiency of fusion events by providing multiple fusion sites. Multiple lysosomes could then fuse with one autophagosome for efficient cargo degradation[212]. Based on these reports, I hypothesize that lysosomes that are hindered from contacting other organelles, such as the ER or the Golgi, cluster around the MTOC to participate in autophagy processes. However, increased sphingolipid degradation (as measured by increased levels of PC) has not been shown in VAPA/B knock-out cells, assuming that lysosomal re-positioning does not necessarily associate with the activation of the sphingolipid degradation pathway. Apart from that, diminished Sph incorporation into higher sphingolipids found in FFAT mutant or FB1 treated cells leads to sphingolipid degradation. Therefore, it is tempting to speculate that sphingolipid degradation is decoupled from autophagy.

2.2.5 MOSPD2 as a potential STARD3 interacting partner

Many proteins have been found to contribute to membrane contact site formation[117]. For example, VAPs have been extensively studied for their impact on ER-mediated contact site formations[137]. Recently, another ER-resident surface protein family has been reported to mediate ER-organelle contact site formations. This protein family is named motile sperm domain-containing proteins (MOSPD) and can be grouped into three classes: MOSPD1, 2, and 3. MOSPD proteins are sometimes described as VAP homologs since they share the same, highly conserved MSP domain that interacts with many LTPs at membrane contact sites[137]. However, it has been shown that the three MOSPD proteins interact with different FFAT motif variants of their interacting proteins[136]. While VAPA, B, and MOSPD2 interact with classical FFAT motifs, MOSPD1 and 3 are selective for unconventional FFAT motifs named FFNT (two phenylalanines in a neutral tract) motifs. Besides the MSP domain, MOSPD2 has also been shown to contain a cellular retinaldehyde-binding domain (CRAL) that suggests MODPD2 as a triple functional domain protein. Therefore, this domain is named CRAL-TRIO[145]. Notably, it has been shown that MOSPD2 and STARD3 (Fig. 2.17a), but not MOSPD2 and CERT, interact with each other[136]. Therefore, MOSPD2 is a promising target to investigate STARD3-mediated lysosome-ER contact site formation without affecting ER-Golgi contacts.

To investigate whether STARD3-MOSPD2 interaction is essential for sphingolipid transfer across the lysosome-ER contact site, I generated MOSPD2 knock-out cells overexpressing STARD3. Afterwards, a master student in the lab, Yannis Stahl, investigated sphingolipid transfer using the TLC-based lyso-pacSph assay with 30 min chase.

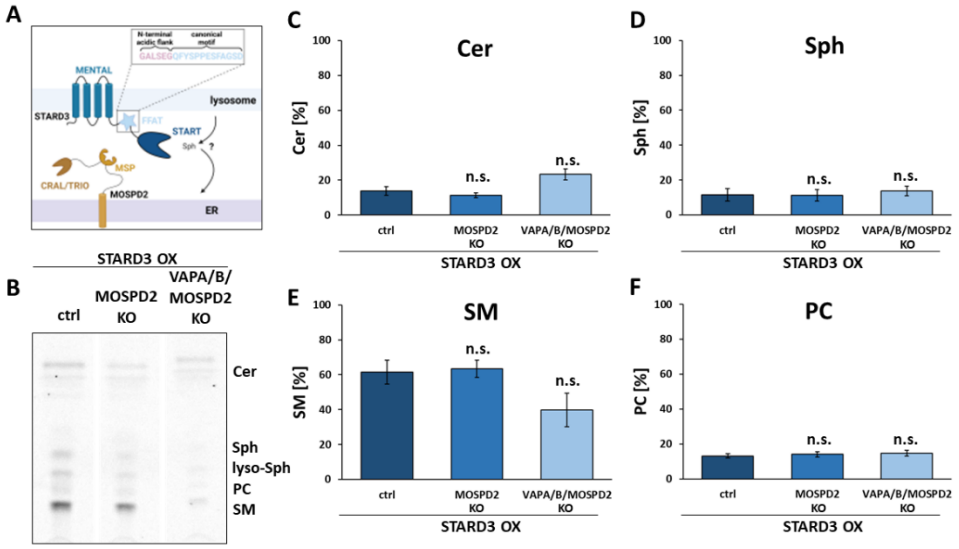

Figure 2.17: Sphingolipid metabolism in MOSPD2 and MOSPD2/VAPA/B knock-out cells. A| MOSPD2 that can bind to STARD3 to possibly transport Sph at lysosome-ER contact sites. B| TLC of WT (ctrl), MOSPD2, MOSPD2/VAPA/B knock-out cells stably overexpressing STARD3 (STARD3 OX). Cells were labelled with 5 µM lyso-pacSph and chased after probe activation for 30 min. C| Quantification of lyso-pacSph fate after 30 min shown as Cer, D| Sph, E| SM, and F| PC. Error bars show the standard error of the mean and Welch two-sample *t*-tests were performed between ctrl and MOSPD2 or MOSPD2/VAPA/B knock-out cells (n.s. *p*-value ≥ 0.05; * *p*-value < 0.05; ** *p*-value < 0.01, *** *p*-value < 0.001).

These studies did not result in any significant difference in MOSPD2 knock-out (MOSPD2 KO) cells compared to control (ctrl) cells (Fig. 2.17b). When particularly investigating Cer levels in MOSPD2 knock-out cells, a slight but not significant decrease from 14 to 11 % Cer was found (Fig. 2.17c). In general, after 30 min of chase, Cer levels were very low, so that a minor decrease might indicate a role of MOSPD2 in STARD3-mediated Sph transfer at lysosome-ER contact sites. To investigate the interplay of STARD3, MOSPD2 and VAPs, I generated triple knock-out cells containing MOSPD2 and VAPA/B deficiencies, and Yannis Stahl applied the same sphingolipid analysis approach to these cells. He found increased Cer (Fig. 2.17c) and similar PC (Fig. 2.17f) levels in MOSPD2/VAPA/B knock-out cells compared to single MOSPD2 knock-out and control cells, a trend already observed in VAPA/B knock-out cells (Fig. 2.14c and f). SM levels in the triple knock-out dramatically

decreased, while Sph levels stayed the same as in control and MOSPD2 knock-out cells and SM levels dramatically decreased (Fig. 2.17d and e). Interestingly, this finding did not match with findings on VAPA/B knock-out cell experiments, where Sph levels increased to 50 % in VAPA/B knock-out cells (Fig. 2.14d). Moreover, also SM levels showed differences in the VAPA/B compared to VAPA/B/MOSPD2 knock-out cells. Even if the trend of SM decrease compared to control cells was the same, VAPA/B knock-out cells had only 10 % SM, while VAPA/B/MOSPD2 knock-out cells contained 40 % SM. Either the triple knock-out facilitated an unknown way to convert Sph to SM in a MOSPD2-, VAPA- and VAPB-independent manner, or, more likely, the MOSPD2/VAPA/B TLC preparations, including cell harvesting and lipid extraction, were performed not as fast as VAPA/B TLC preparations due to the fact that two different persons performed these assays. In detail, when incubating longer than 30 min, the cells have more time to transfer Sph to the ER (indicated by lower Sph levels), incorporate it into Cer (these levels stay the same since ER Cer levels are highly controlled), transport it to the Golgi and finally incorporate Cer into SM (indicated by higher SM levels).

In conclusion, MOSPD2 might play a minor role in STARD3-mediated Sph transfer across the lysosome-ER contact site, but it is not essential for this transport. MOSPD2 knock-out cells overexpressing STARD3 still favor Sph incorporation into higher sphingolipids, such as SM, and thereby activating the biosynthetic pathway. Even if all currently known STARD3 interacting ER-resident surface proteins, namely VAPA, B, and MOSPD2, were diminished, it did not result in activation of the sphingolipid degradation pathway. In conclusion, these studies on lysosome-ER interaction could not reveal one single ER protein that significantly influenced the STARD3-mediated lysosome-ER contact in order to facilitate Sph transfer. It is tempting to speculate that more ER-located proteins that bind FFAT motifs exist, which potentially interact with STARD3 to facilitate Sph transfer at lysosome-ER contact sites. Also, clearly, other transfer proteins of Sph exist.

In summary, Sph is actively transported by STARD3, most likely at lysosome-ER contact sites. Under lysosome-ER tethering conditions, lysosomal Sph export was boosted

towards the biosynthetic pathway, while when impairing lysosome-ER contacts or inhibiting Sph incorporation into higher sphingolipids such as Cer or SM, the degradative sphingolipid pathway was activated. This process occurred in a STARD3-dependent manner. Moreover, contact site impairment either between the lysosome and the ER or the ER and the Golgi led to alterations in cellular lysosomal positioning, which seemed to be independent of the activation of the degradation pathway. STARD3 has been shown to not only act at lysosome-ER contact sites but also increase lysosome-mitochondria contacts in NPC1 diseased cells[112]. These STARD3-dependent contacts have been suggested to mediate cholesterol egress towards mitochondria when proteins involved in lysosome-ER contacts, such as NPC1 or GramD1b, are deficient[112,213]. Accordingly, it is tempting to speculate that STARD3 mediates lysosome-mitochondria contacts when VAPs or MOSPD2 proteins, that are majorly involved in lysosome-ER contacts, are not available and thereby prevent Sph degradation.

In conclusion, these studies revealed novel findings on STARD3-mediated Sph transfer at lysosome-ER contact sites by challenging already known STARD3 interaction partners, such as VAPA/B and MOSPD2, to not exclusively contribute to it.

2.3 Endogenous sphingolipid analysis confirms STARD3 as a lysosomal sphingosine exporter

The application of functionalized lipids is a revolutionary tool to investigate lipid metabolism and trafficking, yet, it is still limited in some approaches. A major drawback of these modified lipids is the use of unnatural modifications that could affect their metabolism. Moreover, only the acute effect of lipid transfer can be examined, while their steady-state cellular status is neglected. Furthermore, only a limited number of (sphingo-)lipid species can be detected by TLC. Polar lipids, such as S1P, cannot be separated by TLC. Species that can indeed be detected by TLC, such as Cer, cannot be

separated into their single species that differ in saturation and chain length of the attached fatty acid. Notably, another disadvantage is that the usage of functionalized lipids always necessitates working with an excess of lipids. This could lead to a lipid transfer according to their cellular concentration gradient. Lysosomal Sph export could potentially be boosted in conditions of prior accumulation of Sph inside lysosomes by using probes, such as lyso-pacSph.

To investigate the effects of STARD3 on endogenous sphingolipid levels, lipid mass spectrometry was performed in collaboration with the lab of Sarah Spiegel (VCU, USA).

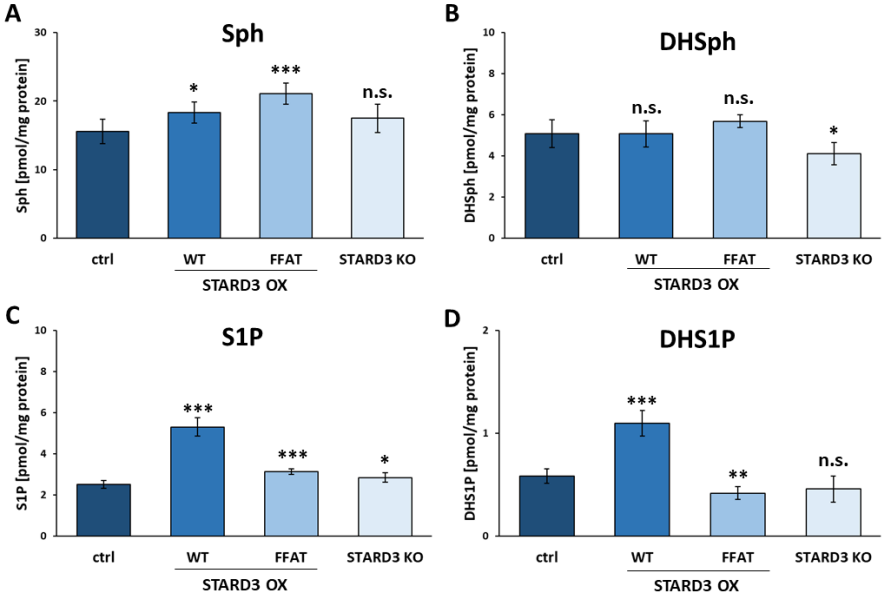

Figure 2.18: Lipid mass spectrometry of sphingoid bases. A| Amount of Sph, B| DHSph, C| S1P and D| DHS1P in control (ctrl), STARD3 overexpression (WT STARD3 OX), STARD3 FFAT mutant overexpression (FFAT STARD3 OX), and STARD3 knock-out (STARD3 KO) cells measured by lipid mass spectrometry performed in the lab of Sarah Spiegel (VCU, USA). Error bars show the standard deviation of the mean and Welch two-sample *t*-tests were performed between ctrl and WT STARD3 OX, FFAT STARD3 OX or STARD3 knock-out cells (n.s. *p*-value ≥ 0.05; * *p*-value < 0.05; ** *p*-value < 0.01, *** *p*-value < 0.001).

The levels of sphingoid bases including Sph, dihydro-Sph (DHSph), S1P, and dihydro-S1P (DHS1P) were measured in cell lines overexpressing STARD3 and the FFAT mutant, as well as STARD3 knock-out cells. Interestingly, Sph levels were found to be significantly elevated in cells overexpressing functional STARD3. This could be explained by the enlargement of lysosomes in STARD3 overexpression conditions accompanied by an increased capacity to store Sph. This Sph storage was even more pronounced in STARD3 FFAT mutant cells, indicating defective lysosomal Sph export mechanisms (Fig. 2.18a). The *de novo* pathway of sphingolipid biosynthesis, analyzed by measuring DHSph, is not affected by overexpressing STARD3. In contrast, when STARD3 is diminished (STARD3 KO), DHSph levels were decreased (Fig. 2.18b), suggesting a lysosomal sensing machinery that lowers sphingolipid biosynthesis when LTPs are defective or deficient. However, S1P (Fig. 2.18c) and DHS1P (Fig. 2.18d) were dramatically increased in STARD3 overexpressing cells, indicating Sph phosphorylation as a signal for Sph incorporation into the biosynthetic pathway. Sph phosphorylation has previously been reported to regulate Sph recycling by the action of SphK2 but not SphK1[96]. This is supported by SphK1 western blot analysis, in which SphK1 levels are not increased in STARD3 overexpressing cells (Fig. 2.13). It is tempting to speculate that the S1P increase in STARD3 overexpression conditions stems from SphK2-mediated Sph phosphorylation, while the slight S1P increase in STARD3 FFAT mutant and STARD3 knock-out cells is mediated by SphK1.

The levels of complex sphingolipids, such as Cer, were also investigated by lipid mass spectrometry in cells featuring STARD3 overexpression or deficient conditions. Surprisingly, total Cer levels and, consequently, all higher abundant Cer species, including Cer C16:0, C22:0, C24:1, and C24:0, were significantly increased in STARD3 overexpression conditions (Fig. 2.19a and b). The attachment of different fatty acids is performed by six different CerS isoforms which are all located in the ER. CerS1 is highly specific for C18 fatty acids. CerS2 is responsible for the incorporation of different chain-length fatty acids, including C20, C22, C24, and C26. CerS3 attaches only long-chain fatty acids, including C22, C24, and C26. CerS4 incorporates C18 and C20 fatty acids. CerS5 mediates the attachment of C16 fatty acids, and CerS6 introduces C14 and C16 fatty

acids[214]. Our results suggest an equal contribution of especially CerS2, CerS3, CerS5, and CerS6 for recycled Sph incorporation of recycled Sph into Cer.

Interestingly, STARD3 knock-out conditions showed slight but significantly decreased Cer levels (Fig. 2.19a). Here, mainly C16:0 and C22:0 Cer are affected. Overall, this indicates a STARD3-dependent impairment in Sph recycling in the steady-state and supports our hypothesis that STARD3 mediates the transfer of Sph from lysosomes directly to the ER.

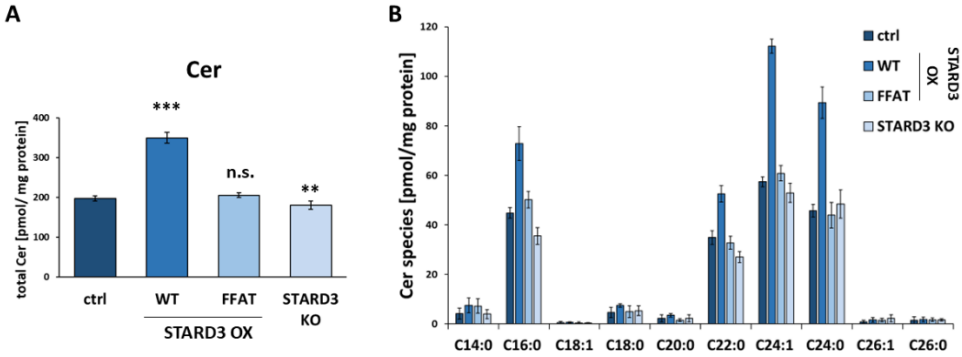

Figure 2.19: Lipid mass spectrometry of Cer. A| Total Cer levels and B| Single Cer species in control (ctrl), STARD3 overexpression (WT STARD3 OX), STARD3 FFAT mutant overexpression (FFAT STARD3 OX), and STARD3 deficient (STARD3 KO) conditions analyzed by lipid mass spectrometry performed in the lab of Sarah Spiegel (VCU, USA). Error bars show the standard deviation of the mean and Welch two-sample *t*-tests were performed between ctrl and WT STARD3 OX, FFAT STARD3 OX or STARD3 knock-out cells (n.s. p-value ≥ 0.05; * p-value < 0.05; ** p-value < 0.01, *** p-value < 0.001).

When analyzing more complex sphingolipids, such as monohexosylceramide (HexCer), a significant increase in STARD3 overexpression conditions was visible (Fig. 2.20a). Especially C16:0, C24:1, and C24:0 were affected (Fig. 2.20b). This increase in HexCer indicates an efficient ER-Golgi transport since enzymes responsible for attaching sugars on the Cer backbone are located in the Golgi. Additionally, an unexpected, slight increase of HexCer was also measured in STARD3 FFAT mutant cells, mainly resulting from an increase in HexCer C16:0. Since Cer levels are stable (Fig. 2.19) and Sph levels are increased (Fig. 2.18) in FFAT mutant conditions, this increase in HexCer does not fit to

the hypothesis of a delayed Sph recycling when lysosome-ER contact sites are impaired. However, the increase in HexCer could be an effect of other physiological consequences of FFAT mutant overexpression that might result from artificially increased lysosome-Golgi contacts that are potentially induced in FFAT mutant cells.

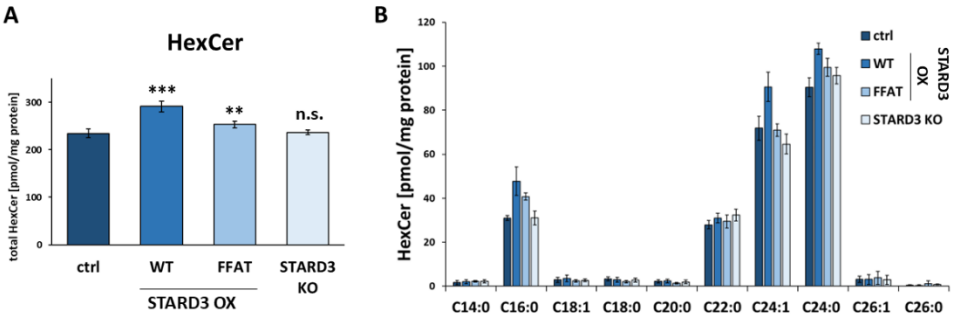

Figure 2.20: Lipid mass spectrometry of HexCer. A| Total HexCer levels and B| Single HexCer species in control (ctrl), STARD3 overexpression (WT STARD3 OX), STARD3 FFAT mutant overexpression (FFAT STARD3 OX), and STARD3 deficient (STARD3 KO) conditions analyzed by lipid mass spectrometry performed in the lab of Sarah Spiegel (VCU, USA). Error bars show the standard deviation of the mean and Welch two-sample *t*-tests were performed between ctrl and WT STARD3 OX, FFAT STARD3 OX or STARD3 knock-out cells (n.s. p-value ≥ 0.05; * p-value < 0.05; ** p-value < 0.01, *** p-value < 0.001).

Surprisingly, the levels of SM were not significantly different, neither in STARD3 overexpression nor in STARD3 deficient conditions compared to control cells (Fig. 2.21a). Only a minor decrease in C16:0 SM in FFAT mutant and a slight but significant increase in STARD3 knock-out cells could be found (Fig. 2.21b). Generally, SM is a highly abundant sphingolipid, so that STARD3-dependent minor changes in its biosynthesis are not visible when analyzing the total SM content of a cell and not only the acute transport such as lyso-pacSph experiments do.

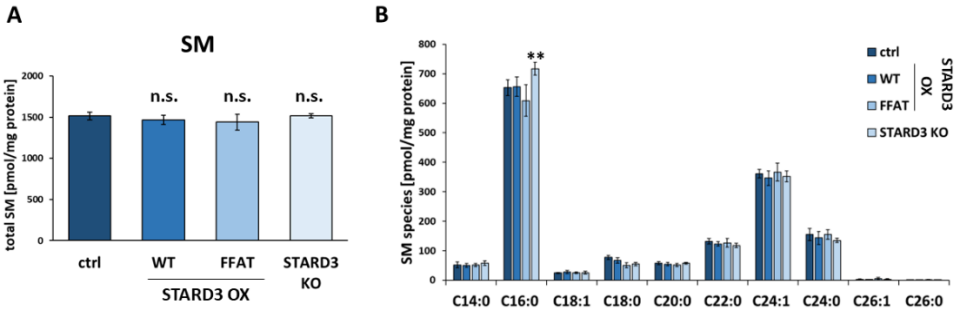

Figure 2.21: Lipid mass spectrometry of SM. A| Total SM levels and B| single SM species in control (ctrl), STARD3 overexpression (WT STARD3 OX), STARD3 FFAT mutant overexpression (FFAT STARD3 OX), and STARD3 deficient (STARD3 KO) conditions analyzed by lipid mass spectrometry performed in the lab of Sarah Spiegel (VCU, USA). Error bars show the standard deviation of the mean and Welch two-sample *t*-tests were performed between ctrl and WT STARD3 OX, FFAT STARD3 OX or STARD3 knock-out cells (n.s. p-value ≥ 0.05; * p-value < 0.05; ** p-value < 0.01, *** p-value < 0.001).

In summary, measuring endogenous sphingolipids in STARD3 overexpression and deficient conditions gives a different view on cellular lipid distribution compared to investigating the acute effect of sphingolipid transfer. While the lyso-pacSph approach showed a STARD3-dependent increase of SM, the analysis of endogenous SM did not show any STARD3-dependent change. This is explainable since SM is highly abundant, and a minor STARD3-dependent SM shift towards the biosynthetic pathway would be of no detectable consequence in total SM levels. However, glycosphingolipids showed higher total levels in STARD3 overexpression conditions, potentially due to the fact that these lipids are not as abundant as SM. Since glycosphingolipids (or HexCer) were not detectable in lyso-pacSph TLC-based assays, no direct comparison between out-of-equilibrium and steady-state results could be made. However, lipid mass spectrometry revealed that Sph entering the recycling pathway is not only incorporated into SM but also into HexCer and, therefore, potentially also into glycosphingolipids.

Additionally, our hypothesis of direct STARD3-mediated Sph transport at lysosome-ER contact sites was supported by significantly increased endogenous Cer levels in STARD3

overexpression conditions as well as by slightly decreased Cer levels in STARD3 deficient conditions. The fact that Cer increase in overexpression and Cer decrease in knock-out conditions are not at the same magnitude is due to highly elevated STARD3 levels in overexpression conditions. In contrast, its knock-out has only minor effects due to low cellular STARD3 levels. Moreover, the entry of Sph into the recycling pathway seems to be regulated by Sph phosphorylation, as shown by the accompanying increase in S1P levels. These results are consistent with previous findings in which phosphorylation of Sph mediated by SphK2 was shown to play an important role in recycling of Sph in mammalian cells[96]. Furthermore, it could be corroborated that functional lysosome-ER contacts are needed for efficient Sph transfer. This has been shown by an increase in Sph levels in STARD3 FFAT mutant overexpressing cells, most likely indicating lysosomal storage of Sph, supporting that STARD3-dependent Sph transfer necessarily takes place at lysosome-ER contact sites, as its the case for STARD3-dependent cholesterol traffic.

In conclusion, lipid mass spectrometry is a valuable method for investigating the steady-state status of cellular lipids. Here, we show that STARD3 overexpression or knock-out impacts cellular sphingolipid biosynthesis and degradation, supporting the hypothesis that STARD3 activity directly affects sphingolipid metabolism, likely through its transport function.

2.4 The START domain is involved in Sph transfer

The steroidogenic acute regulatory protein-related (StAR) lipid transfer (START) domain is a highly conserved lipid-binding domain found in many proteins[215]. In different proteins, the domain has been reported to bind different lipid species, including cholesterol, PC, and Cer[166]. The START domain of STARD3 is attached to the C-terminus of the protein and faces towards the cytoplasm[169]. In 2000, the protein structure of the STARD3 START domain was solved by X-ray crystallography (Fig. 2.22a), and it has been shown that the START three-dimensional organization builds a 26 × 12 × 11 Å

hydrophobic cavity that is large enough to bind one cholesterol molecule[171]. Indeed, the STARD3 START domain-mediated cholesterol transfer has been reconstituted *in vitro*[196]. However, if the STARD3 START domain also mediates Sph transfer is still unclear.

2.4.1 The known cholesterol-binding mutants ΔSTART and MR/ND are essential for Sph transfer

STARD3-mediated cholesterol transfer has been extensively studied in the past years and the START domain has been shown to play an important role in this transfer. Cell biology studies have reported a truncated STARD3, deficient of the entire START domain, and a START mutant with point mutations in M307R/N311D (Fig. 2.22b) to prevent STARD3-mediated cholesterol transfer towards the lysosome[196]. In this chapter, I will investigate whether these STARD3 mutants impact subcellular sphingolipid transfer.

To this end, I generated HeLa 11ht cells stably expressing either a truncated STARD3 deficient of the entire START domain (ΔSTART) or a STARD3 mutant with point mutations in M307R/N311D (MR/ND). Expression levels were analyzed by qPCR and a similar expression compared to the WT STARD3 was observed (Fig. 2.22c). Firstly, I investigated the Sph-binding ability of both constructs. For that reason, I labelled the cells with 2 µM pacSph for 1 h continuously, crosslinked pacSph to proteins in close proximity in cells, and clicked a biotin-azide to lipid-protein complexes in lysate. Afterwards a streptavidin immunoprecipitation was performed, and STARD3-sphingolipid binding was analyzed by western blot using a specific FLAG-antibody.

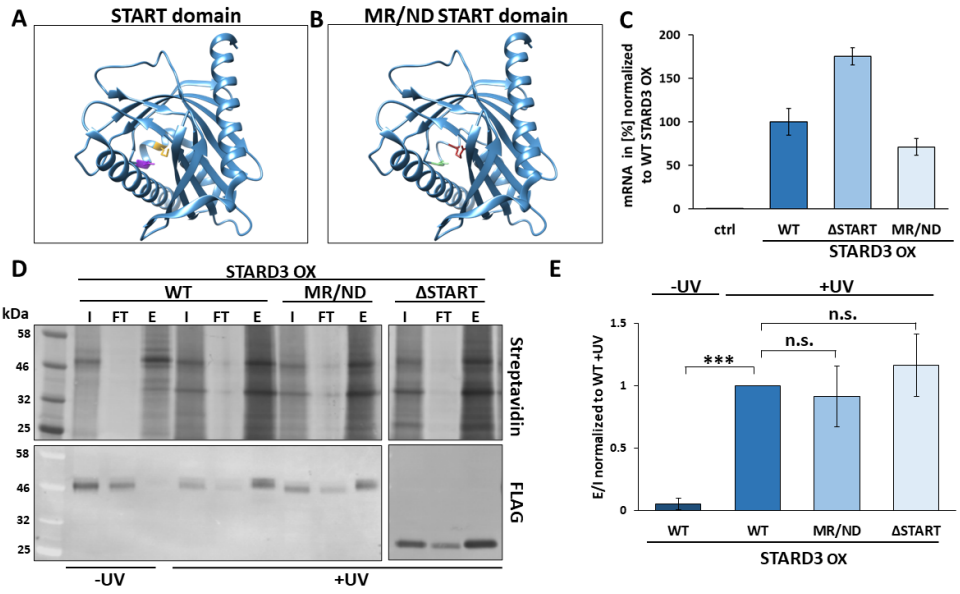

Figure 2.22: Immunoprecipitation of pacSph and START mutants. A| Protein structure of the STARD3 START domain (PDB 5I9J) with highlighted M307 (goldenrod) and N311 (purple). B| Protein structure of STARD3 MR/ND START mutant, manually created in Coot[216] and modeled in chimera[217] with highlighted R307 (dark red) and D311 (light green). C| qPCR of ctrl, STARD3 OX, and STARD3 ΔSTART and MR/ND mutant OX expressing cells. mRNA levels are normalized to STARD3 OX, and error bars show the standard deviation of the mean. D| Streptavidin-based immunoprecipitation of pacSph-STARD3 complexes in HeLa 11ht WT cells overexpressing functional STARD3 (WT), MR/ND mutant STARD3 (MR/ND) or ΔSTART STARD3. E| Quantification of three independent immunoprecipitation experiments showing eluates (E) over inputs (I) normalized to functional STARD3 (WT) +UV sample. Error bars show the standard error of the mean and Welch two-sample *t*-tests were performed between WT STARD3 + UV and WT STARD3 -UV, MR/ND +UV or ΔSTART +UV (n.s. *p*-value ≥ 0.05; * *p*-value < 0.05; ** *p*-value < 0.01, *** *p*-value < 0.001).

The western blot analysis showed a 20 kDa shift from full-length STARD3 to the ΔSTART mutant, confirming the truncation of the START domain. It further revealed that the MR/ND as well as the ΔSTART mutant bind to pacSph shown by the FLAG signal in the respective eluates (E) (Fig. 2.22d). The eluates (E) were quantified over their respective inputs (I), and the ratio indicates no significant difference between WT STARD3 +UV and MR/ND or ΔSTART STARD3 (Fig. 2.22e). Since most of the cytoplasmic domain is truncated in ΔSTART STARD3, it is most likely that pacSph crosslinked to the MENTAL

domain in the lysosomal lumen. This phenomenon has previously been shown to also happen with cholesterol. Photo-cholesterol binding assays revealed the STARD3 MENTAL domain as a cholesterol-binding domain. This binding is speculated to maintain cholesterol levels at the limiting membranes of lysosomes prior to its transfer to other organelles[152]. The binding of Sph at the MENTAL domain at the lysosomal limiting membrane could occur for the same reason, to maintain Sph levels at the limiting membrane of lysosomes prior to its lysosomal exit. However, this does not necessarily imply a MENTAL domain-mediated Sph transfer.

To investigate the Sph transfer ability of MR/ND as well as ΔSTART STARD3 mutants, cells were labelled with 2 µM lyso-pacSph, and activated by uncaging at the next day. After 30 min chase, lipids were extracted, and sphingolipid metabolites were analyzed by TLC.

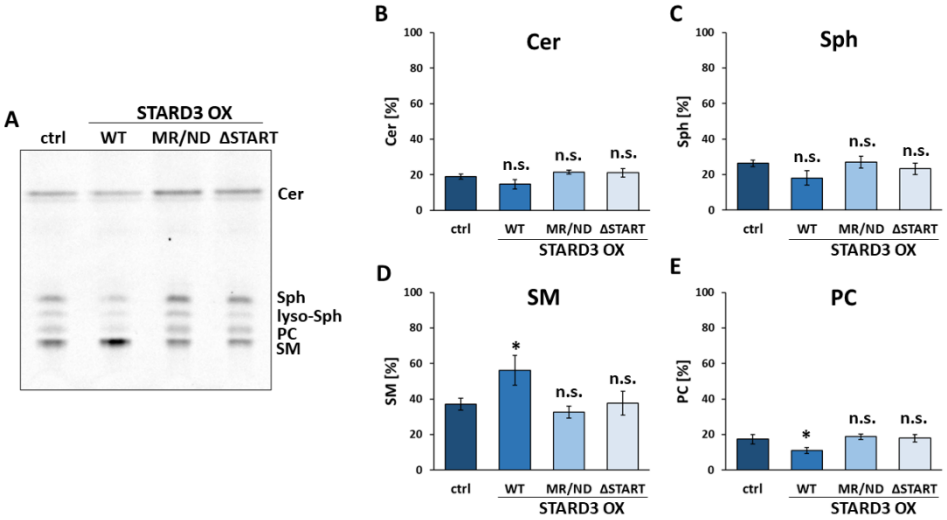

Figure 2.23: Sphingolipid metabolism in STARD3 ΔSTART and MR/ND mutant overexpressing cells. A| TLC of HeLa 11ht WT (ctrl), STARD3 overexpressing (WT STARD3 OX), MR/ND, and ΔSTART STARD3 mutant cells, labelled with 5 µM lyso-pacSph and chased after probe activation for 30 min. B| Quantification of lyso-pacSph fate after 30 min shown as Cer, C| Sph, D| SM, and E| PC. Error bars show the standard error of the mean and Welch two-sample *t*-tests were performed between ctrl and STARD3 OX WT, MR/ND or ΔSTART cells (n.s. p-value ≥ 0.05; * p-value < 0.05; ** p-value < 0.01, *** p-value < 0.001).

The visualizable lipid species pattern on TLC plates already exhibited similar band intensities between control and MR/ND or ΔSTART STARD3 mutants. At the same time, WT STARD3 overexpressing cells show strong labelling of SM (Fig. 2.23a). When quantifying the single lipid species, this assumption was confirmed. All detectable lipid species in MR/ND and ΔSTART STARD3 cells, including Cer (Fig. 2.23b), Sph (Fig. 2.23c), SM (Fig. 2.23d), and PC (Fig. 2.23e), did not show significant differences compared to control cells. However, functional STARD3 overexpressing cells (WT) still showed significantly enriched SM and decreased PC levels. This indicates a STARD3-mediated Sph transport defect in both, START domain deficient conditions and when the hydrophobic cavity is altered by mutating M307 and N311 residues.

In conclusion, STARD3-dependent Sph transfer seemed similar to STARD3-mediated cholesterol transport. Cholesterol has been shown to interact with the STARD3 MENTAL domain for a potential provision of cholesterol molecules at the lysosomal membrane prior to its transfer to target organelles, such as the ER[152]. Since Sph crosslinked to STARD3 proteins deficient of the entire START domain, it is most likely that it also interacts with the MENTAL domain. This mechanism might also maintain Sph levels at the lysosomal limiting membrane to either follow the sphingolipid degradation pathway or the sphingolipid biosynthetic pathway. However, Sph transport was impaired when STARD3 did not comprise a complete START domain, indicating an important role of the START domain for Sph transfer. Moreover, the START residues M307 and N311, located deeply inside the hydrophobic cavity, have been shown to be essential for STARD3-dependent cholesterol transfer. In particular, mutating them by exchanging methionine 307 to arginine (M307R) and asparagine 311 to aspartate (N311D) results in a dramatic conformational change leading to an impaired cholesterol transfer[210]. However, M307 and N311 seemed to be essential for Sph transfer, too. It is tempting to speculate that Sph enters the hydrophobic tunnel of the START domain orientated with either its head or chain facing towards the cavity. Potentially, it interacts with residues buried inside the pocket, such as M307 and N311, to get into a stabilized position that allows its transfer across the polar cytoplasmic gap at membrane contact sites.

In summary, the START domain of STARD3 is essential for Sph transfer at lysosome-ER contact sites. Similar to cholesterol positioning inside the START domain, Sph might enter the hydrophobic tunnel in a favored direction to get stabilized by specific amino acids inside the pocket. If other residues of the START domain also facilitate Sph positioning inside its cavity needs further investigations.

2.4.2 Molecular dynamic simulations revealed R351 as a potential Sph interacting residue

Previously, the START domain was suggested as the most likely Sph interacting domain of STARD3. To further investigate whether other START residues are involved in Sph-binding, a PostDoc in the lab, Denisa Jamecna (Höglinger group, BZH, DE), purified the STARD3 START domain and investigated Sph binding in collaboration with Juri Rappsilber (University of Edinburgh, UK) by crosslinking mass spectrometry. They identified the peptide containing the serine 343 as a potential Sph interacting partner. S343 is located at the opening of the hydrophobic cavity of the START domain. To confirm this serine as Sph interacting residue, we collaborated with the group of Walter Nickel (BZH, DE). A PostDoc, Fabio Lolicato, used molecular dynamic simulations to identify potential Sph-binding residues inside the START domain. He simulated how Sph could potentially enter the hydrophobic cavity of START in an aqueous environment. He found two possible orientations in which Sph might enter the pocket. On the one hand, Sph could enter the cavity with its “head out”, meaning the acyl chain facing towards the pocket (Fig. 2.24a). On the other hand, Sph could invade the pocket in the opposite orientation with its “head in”, implying its polar amino head group facing towards the cavity (Fig. 2.24b). Further simulations suggested the “head out” orientation as the favored position of Sph entry into the START pocket (data shown at DOI 10.17632/768hbxwt9j.1)[208].

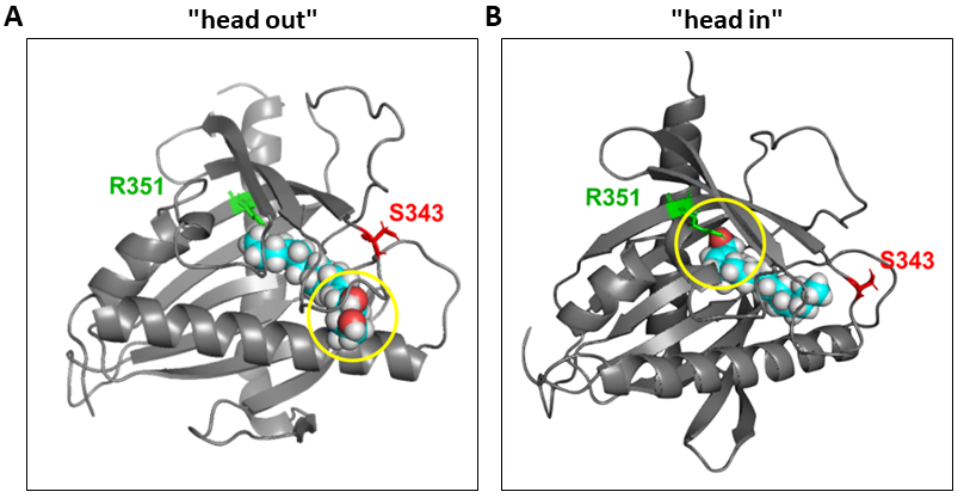

Figure 2.24: Molecular dynamic simulations of STARD3 START domain and Sph. A| Modelling of Sph inside the START hydrophobic cavity with "head out" or B| "head in" orientation. Potential interacting residues such as R351 (green) and S343 (red) are highlighted. This figure was created by Fabio Lolicato and Denisa Jamecna.

Moreover, Fabio Lolicato suggested the deeply buried arginine 351 (R351) residue as a potential Sph interacting amino acid, while he could not find S343 to interact with Sph after it fully entered the pocket.

To follow up on his suggestion, I generated STARD3 R351 mutants by replacing the arginine with either phenylalanine (Phe) or leucine (Leu) and created cells stably overexpressing them. On the one hand, Phe comprises a bulky conjugated ring that potentially faces towards to cavity. This blockade might prevent Sph from fully entering the cavity. On the other hand, Leu is shorter and not as polar as Arg. Therefore, Sph might not reach Leu, which could also prevent the stabilization of Sph inside the pocket (Fig. 2.25a).

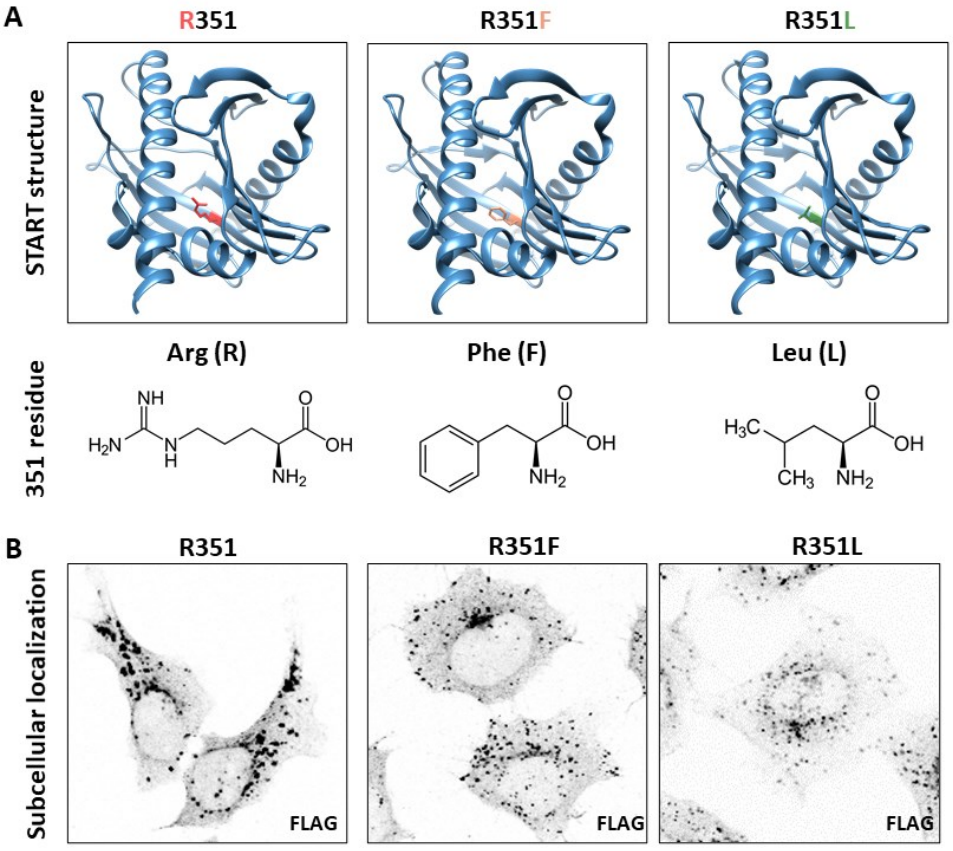

Figure 2.25: Structure and subcellular localization of START 351 mutants. A| Protein structure of the STARD3 START domain (PDB 5I9J) and START R351 mutants, manually mutated in Coot[216] and modeled in chimera[217] with highlighted R351 (red), F351 (coral), and L351 (dark green). The respective amino acid is shown below. B| Immunofluorescence microscopy of cells stably overexpressing an N-terminal FLAG-tagged STARD3 WT (R351), STARD3 R351F, or R351L mutant induced with 100 ng/mL doxycycline and visualized using a specific FLAG antibody.

The subcellular localization was investigated by immunofluorescence microscopy (Fig. 2.25b), and expression levels were analyzed by qPCR (2.26a), which confirmed lysosomal localization and comparable STARD3 expression levels in WT, R351F, and R351L cell lines, respectively.

The Sph transferability of STARD3 R351 mutants was investigated by using the lyso-pacSph TLC-based assay with 30 min chase. Therefore, the cells were labelled with 5 µM lyso-pacSph, which was activated by uncaging after the lysosomal pre-localization of the probe. Lipids were extracted, and single lipid species were analyzed by TLC (Fig. 2.26b).

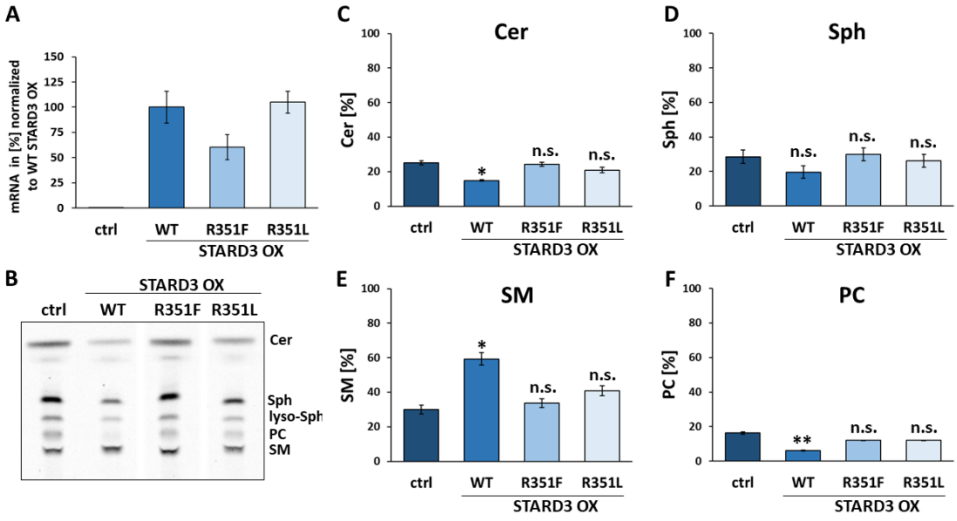

Figure 2.26: Sphingolipid metabolism in STARD3 R351F and R351L mutant overexpressing cells. A| qPCR of ctrl, STARD3 OX and STARD3 R351F and R351L mutant OX expressing cells. mRNA levels are normalized to STARD3 OX, and error bars show the standard deviation of the mean. B| TLC of HeLa 11ht WT (ctrl), STARD3 overexpressing (WT STARD3 OX), R351F STARD3, and R351L STARD3 mutant cells, labelled with 5 µM lyso-pacSph and chased after probe activation for 30 min. C| Quantification of lyso-pacSph fate after 30 min shown as Cer, D| Sph, E| SM, and F| PC. Error bars show the standard error of the mean and Welch two-sample *t*-tests were performed between ctrl and STARD3 OX WT, R351F or R351L cells (n.s. *p*-value ≥ 0.05; * *p*-value < 0.05; ** *p*-value < 0.01, *** *p*-value < 0.001).

As expected, SM levels increased (Fig. 2.26e), while PC levels decreased (Fig. 2.26f) in STARD3 overexpression (WT) conditions compared to control cells. Interestingly, STARD3 R351F and R351L did not show enhanced incorporation of lyso-pacSph into the biosynthetic pathway as observed in WT STARD3 (Fig. 2.26e). Moreover, their PC levels were not significantly decreased. Given that neither the boost in sphingolipid biosynthesis (as measured by SM) nor the decreased degradation (as measured by PC)

was observed in the mutants, mutations of R351 residue were suggested to abolish the Sph transfer activity of STARD3. A slight but not significant increase in SM levels in cells overexpressing STARD R351L suggests a residual functionality of this mutant, while R351F expressing cells lose the ability of enhanced Sph transfer.

In conclusion, the START residue R351 is essential for STARD3-mediated Sph transfer. The size and the charge of the alternative amino acid, in this case Phe and Leu, influenced Sph binding. *In vitro* studies using the purified START domain of STARD3 performed by Denisa Jamecna (Höglinger group, BZH, DE) revealed that R351 mutants give an unexpected higher crosslinking ability with Sph compared to not mutated START domains (data not shown). We believe that the positive charge of R351 repels Sph in the pocket, so it can be unloaded after a successful transfer. However, when mutated to non-charged amino acids, such as Phe or Leu, Sph potentially gets stuck, thereby preventing an efficient lipid transfer at lysosome-ER contact sites. Notably, modeling studies have reported a role for R351 to potentially interact with the 3-hydroxyl group of cholesterol as well[171]. However, this has not been followed up yet.

The START domain has been shown to not only transport cholesterol but also Sph. Moreover, I found START residues which have been shown to be essential for cholesterol transfer, to be also important for stabilizing Sph inside the hydrophobic pocket. However, since modeling studies showed a capacity for only one single cholesterol molecule inside the pocket[171], it is most likely that also only one Sph molecule fits inside, which was supported by molecular dynamic simulations of Fabio Lolicato. Assuredly, the START domain does not accommodate both lipids simultaneously. Moreover, it has been shown that cholesterol, under physiological conditions, is most likely transported from the ER towards the lysosome[196], while I found STARD3-mediated Sph transport to happen in the opposite direction. Therefore, our working hypothesis is that STARD3 mediates a counter transport of cholesterol and Sph between lysosomes and the ER.

2.4.3 Lipid competition studies in cells overexpressing STARD3

START-mediated cholesterol transfer has been extensively studied in the past years[150,171,218]. However, START-mediated Sph transfer is a novel feature of STARD3, which allows Sph entry into the sphingolipid recycling pathway.

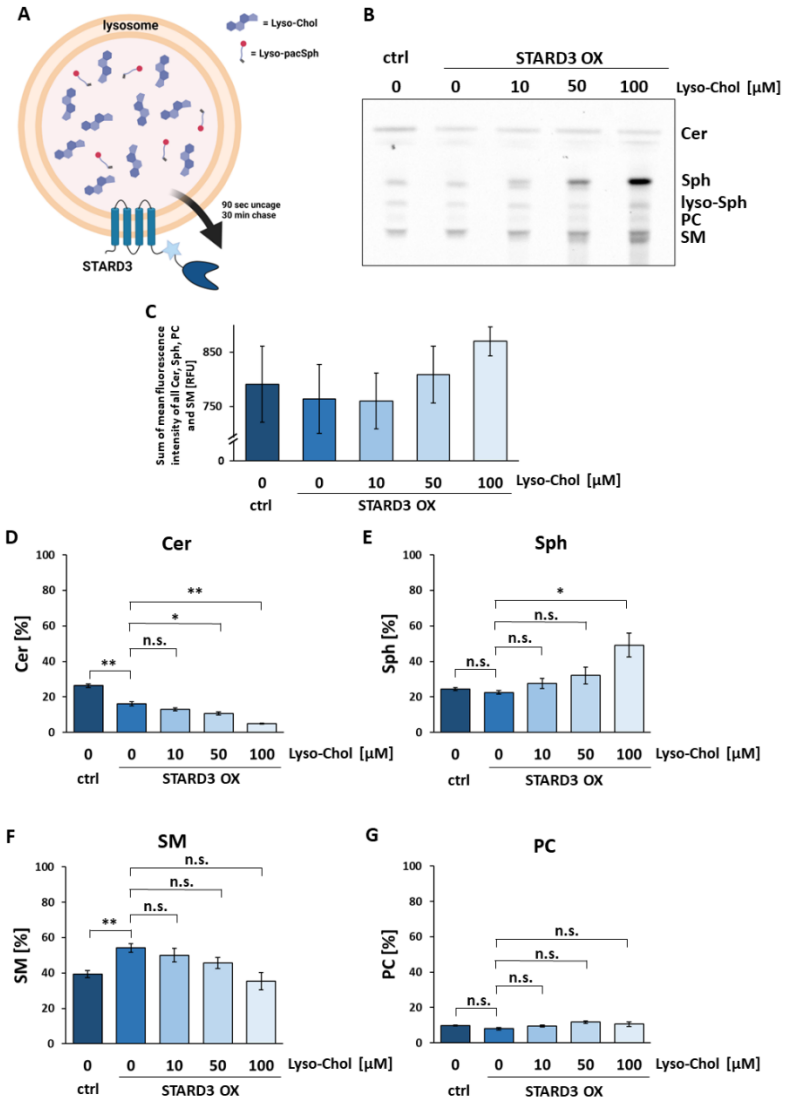

Figure 2.27: Cholesterol competition. A| Lysosomal labelling of lyso-pacSph and lyso-Chol and their potential STARD3-mediated lysosomal export. B| TLC of HeLa 11ht WT (ctrl), STARD3

overexpressing (WT STARD3 OX) cells, labelled simultaneously with 5 µM lyso-pacSph and 0 to 100 µM lyso-Chol and chased after probe activation for 30 min. C| Quantification of total fluorescence intensity of all clickable lipids. Error bars show the standard error of the mean. D| Quantification of lyso-pacSph fate after 30 min shown as Cer, E| Sph, F| SM, and G| PC. Error bars show the standard error of the mean and Welch two-sample *t*-tests were performed as indicated (n.s. *p*-value ≥ 0.05; * *p*-value < 0.05; ** *p*-value < 0.01, *** *p*-value < 0.001).

I performed lipid competition experiments to investigate whether cholesterol and Sph use the same population of STARD3 proteins. To this end, cells overexpressing STARD3 were simultaneously labelled with 5 µM lyso-pacSph and an excess (0 – 100 µM) of lyso-Chol, a novel cholesterol probe having the same lysosome-targeting motif and coumarin-cage group attached as lyso-pacSph but lacking the photocrosslinkable and clickable groups[140]. After uncaging, the ability of STARD3 to transfer Sph, in the presence of available cholesterol molecules, was investigated by TLC using a 30 min chase (Fig. 2.27a and b).

The quantification of total lipid amounts showed a lyso-Chol concentration-dependent increase in the total intensity of metabolized lyso-pacSph species (Fig. 2.27c). The fact that lysosomes were pre-loaded with an unnatural amount of lipids might lead to lysosomal enlargement accompanied by an artificially induced lysosomal storage disorder. This would lead to an increased lysosomal lipid capacity, explaining the observed enhanced lyso-pacSph uptake. When quantifying the single sphingolipid species, a significant decrease in Cer (Fig. 2.27d), and a non-significant increase in Sph levels (Fig. 2.27e) was shown with increasing lyso-Chol concentration. This indicates a diminished exit of Sph out of the lysosome when an excess of cholesterol is present. Moreover, a trend of SM decrease in a lyso-Chol concentration-dependent manner was detected (Fig. 2.27f). This showed a reduced STARD3-mediated transfer of Sph towards the biosynthetic pathway. It is tempting to speculate that cholesterol occupied the STARD3 START domain, most likely for its transfer out of the lysosome to the ER, leading to a diminished STARD3-dependent Sph transfer. Interestingly, PC levels stay constant in all conditions (Fig. 2.27g), indicating that the cholesterol-dependent lysosomal Sph

storage is not necessarily accompanied by switching on of the sphingolipid degradation pathway. However, the most pronounced effect on sphingolipid metabolism in this competition study was observed in 100 µM cholesterol excess conditions. In these conditions, the lysosomes might be severely affected in size, stress, and metabolism. With lower cholesterol concentrations the effects are only moderate. For that reason, speculations about STARD3-mediated counter-transfer of Sph and cholesterol must be taken with caution.

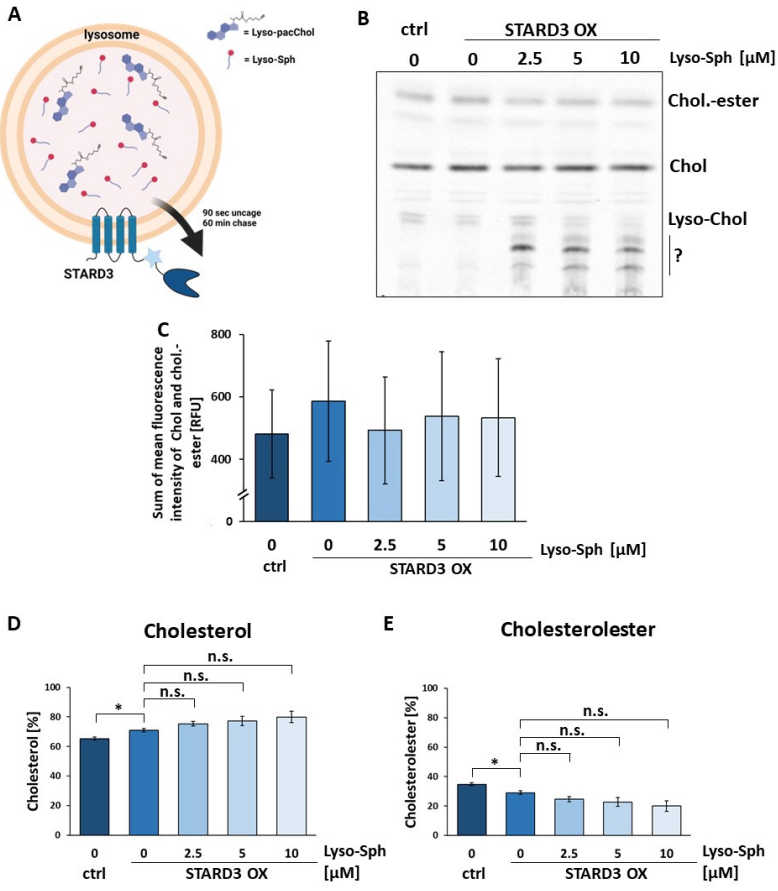

Figure 2.28: Sph competition. A| Lysosomal labelling of lyso-pacChol and lyso-Sph and their potential STARD3-mediated lysosomal export. B| TLC of HeLa 11ht WT (ctrl), STARD3 overexpressing (WT STARD3 OX) cells, labelled simultaneously with 2.5 µM lyso-pacChol and 0 to 10 µM lyso-Sph and chased after probe activation for 60 min. C| Quantification of total

fluorescence intensity of each lane. Error bars show the standard error of the mean. D| Quantification of lyso-pacChol fate after 60 min shown as cholesterol (Chol), and D| Cholesterolester (Chol.-ester). Error bars show the standard error of the mean and Welch two-sample *t*-tests were performed as indicated (n.s. *p*-value ≥ 0.05; * *p*-value < 0.05; ** *p*-value < 0.01, *** *p*-value < 0.001).

To further investigate the transfer of cholesterol and Sph, I performed the competition experiment vice versa. To this end, cells overexpressing STARD3 were simultaneously labelled with 2.5 µM lyso-pacChol, a multifunctionalized cholesterol probe, and an excess (0 – 10 µM) of lyso-Sph, an Sph probe containing the lyso-cage group, but not the click and crosslinking group[140]. After uncaging, the ability of STARD3 to transfer cholesterol in the presence of available Sph molecules was investigated by TLC using a 60 min chase (Fig. 2.28a and b).

As known so far, cholesterol can only be metabolized to cholesterol esters, which are made at the ER by the action of acyl-CoA-acetyltransferase (ACAT). These esters are then stored in lipid droplets or unesterified by esterases to release free cholesterol[219]. In a previous study, I already identified cholesterol and cholesterol ester bands in TLC-based assays, using cholesterol standards and ACAT inhibition approaches, respectively[155]. This time, total quantification of the fluorescence intensity of cholesterol and cholesterol esters did not show an Sph-dependent increase (Fig. 2.28c). This might be due to the fact that this experiment was performed with lower concentrations of lyso-pacChol as well as lyso-Sph, to prevent cell death accounted by high Sph concentrations. Notably, cell death started already at 50 µM lyso-pacSph concentrations. However, with increasing lyso-Sph concentrations, several non-identified bands appear on the TLC. On the one hand, these bands ran at the same height as SM and PC, and they only appear in the presence of Sph excess. Since the click group of lyso-pacChol is attached to the esterified side chain of the molecule, it is tempting to speculate that cellular esterases can cleave the alkyne comprising chain off, which is then subsequently incorporated into the sphingolipid metabolism resulting in short-chain sphingolipids or their degradative products. This process might be driven by the excess of Sph. On the other hand, it is also possible that these unidentified bands correlate with unusual cholesterol metabolites,

appearing upon lysosomal stress, as caused by an excess of Sph. However, the nature of these potential cholesterol metabolites is unknown and would need further investigation.

Interestingly, quantification of cholesterol (Fig. 2.28d) and cholesterol esters (Fig. 2.28e) showed increased cholesterol and ester levels in STARD3 overexpression cells compared to control cells, when lyso-Sph was not added. Since cholesterol esters are made at the ER, it is most likely that STARD3 preferred an ER to lysosome transfer of cholesterol, leading to lower cholesterol ester levels. This is possible since the chase of 60 min allows the priorly lysosomal targeted cholesterol to distribute throughout the entire cell, including internal membranes, such as the ER[140].

Although not significant, in lyso-Sph increasing conditions, this phenotype got even more pronounced. This could stem from a counter transport of Sph and cholesterol, meaning more Sph transfer from lysosomes to the ER, as expected in Sph-rich conditions, induces a more efficient cholesterol transfer from the ER to lysosomes, leading to less esterification. In contrast, the phenotype could also be explained by a slower cholesterol transfer from lysosomes to the ER in Sph-rich conditions, also leading to less esterification. The latter hypothesis is more likely since it has been reported that an excess of Sph induces a lysosomal cholesterol accumulation phenotype[140].

Together, these lipid competition studies revealed a correlation between STARD3-mediated Sph and cholesterol transfer. Moreover, these data give a first hint that Sph and cholesterol transport mediated by STARD3 potentially occurs in exchange for each other at lysosome-ER contact sites. However, these lipid competition experiments were performed with high lipid concentrations, which potentially induced a lysosomal lipid storage phenotype. For that reason, the interpretation of these data needs to be taken with caution.

2.5 Conclusion and outlook

Sphingolipid-protein interactions and sphingolipid metabolism have already been studied for decades. Several receptors and transport proteins, such as S1P receptors[220] or the Cer transfer protein CERT[221], have been described to participate in sphingolipid metabolism, signaling, and transfer. However, advanced novel tools, such as functionalized lipid probes, allow a sophisticated way to investigate lipids and their interacting proteins not only in steady-state but also in a highly dynamic manner. Using these lipid probes, two lysosomal Sph-binding proteins, namely NPC1 and LIMP2, have been discovered recently[140]. While these proteins were shown to participate in Sph export from the lysosomal lumen towards the limiting lysosomal membrane, here I found the first known example of an Sph transporter between lysosomes and the ER.

In vitro and *in cellulo* lipid-protein immunoprecipitation, as well as TLC-based Sph transfer assays, revealed STARD3 as an Sph transporter. Interestingly, Sph seems to bind not only to the lipid-transferring START domain but also to the MENTAL domain of STARD3. This MENTAL-lipid binding ability has also been shown for cholesterol binding[152]. The MENTAL domain was suggested as a reservoir that stores an excess of lipid molecules prior to START-mediated lipid transfer to target organelles[152]. This hypothesis matches with STARD3-Sph binding findings and would explain why START deficient STARD3 mutants are still able to crosslink with Sph. Before Sph can reach the MENTAL domain, it needs to be transferred out of the lysosomal lumen, where hydrolases act on intraluminal membranes for prior degradation of higher sphingolipids. For cholesterol, it is known that it reaches the limiting membrane of lysosomes by an active transfer driven by NPC1 and NPC2[128]. Since NPC1 and STARD3 are reported to occur in the same type of lysosomes[173] and NPC1 has been shown to bind Sph[140], it is tempting to speculate that the NPC proteins facilitate Sph transfer from the lumen to the limiting membrane of lysosomes and forwarded it to STARD3 for lysosomal exit and its transfer towards the ER. To investigate this assumption, STARD3-mediated Sph transfer could be analyzed in NPC1-deficient cells to investigate whether NPC1s act as a mediator between the

lysosomal lumen and the lysosomal limiting membrane. However, since the knock-out of STARD3 still resulted in successful Sph exit out of the lysosome, STARD3 is certainly one of more, still unknown proteins, that regulate the entry of Sph into the sphingolipid recycling pathway.

Furthermore, lipid-protein binding assays found that the functionality of lysosome-ER contact sites impacts STARD3-Sph binding. Impaired membrane contact site formation between lysosomes and the ER by mutating the FFAT motif of STARD3 decreased the STARD3-Sph binding efficiency. This implies a highly regulated cellular sensing machinery that adapts to subcellular changes, such as decreased contact site between lysosomes and the ER in FFAT mutant conditions. It has been reported that phosphorylation of the FFAT motif controls the formation of membrane contact sites and lipid transfer function and acts as a general switch at inter-organelle contacts[134]. However, the respective kinase that mediates FFAT-phosphorylation has not been identified so far. Since the prominent serine/threonine kinase mTOR, a major regulator of cell growth, localizes in its active form to the surface of lysosomes, it is not unreasonable to speculate that mTOR might regulate lysosome-organelle contacts by phosphorylation of the cytosolic FFAT motif of STARD3 and thereby act as lysosomal sensor for subcellular changes. In order to investigate whether mTOR acts as a potential kinase to regulate lysosomal contact sites, FFAT phosphorylation mutation studies, as well as mTOR inhibition experiments, could be performed.

Besides decreased Sph-STARD3 binding in lysosome-ER impaired cells, also sphingolipid metabolism is affected by defective contacts. When Sph incorporation into Cer at the ER is impaired, either by defective lysosome-ER contact site formation in a STARD3 FFAT mutant or by inhibition of the biosynthetic pathway using specific drugs, such as FB1, the sphingolipid degradation pathway is switched on. This confirms the suggestion that a highly regulated cellular machinery senses lysosome-ER contacts to switch on either the Sph recycling or degradation pathway. However, S1P, a bioactive sphingolipid metabolite, has been reported to be synthesized prior to Sph degradation[179]. Two

different isoforms of SphKs are known and have been reported to have opposing effects. While overexpression of the pro-survival SphK1 reduces Sph incorporation into Cer, overexpression of the pro-apoptotic SphK2 has been shown to facilitate Sph incorporation into C16:0 Cer by increasing the incorporation of palmitate, which is a substrate for CerS[100]. I could show an increase in SphK1 levels in STARD3 FFAT mutant but not in functional STARD3 overexpression conditions, suggesting an SphK1 regulated sphingolipid degradation. However, in inhibitory biosynthesis conditions using FB1, this SphK1 increase did not occur, implying a complex sphingolipid degradation regulation that is not always accompanied by increased amounts of SphK1. Additionally, increased amounts of SphK1 do not necessarily equal with enhanced kinase activity. Therefore, I can only speculate that Sph phosphorylation prior to its degradation is mainly facilitated by SphK1.

Interestingly, endogenous S1P levels were dramatically increased in STARD3 overexpression conditions that potentially favor Sph incorporation into higher sphingolipids. It is tempting to speculate that these increased S1P levels occur from SphK2 activity, thereby increasing palmitate levels and C16:0 Cer[100], which has been indeed shown by lipid mass spectrometry. SphK knock-out studies and activity assays could give more insights into sphingolipid degradation regulation via SphK1 and Sph entry into the recycling pathway via SphK2, and thereby shed light on the opposing roles of both kinases.

Nevertheless, the final step in sphingolipid degradation facilitated by S1PL occurs at the ER[222], implying a transfer of Sph or S1P between lysosomes and the ER in FFAT mutant or FB1 treatment conditions. Since, at least in FFAT mutant conditions, the contacts between lysosomes and the ER are dramatically decreased, it could be considered that SphK1 (or SphK2) might be recruited to lysosomes for Sph phosphorylation rather than that the phosphorylation occurs at the ER. Presumably, down-regulation of SphKs, by inhibitory or knock-out approaches, would result in an artificial Sph lysosomal storage disorder as found in NPC disease[223]. As already mentioned, cleavage of the Sph backbone

occurs at the ER, implying a transfer of S1P towards the ER. The observed increased PC levels in lyso-pacSph studies already after a short period of time presume an efficient lysosome-to-ER transfer. It is unlikely that this transfer is facilitated via vesicular trafficking, which is presumably not fast enough, or at lysosome-ER contact sites since these contacts are reduced in FFAT mutant cells. For that reason, it is tempting to speculate that S1P reaches the ER via a still unknown protein or transfer mechanism. S1P-protein interaction studies could be performed to investigate potential interaction partners that might facilitate its transfer towards the ER.

Furthermore, molecular dynamic simulation studies confirmed that Sph fits inside the hydrophobic cavity of the START domain. In an aqueous environment, it has been shown that Sph favors entering the pocket with its tail first. This position might stabilize Sph inside the START domain in an aqueous solution since its polar headgroup faces towards the cytosol. However, in a membranous environment, as such of cells, Sph might enter the pocket with its head first. Polar lipids, including Sph, are anchored in biomembranes with their heads facing towards the polar cytosol and could thereby be extracted from LTPs only in head-first orientation. To further investigate this hypothesis, simulations of START-Sph interactions need to be done in a membranous environment.

Moreover, the R351 residue that is deeply buried inside the pocket seems to be essential for START-mediated Sph transfer. This residue, which is highly conserved through evolution, has already been shown by molecular docking studies to potentially also interact with the hydroxyl group of cholesterol[171]. Its polarity might be essential for releasing lipids out of the START domain, as supported by increased Sph-R351 START mutant crosslinking in *in vitro* studies (Denisa Jamecna, unpublished data). This also supports the assumption that Sph enters the START pocket with its polar head first in a membranous environment. R351 replacement by other positively charged amino acids, such as His or Lys, in START-mediated Sph trafficking studies, could give further evidence if charged amino acids at the end of the cavity are essential for its lipid release.

In conclusion, the cholesterol transfer protein STARD3 has been shown to also transport Sph at lysosome-ER contact sites in a START-dependent manner, while the MENTAL domain presumably supplies Sph prior to its transfer at membrane contact sites. STARD3 seems to be a highly flexible lipid transfer protein that adapts its lipid transfer direction along the subcellular lipid concentration gradient, presumably Sph transfer from lysosomes to the ER and cholesterol transfer in exchange from the ER to lysosomes. Therefore, STARD3 could play a, yet unknown, role in many lysosomal storage diseases to ensure cellular lipid homeostasis when major lysosomal lipid breakdown or transfer proteins are defective.

Chapter III – Experimental Methods

3.1 Reagents

All common reagents used in this thesis were purchased from commercial sources such as Sigma Aldrich/Merck (Darmstadt, DE), ThermoFisher Scientific (Massachusetts, USA), or Carl Roth (Karlsruhe, DE) without further purification. All enzymes and cloning reagents were purchased from New England Biolabs (Frankfurt am Main, DE). Commercially available functionalized lipids such as pacSph were obtained from Avanti Polar Lipids (Birmingham, USA). Lyso-pacSph, lyso-pacChol, lyso-Sph, and lyso-Chol were originally synthesized by Janathan Juarez in the Höglinger laboratory (Heidelberg University, DE) and provided by him. CerS inhibitor Fumonisin B1 (FB1) was purchased from Biomol (Hamburg, DE).

3.2 Buffers and media

3.2.1 Buffers and solutions

PBS

137 mM NaCl

2.7 mM KCl

10 mM Na_2HPO_4

1.8 mM KH_2PO_4

The pH was adjusted to 7.4 using HCl. PBS was prepared as sterile filtrated 10x stock in the media kitchen of the BZH.

PHEM buffer

60 mM PIPES, pH 6.9

25 mM HEPES, pH 6.9

10 mM EGTA, pH 7.0

2 mM $MaCl_2$

PHEM buffer was sterile filtrated and used at pH 6.9.

Imaging buffer

20 mM HEPES

115 mM NaCl

1.2 mM $MgCl_2$

1.2 mM glucose

1.8 mM $CaCl_2$

The pH was adjusted to 7.4 using NaOH and the solution was sterile filtrated before usage.

IP equilibration buffer

50 mM Tris, pH 7.4

150 mM NaCl

0.05 % (v/v) Trition-X-100

1 mM DTT

Equilibration buffer was prepared freshly before each experiment.

IP wash buffer 1

2 % (w/v) SDS

IP wash buffer 2

50 mM HEPES, pH 7.4

1 mM EDTA, pH 8.0

500 mM NaCl

1 % (v/v) Triton-X-100

0.1 % (w/v) Na-deoxycholate

IP wash buffer 3

10 mM Tris, pH 8.0

250 mM LiCl

1 mM EDTA, pH 8.0

0.5 % (v/v) NP-40

0.5 % (w/v) Na-deoxycholate

IP wash buffer 4

50 mM Tris, pH 7.4

50 mM NaCl

0.1 % (v/v) NP-40

IP elution buffer

10 mM Tris, pH 7.4

2 % (w/v) SDS

5 % (v/v) β-mercaptoethanol

2 mM Biotin

Elution buffer was prepared freshly before each experiment.

Amido black solution

1 g/L amido black

90 % (v/v) MeOH

10 % (v/v) acetic acid

Amido black wash solution

90 % (v/v) MeOH

10 % (v/v) acetic acid

MOPS

MOSPS SDS Running buffer (20×) from novex life technologies (Carlsbad, CA)

MOPS buffer was diluted to 1× concentration before usage.

Transfer buffer

25 mM Tris

192 mM glycine

20 % (v/v) MeOH

PBS-T

137 mM NaCl

2.7 mM KCl

10 mM Na_2HPO_4

1.8 mM KH_2PO_4

0.1 % (v/v) Tween

The pH was adjusted to 7.4 using HCl. PBS was prepared as sterile filtrated 10x stock in the media kitchen of the BZH.

RIPA lysis buffer

150 mM NaCl

5 mM EDTA, pH 8.0

50 mM Tris, pH 8.0

1 % (v/v) NP-40

0.5 % (w/v) Na-deoxycholate

0.1 % (w/v) SDS

1x Protease inhibitor cocktail (Serva, Heidelberg, DE) was added to RIPA lysis buffer before usage.

SDS lysis buffer

0.1 % (w/v) SDS

1 % (v/v) Triton-X-100

All ingredients of SDS lysis buffer were dissolved in PBS. 1x Protease inhibitor cocktail (Serva, Heidelberg, DE) was added to SDS lysis buffer before usage.

4x Lämmli buffer

250 mM Tris

280 mM SDS

40 % (v/v) glycerol

20 % (v/v) β-mercaptoethanol

Spatula tip bromephenol blue

The pH was adjusted to 6.8. and 100 µL of 1 M DTT was freshly added to 900 µL of 4× lämmli buffer aliquot and stored at RT.

3.2.2 Bacterial culture medium

LB Medium

1 % (w/v) tryptone

1 % (w/v) NaCl

0.5 % (w/v) yeast extract

The pH was adjusted to 7.0 using NaOH. Luria-Bertani (LB) medium was prepared and autoclaved in the media kitchen of the BZH.

LB plates

1.5 % (w/v) bacto agar in LB

LB plates were supplemented with 100 µg/mL ampicillin or 30 µg/mL kanamycin and cast in the media kitchen of the BZH. LB plates were stored upside down at 4 °C.

SOC Medium

0.5 % (w/v) yeast extract

2 % tryptone

10 mM NaCl

2.5 mM KCl

10 mM $MgCl_2$

10 mM $MgSO_4$

20 mM glucose

The pH was adjusted to 7.0 with NaOH. Super optimal broth medium with catabolite repression (SOC) medium was prepared and autoclaved in the media kitchen of the BZH.

3.2.3 Eukaryotic cell medium

HeLa cell complete medium

Dulbecco's Modified Eagle Medium (DMEM) (4.5 g/L glucose, Sigma Aldrich)

10 % fetal calf serum (Bio & Sell)

1 % penicillin/streptomycin (Sigma Aldrich)

HeLa 11ht cell selection medium

Dulbecco's Modified Eagle Medium (DMEM) (4.5 g/L glucose, Sigma Aldrich)

10 % fetal calf serum (Bio & Sell)

1 % penicillin/streptomycin (Sigma Aldrich)

50 mM Ganciclovir

HeLa CRISPR Cas9 selection medium

Dulbecco's Modified Eagle Medium (DMEM) (4.5 g/L glucose, Sigma Aldrich)

10 % fetal calf serum (Bio & Sell)

1 % penicillin/streptomycin (Sigma Aldrich)

6 µg/mL 6-thioguanine

Starvation medium

Dulbecco's Modified Eagle Medium (DMEM) (4.5 g/L glucose, Sigma Aldrich)

3.3 Cloning and bacterial culture

3.3.1 Plasmid construction

For transient overexpression of STARD3, the STARD3 gene sequence was amplified by PCR using a Q5 DNA polymerase introducing a FLAG-tag sequence at the N-terminus of STARD3 and sites for restriction enzymes, namely BamHI and FseI for the N- and C-terminus, respectively. A pCMV6 vector was digested for 1 h at 37 °C using BamHI and FseI and the amplified PCR product was inserted by ligation using a T4 ligase overnight at 16 °C. Afterwards, T4 ligase was inactivated at 65 °C for 10 min.

The plasmid for transient STARD3 ΔSTART overexpression was produced in the same way as described above, but the reverse primer for PCR amplification bound before the START domain of STARD3. Consequently, the construct only consists of the FLAG-tagged N-terminus and the MENTAL domain but does not contain the START domain of STARD3.

Mutagenesis of STARD3 FFAT/Ala, FA/YA, MR/ND, R351A, R351D, R351E, R351F, and R351L was done by PCR amplification introducing the desired nucleotides by primer design. The whole plasmid was amplified using a Q5 DNA polymerase. In one step, the resulting linear DNA sequence was phosphorylated at the 5'-ends using a T4 polynucleotide kinase (4-PNK) and re-ligated using a T4 ligase. Additionally, DpnI was added to digest methylated original plasmids which do not contain the desired mutations. This KDL reaction was performed for 30 min at room temperature (RT).

For the preparation of HeLa 11ht cells stably overexpressing STARD3 (and the corresponding mutants) or ORP1L ΔORD, a PSF3 vector, which was a kind gift from Julien Bethuné (BZH, Heidelberg, DE), was used. FLAG-STARD3 (and the corresponding

mutants) and ORP1L-FLAG ΔORD were amplified by PCR using a Q5 DNA polymerase introducing EcoRI and NotI restriction sites at the N- and C-terminus, respectively. The PSF3 vector was digested for 1 h at 37 °C using EcoRI and NotI and the amplified PCR product was inserted by ligation using a T4 ligase overnight at 16 °C. Afterwards, T4 ligase was inactivated at 65 °C for 10 min.

For generating polyclonal CRISPR Cas9 knock-out cells, the respective gRNA sequence (for STARD3, MOSPD2, and SGPL1) was introduced into a pX330 backbone. For that purpose, oligonucleotides for the gRNA sequence with flanking BbsI restriction sites were designed using CISPOR (http://crispor.tefor.net) and annealed for 30 min at 37 °C and afterwards 5 min at 95 °C with a subsequent cool down to 25 °C in 5°C/min steps. pX330 backbone was digested using BbsI for 1 h at 37 °C and annealed oligonucleotides were inserted into the digested pX330 backbone using a t4 ligase overnight at 16 °C. The empty pX330 plasmid and the pX330 plasmid containing VAPA/B gRNA targets were a kind gift from Takeshi Harayama (University of Geneva, CHE).

3.3.2 Bacteria transformation

For transforming the constructed plasmids in bacteria, 100-200 µL E.coli (DH5α or 10β strains) bacteria were thawed on ice and mixed by flicking the tube. Afterwards, 2-10 µL of heat-inactivated ligation or KDL mixture were added and incubated for 30 min on ice. A heat-shock was performed at 42 °C for 45 sec and bacteria were recovered for 5 min on ice. Next, 1 mL of pre-warmed SOC-media was added, and bacteria were grown for 1 h at 37 °C while shaking at 500 rpm. Afterwards, bacteria were pelleted for 3 min at 1500 rpm and approximately 900 µL of supernatant were discarded. Residual 100 µL bacterial culture were re-dissolved to a homogenous solution by pipetting up and down and subsequently distributed on an LB plate containing 50 µg/mL Kanamycin or 100 µg/mL Ampicillin for CMV6 or PSF3 and pX330 plasmids, respectively. LB plates were incubated overnight at 37 °C.

The next day, single colonies were picked and grown in 5 mL LB media containing 50 µg/mL kanamycin or 100 µg/mL ampicillin overnight at 37 °C while shaking at 180 rpm. From bacterial culture, plasmids were extracted using a MiniPrep Kit (Sigma Aldrich) and DNA concentration was measured at a NanoDrop.

3.4 Cell culture

3.4.1 Cell lines

All HeLa (human cervical adenocarcinoma cells, No. CCL-2) and HeLa 11ht (human cervical adenocarcinoma cells, No CCL-2, stably expressing the reverse tetracycline-controlled transcription activator rtTA-M2 and containing a locus for Flp-recombinase-mediated cassette exchange[224,225]) cell lines were cultured in Dulbecco's Modified Eagle's Medium supplemented with 10 % FCS, 500 units penicillin and 0.1 mg/mL streptomycin in a humidified incubator at 37 °C with 5 % CO_2. Cells were regularly tested for mycoplasma contamination.

Cells used in this thesis is listed below:

Cell type	**Knock-out**	**Inducible expression**
HeLa	WT	-
HeLa	*SGPL1*	-
HeLa 11ht	WT	-
HeLa 11ht	WT	FLAG-STARD3
HeLa 11ht	WT	FLAG-STARD3 Q206A/F207A/Y208A/ S209A/P210A/P211A/E212A (FFAT/Ala)

HeLa 11ht	WT	FLAG-STARD3 ΔSTART
HeLa 11ht	WT	FLAG-STARD3 M307R/N311D (MR/ND)
HeLa 11ht	WT	ORP1L-FLAG ΔORD
HeLa 11ht	WT	FLAG-STARD3 R351F
HeLa 11ht	WT	FLAG-STARD3 R351L
HeLa 11ht	*VAPA*	-
HeLa11ht	*VAPA*	FLAG-STARD3
HeLa 11ht	*VAPB*	-
HeLa 11ht	*VAPB*	FLAG-STARD3
HeLa 11ht	*VAPA/B*	-
HeLa 11ht	*VAPA/B*	FLAG-STARD3
HeLa 11ht	*STARD3*	-
HeLa 11ht	*MOSPD2*	-
HeLa 11ht	*MOSPD2*	FLAG-STARD3
HeLa 11ht	*MOSPD2/VAPA/B*	FLAG-STARD3

HeLa WT and HeLa SGPL1$^{-/-}$ cells were a kind gift from Britta Brügger (BZH, Heidelberg, DE) and HeLa 11ht WT cells were a kind gift from Julien Bethuné (BZH, Heidelberg, DE). All other cell lines were generated by me.

3.4.2 Transfection and preparation of HeLa 11ht cells stably expressing modified proteins

Hela 11ht cells harbor a stably integrated hygromycin cassette flanked by a flippase (Flp) recognition target (FRT) site. These FRT sites were used to stably integrate a gene sequence of interest using a PSF3 vector containing the gene of interest flanked by the same FRT sites which are therefore compatible with the Flp-recombinase-mediated cassette in HeLa 11ht cells. To exchange the integrated hygromycin cassette with the gene of interest, a Flp enzyme, specifically targeting the FRT sites, is expressed[224].

For that reason, cells were grown in a 6-well plate to 70-80 % confluency and co-tansfected with 2 µg of PSF3-based plasmid and 2 µg of Flp-based plasmid using polyethylenimine (PEI) in a 1:2 ratio in recovery medium. After 24 h, the cells were transferred into a 10 cm dish, and two days later the recovery medium was replaced by HeLa 11ht selection medium containing 10 % FCS, 1 % Pen/Strep, and 50 mM Ganciclovir to select transfected cells. Cells were cultured for one week in selection medium and afterwards seeded in a 10 cm dish at a very low density. Approximately after one week, colonies of around 20 to 100 cells were grown, picked using sterile cloning disks, and expanded to 10 cm dishes. Cells were genetically validated by extracting the genomic DNA (gDNA) (Blood and Tissue Kit, Qiagen), amplifying the stably integrated gene of interest by PCR, and sequencing the PCR product.

3.4.3 Generation of polyclonal CRISPR Cas9 knock-out cells

The highly efficient gene disruption strategy used for producing polyclonal CRISPR Cas9 knock-out cells has been adapted from a protocol by Takeshi Harayama (Geneva, Switzerland)[226]. Emtpy pX330, pX330 VapA/B, and HPRT1-3m13 plasmids were a kind gift from Takeshi Harayama (Geneva, Switzerland), and pX330 Stard3, pX330 MOSPD2 were

produced as described in chapter 3.3.1. HeLa 11ht WT cells were reverse co-transfected with 495 ng of the respective pX330 plasmid and 5 ng of HPRT1-3m13 in a 24-well plate using Lipofectamine 2000. On the next day, cells were detached and seeded in a 10 cm dish. After further 4 days, the cells were detached again and reseeded in a new 10 cm dish in HeLa CRISPR Cas9 selection medium supplemented with 10 % FCS, 1 % Penicillin/Streptomycin and 6 µg/mL 6-thioguanine. Cells were cultured for one week in HeLa CRISPR selection medium and afterwards grown in normal HeLa complete medium. Cells were genetically validated by extracting the genomic DNA (gDNA) (Blood and Tissue Kit, Qiagen), amplifying the exon of interest by PCR, and sequencing the PCR product. If a suitable antibody was commercially available, the cells were validated by western blot as described in chapter 3.10.

3.5 Immunoprecipitation

Cells were grown in 10 cm dishes to 90 % confluency and labeled with 2 µM pacSph for 1 h in starvation medium. Thereafter, cells were washed with PBS and 5 mL pre-cooled imaging buffer was added. Lipids were crosslinked to proteins in proximity by irradiating the cells with UV light at 365 nm wavelength for 5 min. Subsequently, cells were harvested by scraping them in PBS and pelleted in a 1.5 mL tube. Cells were resuspended in 100 - 200 µL SDS lysis buffer containing 0.1 % (w/v) SDS and 1 % (v/v) Triton-X-100 in PBS and sonicated for 5 min, followed by a 1 h incubation at 4 °C while rotating. Cells debris was pelleted for 5 min at 14000 rpm at 4 °C and protein-containing supernatant was collected and transferred into a new 1.5 mL tube. Protein concentration was determined using amido black (see chapter 3.9) and adjusted to 200 µg protein in 100 µL SDS lysis buffer. 7 µL of click mixture containing 500 µM $CuSO_4$, 50 µM TBTA, 500 µM freshly prepared ascorbic acid, and 250 µM picolyl-azide-PEG4-Biotin were added and the solution was pipetted up and down until clear. The click reaction was performed at

37 °C for 1 h while shaking at 500 rpm. Next, to remove all reagents from the click mixture, the proteins were precipitated by adding 400 µL pre-cooled MeOH, 100 µL pre-cooled $CHCl_3$ and 300 µL pre-cooled H_2O, thoroughly vortexted, followed by a centrifugation step at 14000 rpm for 2 min at 4 °C. Two phases were formed, and the protein pellet was located on the actual phase. The upper phase was carefully removed and further 400 µL pre-cooled MeOH was added. The mixture was briefly vortexed and centrifuged again for 3 min at 14000 rpm at 4 °C. The protein pellet was now found on the bottom of the tube and the supernatant was removed. The protein pellet was dissolved in 2 % SDS/PBS by pipetting up and down and incubated for 5 min at 37 °C while shaking. After the pellet is completely dissolved, the precipitation was repeated. This time, after the second centrifuging step, the protein pellet was air-dried for 5 min to evaporate all solvents. Afterwards, the dried protein pellet was resuspended in 200 µL 0.2 % (w/v) SDS/PBS by pipetting up and down, followed by an incubation at 37 °C while shaking until the solution was clear. 20 µL (10 %) were taken as input and the remaining protein was incubated overnight with 20 µL Streptavidin Sepharose beads (cytiva) previously equilibrated in 0.2 % (w/v) SDS/PBS. On the next day, beads were spun down for 1 min at 1000 rpm and 20 µL of the supernatant was taken as flow-through. Beads were washed twice with 1 mL of IP wash buffer 1 (2 % (w/v) SDS), and twice with IP wash buffer 2 (50 mM HEPES pH 7.4, 1 mM EDTA, 500 mM NaCl, 1 % (v/v) Triton-X-100, 0.1 % (w/v) Na-deoxycholate). Protein was eluted by incubating the cells with 20 µL of elution buffer (10 mM Tris pH 7.4, 2 % (w/v) SDS, 5 % (v/v) β-mercaptoethanol, 2 mM biotin) for 15 min at 98 °C while shaking. Beads were removed by spinning them through a Mibicol "Classic" column with an inserted 10 µm filter (Mo Bi Tec) and flow-through was taken as eluate. Afterwards, 7 µL 4×lämmli buffer was added to input, flow-through and eluate and boiled for further 5 min at 98 °C and western blotting was performed as described in chapter 3.10.

3.6 Microscopy

3.6.1 Lipid visualization by click chemistry

Cells were grown on 25 mm glass coverslips placed in a 24-well plate to 60-70 % confluency, labeled with 10 µM lyso-pacSph for 1 h in pre-warmed complete medium and chased overnight in complete medium to allow its pre-localization to lysosomes. The next day, the probe taken up from the cells was uncaged for 90 sec at 405 nm wavelength in pre-warmed imaging buffer. Subsequently, the probe is released out of the lysosome and incorporated into cellular lipid metabolism. Chasing for certain timepoints allows following its way through the cell. After chasing in imaging buffer at 37 °C, the probe was crosslinked for 5 min in pre-cooled imaging buffer to proteins and other cellular material in close proximity using UV light at 365 nm wavelength. Cells were immediately fixed with MeOH for 20 min at -20 °C. Following fixation, lipids not crosslinked to cellular material were extracted by washing three times with $CHCl_3$/MeOH/AcOH (=10:55:0.75 (v/v)) and two times with PBS. Cells were then incubated with 50 µL of click mixture containing 2 mM Cu(I)BF_4, 0.8 µM AlexaFluor594-picolyl-azide in PBS for 1 h at room temperature in the dark. Cells were then washed two times with PBS and incubated with 50 µL of primary antibody (α-LAMP1 rabbit, Cell Signaling, 1:100 in 1 % BSA, 0.3 % Triton-X-100 in PBS) for 1 h at RT in the dark. Coverslips were washed briefly with PBS and cells were incubated with 50 µL of secondary antibody (α-rabbit conjugated with AlexaFluor488, Cell Signaling, 1:800 in 1 % BSA, 0.3 % Triton-X-100 in PBS) for 30 min at room temperature in the dark. Coverslips were washed briefly with PBS and mounted in 5 µL ProLong Gold Antifade mounting medium, Thermofisher Scientific. Cells were imaged at room temperature using a confocal laser scanning microscope (Zeiss LSM800) with a 63× oil objective. Co-localization was analyzed by calculating the Pearson correlation coefficient using the Coloc2 tool in the Fiji software (http://fiji.sc/Fiji).

3.6.2 Immunofluorescence microscopy

Cells were grown on 25 mm glass coverslips placed in a 24-well plate to 60 - 70 % confluency. Culturing media was removed, and cells were washed twice with PBS. Subsequently, cells were fixed using 0.5 mL 4% PFA in PBS for 20 min at RT. After fixation, the fixation solution was aspirated off and the remaining PFA was quenched with 1.5 mg/mL glycine in PBS for 10 min while shaking at RT. Next, cells were washed twice with PBS, and 50 µL of primary antibody was added (α-FLAG mouse, Sigma Aldrich, 1:100 and α-LAMP1 rabbit, Cell Signaling, 1:100 in 1 % BSA, 0.3 % Triton-X-100 in PBS) for 1 h at RT. Afterwards, cells were washed briefly, and cells were incubated with 50 µL of secondary antibody (α-rabbit or α-mouse conjugated with AlexaFluor488 or AlexaFluor649, Cell Signaling, 1:800 in 1 % BSA, 0.3 % Triton-X-100 in PBS) for 30 min at room temperature in the dark. Cells were washed briefly with PBS and mounted on a microscope slide in 5 µL ProLong Gold Antifade mounting medium, Thermofisher Scientific. Cells were imaged at room temperature using a confocal laser scanning microscope (Zeiss LSM800) with a 63× oil objective.

3.6.3 Electron microscopy

Cells were grown on 25 mm coverslips placed in a 24-well plate to 60 - 70 % confluency for conventional electron microscopy. Culturing medium was removed, and cells were washed twice with PBS. Cells were immediately fixed in 4 % PFA in PHEM buffer for 2 h at RT. Coverslips were taken out of the 24-well plated and stored in a 15 mL falcon to the top filled with 1 % PFA in PHEM buffer. For further processing, the falcon was closed properly with Parafilm and shipped to Emily Eden (UCL Institute of Ophthalmology London, UK). She imaged the cells by electron microscopy.

3.7 Thin-layer chromatography

3.7.1 Regular lipid extraction

Cells were grown in a 12- or 6-well plate to 90 % confluency and labeled with different functionalized lipids. For general investigations of cellular sphingolipid metabolism, cells were pulsed for 5 min with 2 µM pacSph and chased for indicated times in starvation medium. For a more precise analysis of Sph export out of the lysosome, a new lyso-pacSph probe was made by Janthan Juarez and Judith Notbohm in the Höglinger laboratory. This probe was given to cells for 1 h at a 5 µM concentration and chased overnight in complete medium to allow its pre-localization to lysosomes. On the next day, an uncaging step was performed for 90 sec at 405 nm wavelength to activate the probe and then a second chase was done for indicated times to precisely analyze its metabolism after lysosomal export. Subsequently after the chase (pacSph) or the second chase (lyso-pacSph), cells were scraped on ice and pelleted in a 1.5 mL tube at 1500 rpm for 5 min at 4 °C.

Lipids were extracted using a two-phase lipid extraction method. In the first step, cells were resuspended in 300 µL PBS and afterwards 600 µL MeOH and 150 µL $CHCl_3$ were added. By centrifuging at 14000 rpm for 5 min, cell debris was pelleted and the supernatant containing the lipids was transferred to a 2 mL tube. Next, 300 µL $CHCl_3$ and 600 µL 0.1 % (v/v) acetic acid were added to purify the lipid mixture. After a second centrifugation step at 14000 rpm for 5 min to phases were formed. The aqueous upper phase and remaining protein at the actual phase were taken off and the lipid-containing lower organic phase was transferred in a new 1.5 mL tube. Lipids were dried using a speed vac at 30 °C for 20 min. Next, the dried lipids were dissolved in a 30 µL click-mixture containing 4.3 µM 3-azido-7-hydroxycoumarin, 2 mM Cu(I)BF_4 in EtOH. Click reaction was performed in a speed vac at 45 °C for 20 min. Clicked lipids were dissolved in 15 µL EtOH/acetonitrile (=5:1 (v/v)) and applied on a 10 × 20 cm TLC Silica gel 60 aluminum plate. TLC plates were developed using two different solvents. The plates were placed into a glass chamber containing the first solvent, $CHCl_3$/MeOH/H_2O/AcOH (=65:25:4:1

(v/v)), until the capillary force pushed the solvent front to 5 cm from the bottom. The plates were dried and afterward placed into a second glass chamber containing the second solvent, cyclohexane/ethylacetate (=1:1 (v/v)). After the solvent front was run to the top of the plate, the plate was dried again and lipids containing the fluorescent coumarin group were visualized at a gel doc system.

The amount of a certain lipid species was analyzed by calculating the ratio of the lipid species of interest and all lipid species having the fluorescent coumarin group and presented as percent of all lipid species.

3.7.2 Quick lipid extraction

The quick lipid extraction protocol was adapted from Christoph Thiele (University of Bonn, DE)[227] and performed to analyze the acute export of lyso-pacSph from lysosomes.

To this end, cells were grown in a 6-well plate to 90 % confluency and labeled with lyso-pacSph for 1 h at a 5 µM concentration and chased overnight in complete medium to allow its pre-localization to lysosomes. On the next day, an uncaging step in imaging buffer was performed for 90 sec at 405 nm wavelength to activate the probe and then a second chase was done for indicated times in the same imaging buffer to precisely analyze its metabolism after lysosomal export. Subsequently after the second chase, the imaging buffer was aspirated off and 500 µL of MeOH/$CHCl_3$ (=5:1 (v/v)) was added in one go. The plate was placed in a sonicator bath, floating on the water surface, and sonicated for 40 sec. The cell debris solution was transferred into a 1.5 mL tube and pelleted for 5 min at 20000 rpm. The supernatant was transferred in a new 2 mL tube and 300 µL $CHCl_3$ and 600 µL 0.1 % (v/v) acetic acid were added and manually mixed for 30 sec. The phase separation step was performed at 20000 rpm for 5 min and the upper phase was discarded. The lower, organic phase was transferred into a new 1.5 mL tube and dried for 20 min at 45 °C in a speed vac. The click reaction and TLC analysis was performed as described in 3.7.1.

3.8 Lipid mass spectrometry

1×10^6 cells were seeded into 10 cm dishes and grown for 2 days. Cells were scaped in PBS and counted using Neubauer Improved cell counting chambers. Cells were pelleted for 5 min at 1500 rpm, supernatant was removed, and cell pellet was snap frozen in liquid nitrogen. Cell pellets were shipped on dry ice to Sarah Spiegel (VCU, Virginia, USA). She extracted the lipids and S1P, DHS1P, Sph, DHSph, Cer, HexCer and SM were quantified by liquid chromatography, electrospray ionization-tandem mass spectrometry.

3.9 Amido black

A serial dilution of 0, 0.025, 0.05. 0.075 and 0.1 µg/µL BSA in a final volume of 100 µL in H_2O was prepared. Next, 2.5 to 5 µL of previously prepared lysate was diluted to 100 µL in H_2O. 400 µL of amido black solution was added to all samples, thoroughly mixed, and incubated for 5 min at RT. Next, the stained protein was pelleted by centrifuging for 5 min at 13000 rpm, the supernatant was discarded, and the pellets were washed twice with 500 µL MeOH/AcOH (= 10:1 (v/v)). In the next step, the stained protein was dissolved in 300 µL 0.1 N NaOH and 150 µL were spotted onto a transparent 96-well plate. The absorbance was measured at 550 nm using a plate reader and the protein concentration of the lysate was calculated by reference to the BSA standard.

3.10 Western blot

To visualize specific proteins, 20 µg protein of a lysate or all of the eluate of an immunoprecipitation experiment were separated by SDS-PAGE analysis for 5 min at 100 V and further 45 min at 200 V in MOPS buffer. Proteins were transferred to a pre-activated PVDF membrane for 1 h at 30 V in transfer buffer. Total protein amount was

measured using the revert 700 total protein stain (Licor Bioscience, Nebraska, USA) according to the user manual. Next, unspecific proteins were blocked in 5 % milk/PBS (w/v) for 1 h and washed three times with PBS-T for 5 min. First antibody (α-FLAG mouse, Sigma Aldrich) 1:1000 or α-STARD3 mouse (Fabien Alpy lab) 1:500 in 2 % (w/v) BSA in PBS-T) was incubated overnight at 4 °C. On the next day, the membrane was washed 3 times with PBS-T and secondary antibody (α-mouse 800 1:10000 in 2 % (w/v) BSA in PBS-T) or streptavidin680 dye (1:15000 in 2 % (w/v) BSA in PBS-T) was incubated for 1 h at RT. Proteins were visualized using an odyssey imaging system (Licor Bioscience, Nebraska, USA).

3.11 qPCR

Cells were grown in a 10 cm dish and induced with 100 ng/mL doxycycline at the next day. After 24 h, cells were harvested, and RNA was extracted using the Direct-zol RNA MiniPrep kit (Zymo Research). RNA concentration was measured at a NanoDrop and 500 ng RNA were used for cDNA using the RevertAid first strand cDNA synthesis kit (thermo scientific). The qPCR was performed using the LUNA kit (NEB) and specific STARD3 and GAPDH primers were added. A qPCR thermo cycler (applied bioscience) was used with following settings: 2 h, SBRGreen, with meting curve. For quantification, the amount of amplified STARD3 product was normalized to the amount of GAPDH product.

Bibliography

1. Ellinger I, Ellinger A. Smallest Unit of Life: Cell Biology. *Comp Med Anat Physiol*. 2014;9783709115596:19-33. doi:10.1007/978-3-7091-1559-6_2
2. Lovinger DM. Communication Networks in the Brain: Neurons, Receptors, Neurotransmitters, and Alcohol. *Alcohol Res Heal*. 2008;31(3):196. /pmc/articles/PMC3860493/. Accessed February 2, 2022.
3. Ali AT, Hochfeld WE, Myburgh R, Pepper MS. Adipocyte and adipogenesis. *Eur J Cell Biol*. 2013;92(6-7):229-236. doi:10.1016/J.EJCB.2013.06.001
4. Lee H, Van Vactor D. Neurons Take Shape. *Curr Biol*. 2003;13(4):R152-R161. doi:10.1016/S0960-9822(03)00080-0
5. Song T, Kuang S. Adipocyte dedifferentiation in health and diseases. *Clin Sci (Lond)*. 2019;133(20):2107. doi:10.1042/CS20190128
6. Rashid HO, Yadav RK, Kim HR, Chae HJ. ER stress: Autophagy induction, inhibition and selection. *Autophagy*. 2015;11(11):1956-1977. doi:10.1080/15548627.2015.1091141
7. Vyas S, Zaganjor E, Haigis MC. Mitochondria and Cancer. *Cell*. 2016;166(3):555. doi:10.1016/J.CELL.2016.07.002
8. Cohen S, Valm AM, Lippincott-Schwartz J. Interacting Organelles. *Curr Opin Cell Biol*. 2018;53:84. doi:10.1016/J.CEB.2018.06.003
9. Saheki Y, De Camilli P. Endoplasmic Reticulum-Plasma Membrane Contact Sites. *Annu Rev Biochem*. 2017;86:659-681. doi:10.1146/ANNUREV-BIOCHEM-061516-044932
10. Baumann O, Walz B. Endoplasmic reticulum of animal cells and its organization into structural and functional domains. *Int Rev Cytol*. 2001;205:149-214. doi:10.1016/S0074-7696(01)05004-5

11. Li C, Qian T, He R, Wan C, Liu Y, Yu H. Endoplasmic Reticulum–Plasma Membrane Contact Sites: Regulators, Mechanisms, and Physiological Functions. *Front Cell Dev Biol*. 2021;9:627700. doi:10.3389/FCELL.2021.627700
12. Alpy F, Rousseau A, Schwab Y, et al. STARD3 or STARD3NL and VAP form a novel molecular tether between late endosomes and the ER. *J Cell Sci*. 2013;126(Pt 23):5500-5512. doi:10.1242/JCS.139295
13. Eden ER, White IJ, Tsapara A, Futter CE. Membrane contacts between endosomes and ER provide sites for PTP1B-epidermal growth factor receptor interaction. *Nat Cell Biol*. 2010;12(3):267-272. doi:10.1038/NCB2026
14. Rocha N, Kuijl C, Van Der Kant R, et al. Cholesterol sensor ORP1L contacts the ER protein VAP to control Rab7-RILP-p150 Glued and late endosome positioning. *J Cell Biol*. 2009;185(7):1209-1225. doi:10.1083/JCB.200811005
15. Peretti D, Dahan N, Shimoni E, Hirschberg K, Lev S. Coordinated lipid transfer between the endoplasmic reticulum and the Golgi complex requires the VAP proteins and is essential for Golgi-mediated transport. *Mol Biol Cell*. 2008;19(9):3871-3884. doi:10.1091/MBC.E08-05-0498
16. D'Angelo G, Polishchuk E, Tullio G Di, et al. Glycosphingolipid synthesis requires FAPP2 transfer of glucosylceramide. *Nature*. 2007;449(7158):62-67. doi:10.1038/NATURE06097
17. Hanada K, Kumagai K, Yasuda S, et al. Molecular machinery for non-vesicular trafficking of ceramide. *Nature*. 2003;426(6968):803-809. doi:10.1038/NATURE02188
18. Stefan C, Cockcroft S. ER platforms for membrane lipid dynamics. *Biochim Biophys acta Mol cell Biol lipids*. 2020;1865(1). doi:10.1016/J.BBALIP.2019.158529
19. Sun Z, Brodsky JL. Protein quality control in the secretory pathway. *J Cell Biol*. 2019;218(10):3171. doi:10.1083/JCB.201906047
20. The Endoplasmic Reticulum - Molecular Biology of the Cell - NCBI Bookshelf. https://www.ncbi.nlm.nih.gov/books/NBK26841/. Accessed April 15, 2022.

21. Appenzeller-Herzog C, Hauri HP. The ER-Golgi intermediate compartment (ERGIC): in search of its identity and function. *J Cell Sci*. 2006;119(11):2173-2183. doi:10.1242/JCS.03019

22. Béthune J, Wieland FT. Assembly of COPI and COPII Vesicular Coat Proteins on Membranes. *https://doi.org/101146/annurev-biophys-070317-033259*. 2018;47:63-83. doi:10.1146/ANNUREV-BIOPHYS-070317-033259

23. Guo Y, Sirkis DW, Schekman R. Protein Sorting at the trans-Golgi Network. *http://dx.doi.org/101146/annurev-cellbio-100913-013012*. 2014;30:169-206. doi:10.1146/ANNUREV-CELLBIO-100913-013012

24. Lorente-Rodríguez A, Barlowe C. Entry and Exit Mechanisms at the cis-Face of the Golgi Complex. *Cold Spring Harb Perspect Biol*. 2011;3(7):1-15. doi:10.1101/CSHPERSPECT.A005207

25. Jackson CL. Mechanisms of transport through the Golgi complex. *J Cell Sci*. 2009;122(4):443-452. doi:10.1242/JCS.032581

26. Robinson MS. Forty Years of Clathrin-coated Vesicles. *Traffic*. 2015;16(12):1210-1238. doi:10.1111/TRA.12335

27. Stalder D, Gershlick DC. Direct trafficking pathways from the Golgi apparatus to the plasma membrane. *Semin Cell Dev Biol*. 2020;107:112. doi:10.1016/J.SEMCDB.2020.04.001

28. Krauss M, Jia JY, Roux A, et al. Arf1-GTP-induced Tubule Formation Suggests a Function of Arf Family Proteins in Curvature Acquisition at Sites of Vesicle Budding. *J Biol Chem*. 2008;283(41):27717. doi:10.1074/JBC.M804528200

29. Chen Y, Gershlick DC, Park SY, Bonifacino JS. Segregation in the Golgi complex precedes export of endolysosomal proteins in distinct transport carriers. *J Cell Biol*. 2017;216(12):4141. doi:10.1083/JCB.201707172

30. Grigoriev I, Splinter D, Keijzer N, et al. Rab6 Regulates Transport and Targeting of Exocytotic Carriers. *Dev Cell*. 2007;13(2):305-314. doi:10.1016/J.DEVCEL.2007.06.010

31. Miserey-Lenkei S, Chalancon G, Bardin S, Formstecher E, Goud B, Echard A. Rab

and actomyosin-dependent fission of transport vesicles at the Golgi complex. *Nat Cell Biol 2010 127*. 2010;12(7):645-654. doi:10.1038/ncb2067

32. Sorre B, Callan-Jones A, Manneville JB, et al. Curvature-driven lipid sorting needs proximity to a demixing point and is aided by proteins. *Proc Natl Acad Sci U S A*. 2009;106(14):5622-5626. doi:10.1073/PNAS.0811243106
33. Contreras FX, Ernst AM, Haberkant P, et al. Molecular recognition of a single sphingolipid species by a protein's transmembrane domain. *Nat 2011 4817382*. 2012;481(7382):525-529. doi:10.1038/nature10742
34. Pike LJ, Han X, Chung KN, Gross RW. Lipid Rafts Are Enriched in Arachidonic Acid and Plasmenylethanolamine and Their Composition Is Independent of Caveolin-1 Expression: A Quantitative Electrospray Ionization/Mass Spectrometric Analysis†. *Biochemistry*. 2002;41(6):2075-2088. doi:10.1021/BI0156557
35. Fridriksson EK, Shipkova PA, Sheets ED, Holowka D, Baird B, McLafferty FW. Quantitative Analysis of Phospholipids in Functionally Important Membrane Domains from RBL-2H3 Mast Cells Using Tandem High-Resolution Mass Spectrometry†. *Biochemistry*. 1999;38(25):8056-8063. doi:10.1021/BI9828324
36. Bartke N, Hannun YA. Bioactive sphingolipids: metabolism and function. *J Lipid Res*. 2009;50 Suppl(Suppl). doi:10.1194/JLR.R800080-JLR200
37. Milhas D, Clarke CJ, Hannun YA. Sphingomyelin Metabolism at the Plasma Membrane: Implications for Bioactive Sphingolipids. *FEBS Lett*. 2010;584(9):1887. doi:10.1016/J.FEBSLET.2009.10.058
38. Yeang C, Ding T, Chirico WJ, Jiang XC. Subcellular targeting domains of sphingomyelin synthase 1 and 2. *Nutr Metab (Lond)*. 2011;8. doi:10.1186/1743-7075-8-89
39. Pakdel M, Von Blume J. Exploring new routes for secretory protein export from the trans-Golgi network. *Mol Biol Cell*. 2018;29(3):235. doi:10.1091/MBC.E17-02-0117
40. Blume J Von, Alleaume AM, Kienzle C, Carreras-Sureda A, Valverde M, Malhotra V. Cab45 is required for Ca2+-dependent secretory cargo sorting at the trans-

Golgi network. *J Cell Biol*. 2012;199(7):1057. doi:10.1083/JCB.201207180

41. DE DUVE C, PRESSMAN BC, GIANETTO R, WATTIAUX R, APPELMANS F. Tissue fractionation studies. 6. Intracellular distribution patterns of enzymes in rat-liver tissue. *Biochem J*. 1955;60(4):604. doi:10.1042/BJ0600604
42. Ballabio A, Bonifacino JS. Lysosomes as dynamic regulators of cell and organismal homeostasis. *Nat Rev Mol Cell Biol 2019 212*. 2019;21(2):101-118. doi:10.1038/s41580-019-0185-4
43. Bonifacino JS, Neefjes J. Moving and positioning the endolysosomal system. *Curr Opin Cell Biol*. 2017;47:1-8. doi:10.1016/J.CEB.2017.01.008
44. Jongsma MLLM, Berlin I, Wijdeven RHHM, et al. An ER-Associated Pathway Defines Endosomal Architecture for Controlled Cargo Transport. *Cell*. 2016;166(1):152-166. doi:10.1016/J.CELL.2016.05.078
45. Starling GP, Yip YY, Sanger A, Morton PE, Eden ER, Dodding MP. Folliculin directs the formation of a Rab34-RILP complex to control the nutrient-dependent dynamic distribution of lysosomes. *EMBO Rep*. 2016;17(6):823-841. doi:10.15252/EMBR.201541382
46. Nakata T, Hirokawa N. Point mutation of adenosine triphosphate-binding motif generated rigor kinesin that selectively blocks anterograde lysosome membrane transport. *J Cell Biol*. 1995;131(4):1039-1053. doi:10.1083/JCB.131.4.1039
47. Harada A, Takei Y, Kanai Y, Tanaka Y, Nonaka S, Hirokawa N. Golgi vesiculation and lysosome dispersion in cells lacking cytoplasmic dynein. *J Cell Biol*. 1998;141(1):51-59. doi:10.1083/JCB.141.1.51
48. Lübke T, Lobel P, Sleat DE. Proteomics of the lysosome. *Biochim Biophys Acta*. 2009;1793(4):625-635. doi:10.1016/J.BBAMCR.2008.09.018
49. Eskelinen EL, Tanaka Y, Saftig P. At the acidic edge: emerging functions for lysosomal membrane proteins. *Trends Cell Biol*. 2003;13(3):137-145. doi:10.1016/S0962-8924(03)00005-9
50. Saftig P, Klumperman J. Lysosome biogenesis and lysosomal membrane

proteins: trafficking meets function. *Nat Rev Mol Cell Biol 2009 109*. 2009;10(9):623-635. doi:10.1038/nrm2745

51. Huotari J, Helenius A. Endosome maturation. *EMBO J*. 2011;30(17):3481. doi:10.1038/EMBOJ.2011.286
52. Maxfield FR, McGraw TE. Endocytic recycling. *Nat Rev Mol Cell Biol*. 2004;5(2):121-132. doi:10.1038/NRM1315
53. Grant BD, Donaldson JG. Pathways and mechanisms of endocytic recycling. *Nat Rev Mol Cell Biol*. 2009;10(9):597. doi:10.1038/NRM2755
54. Zerial M, McBride H. Rab proteins as membrane organizers. *Nat Rev Mol Cell Biol*. 2001;2(2):107-117. doi:10.1038/35052055
55. Rink J, Ghigo E, Kalaidzidis Y, Zerial M. Rab conversion as a mechanism of progression from early to late endosomes. *Cell*. 2005;122(5):735-749. doi:10.1016/J.CELL.2005.06.043
56. Poteryaev D, Datta S, Ackema K, Zerial M, Spang A. Identification of the switch in early-to-late endosome transition. *Cell*. 2010;141(3):497-508. doi:10.1016/J.CELL.2010.03.011
57. Scott CC, Vacca F, Gruenberg J. Endosome maturation, transport and functions. *Semin Cell Dev Biol*. 2014;31:2-10. doi:10.1016/J.SEMCDB.2014.03.034
58. Luzio JP, Pryor PR, Bright NA. Lysosomes: fusion and function. *Nat Rev Mol Cell Biol*. 2007;8(8):622-632. doi:10.1038/NRM2217
59. Mindell JA. Lysosomal Acidification Mechanisms*. *http://dx.doi.org/101146/annurev-physiol-012110-142317*. 2012;74:69-86. doi:10.1146/ANNUREV-PHYSIOL-012110-142317
60. Lysosomes - The Cell - NCBI Bookshelf. https://www.ncbi.nlm.nih.gov/books/NBK9953/. Accessed April 16, 2022.
61. Pu J, Guardia CM, Keren-Kaplan T, Bonifacino JS. Mechanisms and functions of lysosome positioning. *J Cell Sci*. 2016;129(23):4329. doi:10.1242/JCS.196287
62. Laplante M, Sabatini DM. mTOR signaling at a glance. *J Cell Sci*. 2009;122(20):3589. doi:10.1242/JCS.051011

63. Sancak Y, Peterson TR, Shaul YD, et al. The Rag GTPases bind raptor and mediate amino acid signaling to mTORC1. *Science*. 2008;320(5882):1496-1501. doi:10.1126/SCIENCE.1157535

64. Leprivier G, Rotblat B. How does mTOR sense glucose starvation? AMPK is the usual suspect. *Cell Death Discov*. 2020;6(1). doi:10.1038/s41420-020-0260-9

65. Yoon MS. The Role of Mammalian Target of Rapamycin (mTOR) in Insulin Signaling. *Nutrients*. 2017;9(11). doi:10.3390/NU9111176

66. Laplante M, Sabatini DM. MTOR signaling in growth control and disease. *Cell*. 2012;149(2):274-293. doi:10.1016/j.cell.2012.03.017

67. Zoncu R, Bar-Peled L, Efeyan A, Wang S, Sancak Y, Sabatini DM. mTORC1 senses lysosomal amino acids through an inside-out mechanism that requires the Vacuolar H+-ATPase. *Science*. 2011;334(6056):678. doi:10.1126/SCIENCE.1207056

68. Settembre C, Zoncu R, Medina DL, et al. A lysosome-to-nucleus signalling mechanism senses and regulates the lysosome via mTOR and TFEB. *EMBO J*. 2012;31(5):1095-1108. doi:10.1038/emboj.2012.32

69. Medina DL, Fraldi A, Bouche V, et al. Transcriptional Activation of Lysosomal Exocytosis Promotes Cellular Clearance. *Dev Cell*. 2011;21(3):421. doi:10.1016/J.DEVCEL.2011.07.016

70. van Meer G, Voelker DR, Feigenson GW. Membrane lipids: where they are and how they behave. *Nat Rev Mol Cell Biol*. 2008. doi:10.1038/nrm2330

71. Sud M, Fahy E, Cotter D, et al. LMSD: LIPID MAPS structure database. *Nucleic Acids Res*. 2007;35(Database issue). doi:10.1093/NAR/GKL838

72. Voelker DR. Glycerolipid Structure, Function, and Synthesis in Eukaryotes. *Encycl Biol Chem Second Ed*. February 2013:412-418. doi:10.1016/B978-0-12-378630-2.00510-7

73. Donato P, Dugo P, Mondello L. Separation of Lipids. *Liq Chromatogr Appl*. 2013:203-248. doi:10.1016/B978-0-12-415806-1.00009-7

74. Donato P, Cacciola F, Beccaria M, Dugo P, Mondello L. Lipidomics. *Compr Anal*

Chem. 2015;68:395-439. doi:10.1016/B978-0-444-63340-8.00008-X

75. Ekroos K, Ejsing CS, Bahr U, Karas M, Simons K, Shevchenko A. Charting molecular composition of phosphatidylcholines by fatty acid scanning and ion trap MS3 fragmentation. *J Lipid Res*. 2003;44. doi:10.1194/jlr.D300020-JLR200
76. Craig M, Yarrarapu SNS, Dimri M. Biochemistry, Cholesterol. *StatPearls*. August 2021. https://www.ncbi.nlm.nih.gov/books/NBK513326/. Accessed March 7, 2022.
77. Zampelas A, Magriplis E. New Insights into Cholesterol Functions: A Friend or an Enemy? *Nutrients*. 2019;11(7). doi:10.3390/NU11071645
78. Luo J, Jiang LY, Yang H, Song BL. Intracellular Cholesterol Transport by Sterol Transfer Proteins at Membrane Contact Sites. *Trends Biochem Sci*. 2019;44(3):273-292. doi:10.1016/j.tibs.2018.10.001
79. Gault CR, Obeid LM, Hannun YA. An overview of sphingolipid metabolism: from synthesis to breakdown. *Adv Exp Med Biol*. 2010;688:1-23. http://www.ncbi.nlm.nih.gov/pubmed/20919643. Accessed August 27, 2018.
80. Mandon EC, Ehses I, Rother J, Van Echten G, Sandhoff K. Subcellular localization and membrane topology of serine palmitoyltransferase, 3-dehydrosphinganine reductase, and sphinganine N-acyltransferase in mouse liver. *J Biol Chem*. 1992;267(16):11144-11148. doi:10.1016/S0021-9258(19)49887-6
81. Lahiri S, Lee H, Mesicek J, et al. Kinetic characterization of mammalian ceramide synthases: Determination of Km values towards sphinganine. *FEBS Lett*. 2007;581(27):5289-5294. doi:10.1016/J.FEBSLET.2007.10.018
82. Hannun YA, Obeid LM. Many ceramides. *J Biol Chem*. 2011;286. doi:10.1074/jbc.R111.254359
83. Marcus J, Honigbaum S, Shroff S, Honke K, Rosenbluth J, Dupree JL. Sulfatide is essential for the maintenance of CNS myelin and axon structure. *Glia*. 2006;53(4):372-381. doi:10.1002/GLIA.20292
84. Watson P, Stephens DJ. ER-to-Golgi transport: form and formation of vesicular and tubular carriers. *Biochim Biophys Acta*. 2005;1744(3):304-315.

doi:10.1016/J.BBAMCR.2005.03.003

85. Hanada K. Intracellular trafficking of ceramide by ceramide transfer protein. *Proc Jpn Acad Ser B Phys Biol Sci*. 2010;86. doi:10.2183/PJAB.86.426

86. Ichikawa S, Sakiyama H, Suzuki G, Jwa Hidari KIP, Hirabayashi Y. Expression cloning of a cDNA for human ceramide glucosyltransferase that catalyzes the first glycosylation step of glycosphingolipid synthesis. *Proc Natl Acad Sci U S A*. 1996;93(10):4638-4643. doi:10.1073/PNAS.93.10.4638

87. Yamashita T, Wada R, Sasaki T, et al. A vital role for glycosphingolipid synthesis during development and differentiation. *Proc Natl Acad Sci U S A*. 1999;96. http://www.ncbi.nlm.nih.gov/pubmed/10430909. Accessed August 30, 2018.

88. Tafesse FG, Ternes P, Holthuis JCM. The multigenic sphingomyelin synthase family. *J Biol Chem*. 2006;281(40):29421-29425. doi:10.1074/JBC.R600021200

89. Wijesinghe DS, Massiello A, Subramanian P, Szulc Z, Bielawska A, Chalfant CE. Substrate specificity of human ceramide kinase. *J Lipid Res*. 2005;46(12):2706-2716. doi:10.1194/JLR.M500313-JLR200

90. Boath A, Graf C, Lidome E, Ullrich T, Nussbaumer P, Bornancin F. Regulation and traffic of ceramide 1-phosphate produced by ceramide kinase: comparative analysis to glucosylceramide and sphingomyelin. *J Biol Chem*. 2008;283(13):8517-8526. doi:10.1074/JBC.M707107200

91. Breiden B, Sandhoff K. Acid Sphingomyelinase, a Lysosomal and Secretory Phospholipase C, Is Key for Cellular Phospholipid Catabolism. *Int J Mol Sci*. 2021;22(16). doi:10.3390/IJMS22169001

92. Clarke CJ, Wu BX, Hannun YA. The Neutral Sphingomyelinase Family: Identifying Biochemical Connections. *Adv Enzyme Regul*. 2011;51(1):51. doi:10.1016/J.ADVENZREG.2010.09.016

93. Tomiuk S, Zumbansen M, Stoffel W. Characterization and subcellular localization of murine and human magnesium-dependent neutral sphingomyelinase. *J Biol Chem*. 2000;275(8):5710-5717. doi:10.1074/JBC.275.8.5710

94. Wu BX, Rajagopalan V, Roddy PL, Clarke CJ, Hannun YA. Identification and characterization of murine mitochondria-associated neutral sphingomyelinase (MA-nSMase), the mammalian sphingomyelin phosphodiesterase 5. *J Biol Chem*. 2010;285(23):17993-18002. doi:10.1074/JBC.M110.102988

95. Duan RD, Cheng Y, Hansen G, et al. Purification, localization, and expression of human intestinal alkaline sphingomyelinase. *J Lipid Res*. 2003;44(6):1241-1250. doi:10.1194/JLR.M300037-JLR200

96. Le Stunff H, Giussani P, Maceyka M, Lépine S, Milstien S, Spiegel S. Recycling of Sphingosine Is Regulated by the Concerted Actions of Sphingosine-1-phosphate Phosphohydrolase 1 and Sphingosine Kinase 2. *J Biol Chem*. 2007;282(47):34372-34380. doi:10.1074/JBC.M703329200

97. Taha TA, Hannun YA, Obeid LM. Sphingosine kinase: biochemical and cellular regulation and role in disease. *J Biochem Mol Biol*. 2006;39(2):113-131. doi:10.5483/BMBREP.2006.39.2.113

98. Milstien S, Spiegel S. Targeting sphingosine-1-phosphate: a novel avenue for cancer therapeutics. *Cancer Cell*. 2006;9(3):148-150. doi:10.1016/J.CCR.2006.02.025

99. Okada T, Ding G, Sonoda H, et al. Involvement of N-terminal-extended form of sphingosine kinase 2 in serum-dependent regulation of cell proliferation and apoptosis. *J Biol Chem*. 2005;280(43):36318-36325. doi:10.1074/JBC.M504507200

100. Maceyka M, Sankala H, Hait NC, et al. SphK1 and SphK2, sphingosine kinase isoenzymes with opposing functions in sphingolipid metabolism. *J Biol Chem*. 2005;280(44):37118-37129. doi:10.1074/JBC.M502207200

101. Kitatani K, Idkowiak-Baldys J, Hannun YA. The sphingolipid salvage pathway in ceramide metabolism and signaling. *Cell Signal*. 2008;20(6):1010. doi:10.1016/J.CELLSIG.2007.12.006

102. Ikeda M, Kihara A, Igarashi Y. Sphingosine-1-phosphate lyase SPL is an endoplasmic reticulum-resident, integral membrane protein with the pyridoxal

5'-phosphate binding domain exposed to the cytosol. *Biochem Biophys Res Commun*. 2004;325(1):338-343. doi:10.1016/J.BBRC.2004.10.036

103. Schulze H, Sandhoff K. Lysosomal Lipid Storage Diseases. *Cold Spring Harb Perspect Biol*. 2011;3(6):a004804. doi:10.1101/CSHPERSPECT.A004804
104. Ballabio A, Gieselmann V. Lysosomal disorders: From storage to cellular damage. *Biochim Biophys Acta - Mol Cell Res*. 2009;1793(4):684-696. doi:10.1016/J.BBAMCR.2008.12.001
105. Kolter T, Sandhoff K. Sphingolipid metabolism diseases. *Biochim Biophys Acta - Biomembr*. 2006;1758(12):2057-2079. doi:10.1016/J.BBAMEM.2006.05.027
106. Brady RO. Sphingolipidoses. *http://dx.doi.org/101146/annurev.bi47070178003351*. 2003;47:687-713. doi:10.1146/ANNUREV.BI.47.070178.003351
107. Stirnemann JÔ, Belmatoug N, Camou F, et al. A Review of Gaucher Disease Pathophysiology, Clinical Presentation and Treatments. *Int J Mol Sci*. 2017;18(2):441. doi:10.3390/IJMS18020441
108. Yu FPS, Amintas S, Levade T, Medin JA. Acid ceramidase deficiency: Farber disease and SMA-PME. *Orphanet J Rare Dis*. 2018;13(1). doi:10.1186/S13023-018-0845-Z
109. Schuchman EH, Desnick RJ. Types A and B Niemann-Pick Disease. *Mol Genet Metab*. 2017;120(1-2):27. doi:10.1016/J.YMGME.2016.12.008
110. Bradbury AM, Bongarzone ER, Sands MS. Krabbe disease: New hope for an old disease. *Neurosci Lett*. 2021;752:135841. doi:10.1016/J.NEULET.2021.135841
111. Chan B, Adam DN. A Review of Fabry Disease. *Skin Therapy Lett*. 2018;23(2):4-6. https://pubmed.ncbi.nlm.nih.gov/29562089/. Accessed March 9, 2022.
112. Höglinger D, Burgoyne T, Sanchez-Heras E, et al. NPC1 regulates ER contacts with endocytic organelles to mediate cholesterol egress. *Nat Commun*. 2019;10(1). doi:10.1038/S41467-019-12152-2
113. Strauss K, Goebel C, Runz H, et al. Exosome secretion ameliorates lysosomal storage of cholesterol in Niemann-Pick type C disease. *J Biol Chem*.

2010;285(34):26279-26288. doi:10.1074/JBC.M110.134775/ATTACHMENT/784AF232-E429-4A77-AD89-5CB3A1051AE7/MMC1.PDF

114. Pericleous M, Kelly C, Wang T, Livingstone C, Ala A. Wolman's disease and cholesteryl ester storage disorder: the phenotypic spectrum of lysosomal acid lipase deficiency. *lancet Gastroenterol Hepatol*. 2017;2(9):670-679. doi:10.1016/S2468-1253(17)30052-3

115. Spahiu L, Behluli E, Peterlin B, et al. Mucopolysaccharidosis III: Molecular basis and treatment. *Pediatr Endocrinol Diabetes Metab*. 2021;27(3):201-208. doi:10.5114/PEDM.2021.109270

116. Wong LH, Gatta AT, Levine TP. Lipid transfer proteins: the lipid commute via shuttles, bridges and tubes. *Nat Rev Mol Cell Biol 2018 202*. 2018;20(2):85-101. doi:10.1038/s41580-018-0071-5

117. Prinz WA, Toulmay A, Balla T. The functional universe of membrane contact sites. *Nat Rev Mol Cell Biol 2019 211*. 2019;21(1):7-24. doi:10.1038/s41580-019-0180-9

118. Wirtz KWA. Transfer of phospholipids between membranes. *Biochim Biophys Acta*. 1974;344(2):95-117. doi:10.1016/0304-4157(74)90001-X

119. Wirtz KWA, Devaux PF, Bienvenue A. Phosphatidylcholine exchange protein catalyzes the net transfer of phosphatidylcholine to model membranes. *Biochemistry*. 1980;19(14):3395-3399. doi:10.1021/BI00555A046

120. Peretti D, Kim SH, Tufi R, Lev S. Lipid Transfer Proteins and Membrane Contact Sites in Human Cancer. *Front Cell Dev Biol*. 2019;7:371. doi:10.3389/FCELL.2019.00371

121. Lev S. Non-vesicular lipid transport by lipid-transfer proteins and beyond. *Nat Rev Mol Cell Biol 2010 1110*. 2010;11(10):739-750. doi:10.1038/nrm2971

122. Ikonen E. Cellular cholesterol trafficking and compartmentalization. *Nat Rev Mol Cell Biol 2008 92*. 2008;9(2):125-138. doi:10.1038/nrm2336

123. Radhakrishnan A, Goldstein JL, McDonald JG, Brown MS. Switch-like Control of

SREBP-2 Transport Triggered by Small Changes in ER Cholesterol: A Delicate Balance. *Cell Metab*. 2008;8(6):512-521. doi:10.1016/J.CMET.2008.10.008

124. Chiapparino A, Maeda K, Turei D, Saez-Rodriguez J, Gavin AC. The orchestra of lipid-transfer proteins at the crossroads between metabolism and signaling. *Prog Lipid Res*. 2016;61:30-39. doi:10.1016/J.PLIPRES.2015.10.004
125. Inohara N, Nuez G. ML — a conserved domain involved in innate immunity and lipid metabolism. *Trends Biochem Sci*. 2002;27(5):219-221. doi:10.1016/S0968-0004(02)02084-4
126. Im YJ, Raychaudhuri S, Prinz WA, Hurley JH. Structural mechanism for sterol sensing and transport by OSBP-related proteins. *Nat 2005 4377055*. 2005;437(7055):154-158. doi:10.1038/nature03923
127. Kudo N, Kumagai K, Tomishige N, et al. Structural basis for specific lipid recognition by CERT responsible for nonvesicular trafficking of ceramide. *Proc Natl Acad Sci U S A*. 2008;105(2):488-493. doi:10.1073/PNAS.0709191105
128. Kwon HJ, Abi-Mosleh L, Wang ML, et al. Structure of N-Terminal Domain of NPC1 Reveals Distinct Subdomains for Binding and Transfer of Cholesterol. *Cell*. 2009;137(7):1213-1224. doi:10.1016/J.CELL.2009.03.049
129. James C, Kehlenbach RH. The Interactome of the VAP Family of Proteins: An Overview. *Cells*. 2021;10(7). doi:10.3390/CELLS10071780
130. Kim SH, Leal SS, Halevy D Ben, Gomes CM, Lev S. Structural requirements for VAP-B oligomerization and their implication in amyotrophic lateral sclerosis-associated VAP-B(P56S) neurotoxicity. *J Biol Chem*. 2010;285(18):13839-13849. doi:10.1074/JBC.M109.097345/ATTACHMENT/49041FF0-BBB7-4178-8D5C-AB0EB2C271C8/MMC1.PDF
131. Skehel PA, Fabian-Fine R, Kandel ER. Mouse VAP33 is associated with the endoplasmic reticulum and microtubules. 1999. www.pnas.org. Accessed March 10, 2022.
132. Nishimura Y, Hayashi M, Inada H, Tanaka T. Molecular Cloning and Characterization of Mammalian Homologues of Vesicle-Associated Membrane

Protein-Associated (VAMP-Associated) Proteins. *Biochem Biophys Res Commun*. 1999;254(1):21-26. doi:10.1006/BBRC.1998.9876

133. Tarr DEK, Scott AL. MSP domain proteins. *Trends Parasitol*. 2005;21(5):224-231. doi:10.1016/J.PT.2005.03.009

134. Mattia T Di, Martinet A, Ikhlef S, et al. FFAT motif phosphorylation controls formation and lipid transfer function of inter-organelle contacts. *EMBO J*. 2020;39(23). doi:10.15252/EMBJ.2019104369

135. Hanada K, Kumagai K, Tomishige N, Yamaji T. CERT-mediated trafficking of ceramide. *Biochim Biophys Acta - Mol Cell Biol Lipids*. 2009;1791(7):684-691. doi:10.1016/J.BBALIP.2009.01.006

136. Cabukusta B, Berlin I, van Elsland DM, et al. Human VAPome Analysis Reveals MOSPD1 and MOSPD3 as Membrane Contact Site Proteins Interacting with FFAT-Related FFNT Motifs. *Cell Rep*. 2020;33(10):108475. doi:10.1016/j.celrep.2020.108475

137. Neefjes J, Cabukusta B. What the VAP: The Expanded VAP Family of Proteins Interacting With FFAT and FFAT-Related Motifs for Interorganellar Contact. *Contact (Thousand Oaks (Ventura County, Calif))*. 2021;4:251525642110122. doi:10.1177/25152564211012246

138. Neculai D, Schwake M, Ravichandran M, et al. Structure of LIMP-2 provides functional insights with implications for SR-BI and CD36. *Nat 2013 5047478*. 2013;504(7478):172-176. doi:10.1038/nature12684

139. Conrad KS, Cheng TW, Ysselstein D, et al. Lysosomal integral membrane protein-2 as a phospholipid receptor revealed by biophysical and cellular studies. *Nat Commun 2017 81*. 2017;8(1):1-13. doi:10.1038/s41467-017-02044-8

140. Altuzar J, Notbohm J, Stein F, et al. Lysosome-targeted lipid probes reveal sterol transporters NPC1 and LIMP-2 as sphingosine transporters. doi:10.1101/2021.11.10.468010

141. Heybrock S, Kanerva K, Meng Y, et al. Lysosomal integral membrane protein-2

(LIMP-2/SCARB2) is involved in lysosomal cholesterol export. *Nat Commun 2019 101*. 2019;10(1):1-12. doi:10.1038/s41467-019-11425-0

142. Tong J, Tan L, Chun CJ, Im YJ. Structural basis of human ORP1-Rab7 interaction for the late-endosome and lysosome targeting. *PLoS One*. 2019;14(2). doi:10.1371/JOURNAL.PONE.0211724

143. Johansson M, Lehto M, Tanhuanpää K, Cover TL, Olkkonen VM. The Oxysterol-binding Protein Homologue ORP1L Interacts with Rab7 and Alters Functional Properties of Late Endocytic Compartments. *Mol Biol Cell*. 2005;16(12):5480. doi:10.1091/MBC.E05-03-0189

144. Suchanek M, Hynynen R, Wohlfahrt G, et al. The mammalian oxysterol-binding protein-related proteins (ORPs) bind 25-hydroxycholesterol in an evolutionarily conserved pocket. *Biochem J*. 2007;405(Pt 3):473. doi:10.1042/BJ20070176

145. Di Mattia T, Wilhelm LP, Ikhlef S, et al. Identification of MOSPD2, a novel scaffold for endoplasmic reticulum membrane contact sites. *EMBO Rep*. 2018;19(7):e45453. doi:10.15252/embr.201745453

146. Ouimet M, Hennessy EJ, Van Solingen C, et al. miRNA Targeting of Oxysterol Binding Protein-like 6 (OSBPL6) Regulates Cholesterol Trafficking and Efflux. *Arterioscler Thromb Vasc Biol*. 2016;36(5):942. doi:10.1161/ATVBAHA.116.307282

147. Kawasaki A, Sakai A, Nakanishi H, et al. PI4P/PS countertransport by ORP10 at ER–endosome membrane contact sites regulates endosome fission. *J Cell Biol*. 2021;221(1). doi:10.1083/JCB.202103141/VIDEO-1

148. Wong LH, Martello A, Eden ER. Thank ORP9 for FFAT: With endosomal ORP10, it's fission accomplished! *J Cell Biol*. 2022;221(1). doi:10.1083/JCB.202112057/212925

149. Dong R, Saheki Y, Swarup S, Lucast L, Harper JW, De Camilli P. Endosome-ER Contacts Control Actin Nucleation and Retromer Function through VAP-Dependent Regulation of PI4P. *Cell*. 2016;166(2):408. doi:10.1016/J.CELL.2016.06.037

150. Wilhelm LP, Wendling C, Védie B, et al. STARD3 mediates endoplasmic reticulum-to-endosome cholesterol transport at membrane contact sites. *EMBO J*. 2017;36(10):1412. doi:10.15252/EMBJ.201695917

151. Di Mattia T, Tomasetto C, Alpy F. Faraway, so close! Functions of Endoplasmic reticulum–Endosome contacts. *Biochim Biophys Acta - Mol Cell Biol Lipids*. 2020;1865(1):158490. doi:10.1016/J.BBALIP.2019.06.016

152. Alpy F, Latchumanan VK, Kedinger V, et al. Functional Characterization of the MENTAL Domain. *J Biol Chem*. 2005;280(18):17945-17952. doi:10.1074/JBC.M500723200

153. Du X, Kumar J, Ferguson C, et al. A role for oxysterol-binding protein-related protein 5 in endosomal cholesterol trafficking. *J Cell Biol*. 2011;192(1):121-135. doi:10.1083/JCB.201004142

154. Davies JP, Ioannou YA. Topological Analysis of Niemann-Pick C1 Protein Reveals That the Membrane Orientation of the Putative Sterol-sensing Domain Is Identical to Those of 3-Hydroxy-3-methylglutaryl-CoA Reductase and Sterol Regulatory Element Binding Protein Cleavage-activating Protein. *J Biol Chem*. 2000;275(32):24367-24374. doi:10.1074/JBC.M002184200

155. Schoop V, Martello A, Eden ER, Höglinger D. Cellular cholesterol and how to find it. *Biochim Biophys Acta - Mol Cell Biol Lipids*. 2021;1866(9):158989. doi:10.1016/J.BBALIP.2021.158989

156. Leonzino M, Reinisch KM, De Camilli P. Insights into VPS13 properties and function reveal a new mechanism of eukaryotic lipid transport. *Biochim Biophys Acta - Mol Cell Biol Lipids*. 2021;1866(10):159003. doi:10.1016/J.BBALIP.2021.159003

157. Kumar N, Leonzino M, Hancock-Cerutti W, et al. VPS13A and VPS13C are lipid transport proteins differentially localized at ER contact sites. *J Cell Biol*. 2018;217(10):3625-3639. doi:10.1083/JCB.201807019

158. Haberkant P, Stein F, Höglinger D, et al. Bifunctional Sphingosine for Cell-Based Analysis of Protein-Sphingolipid Interactions. *ACS Chem Biol*. 2016;11(1):222-

230. doi:10.1021/ACSCHEMBIO.5B00810/SUPPL_FILE/CB5B00810_SI_002.XLSX

159. Höglinger D, Nadler A, Haberkant P, et al. Trifunctional lipid probes for comprehensive studies of single lipid species in living cells. *Proc Natl Acad Sci U S A*. 2017;114(7):1566-1571. doi:10.1073/PNAS.1611096114/-/DCSUPPLEMENTAL

160. Wagner N, Stephan M, Höglinger D, Nadler A. A Click Cage: Organelle-Specific Uncaging of Lipid Messengers. *Angew Chem Int Ed Engl*. 2018;57(40):13339. doi:10.1002/ANIE.201807497

161. Tomasetto C, Regnier C, Moog-Lutz C, et al. Identification of four novel human genes amplified and overexpressed in breast carcinoma and localized to the q11-q21.3 region of chromosome 17. *Genomics*. 1995;28(3):367-376. doi:10.1006/GENO.1995.1163

162. Alpy F, Tomasetto CL. STARD3: A Lipid Transfer Protein in Breast Cancer and Cholesterol Trafficking. *Cholest Transp START Domain Protein Fam Heal Dis START Proteins-Structure Funct*. 2014;9781493911127:119-138. doi:10.1007/978-1-4939-1112-7_6

163. Watari H, Arakane F, Moog-Lutz C, et al. MLN64 contains a domain with homology to the steroidogenic acute regulatory protein (StAR) that stimulates steroidogenesis. *Proc Natl Acad Sci U S A*. 1997;94(16):8462-8467. doi:10.1073/PNAS.94.16.8462

164. Alpy F, Tomasetto C. START ships lipids across interorganelle space. *Biochimie*. 2014;96(1):85-95. doi:10.1016/J.BIOCHI.2013.09.015

165. Clark BJ. The mammalian START domain protein family in lipid transport in health and disease. *J Endocrinol*. 2012;212(3):257-275. doi:10.1530/JOE-11-0313

166. Alpy F, Tomasetto C. Give lipids a START: the StAR-related lipid transfer (START) domain in mammals. *J Cell Sci*. 2005;118(Pt 13):2791-2801. doi:10.1242/JCS.02485

167. Soccio RE, Breslow JL. StAR-related lipid transfer (START) proteins: mediators of

intracellular lipid metabolism. *J Biol Chem*. 2003;278(25):22183-22186. doi:10.1074/JBC.R300003200

168. Ponting CP, Aravind L. START: a lipid-binding domain in StAR, HD-ZIP and signalling proteins. *Trends Biochem Sci*. 1999;24(4):130-132. doi:10.1016/S0968-0004(99)01362-6

169. Alpy F, Stoeckel ME, Dierich A, et al. The steroidogenic acute regulatory protein homolog MLN64, a late endosomal cholesterol-binding protein. *J Biol Chem*. 2001;276(6):4261-4269. doi:10.1074/jbc.M006279200

170. Wilhelm LP, Tomasetto C, Alpy F. Touché! STARD3 and STARD3NL tether the ER to endosomes. *Biochem Soc Trans*. 2016;44(2):493-498. doi:10.1042/BST20150269

171. Tsujishita Y, Hurley JH. Structure and lipid transport mechanism of a StAR-related domain. *Nat Struct Biol 2000 75*. 2000;7(5):408-414. doi:10.1038/75192

172. Wong LH, Eden ER, Futter CE. Roles for ER:endosome membrane contact sites in ligand-stimulated intraluminal vesicle formation. *Biochem Soc Trans*. 2018;46(5):1055. doi:10.1042/BST20170432

173. Meneses-Salas E, García-Melero A, Kanerva K, et al. Annexin A6 modulates TBC1D15/Rab7/StARD3 axis to control endosomal cholesterol export in NPC1 cells. *Cell Mol Life Sci*. October 2019:1-19. doi:10.1007/s00018-019-03330-y

174. Charman M, Kennedy BE, Osborne N, Karten B. MLN64 mediates egress of cholesterol from endosomes to mitochondria in the absence of functional Niemann-Pick Type C1 protein. *J Lipid Res*. 2010;51(5):1023-1034. doi:10.1194/jlr.M002345

175. Vassilev B, Sihto H, Li S, et al. Elevated Levels of StAR-Related Lipid Transfer Protein 3 Alter Cholesterol Balance and Adhesiveness of Breast Cancer Cells: Potential Mechanisms Contributing to Progression of HER2-Positive Breast Cancers. *Am J Pathol*. 2015;185(4):987-1000. doi:10.1016/J.AJPATH.2014.12.018

176. Fu Y, Finney NS. Small-molecule fluorescent probes and their design. *RSC Adv*.

2018;8(51):29051-29061. doi:10.1039/C8RA02297F

177. Lipsky NG, Pagano RE. Sphingolipid metabolism in cultured fibroblasts: microscopic and biochemical studies employing a fluorescent ceramide analogue. *Proc Natl Acad Sci U S A*. 1983;80(9):2608. doi:10.1073/PNAS.80.9.2608

178. Rother J, Echten G van, Schwarzmann G, Sandhoff K. Biosynthesis of sphingolipids: Dihydroceramide and not sphinganine is desaturated by cultured cells. *Biochem Biophys Res Commun*. 1992;189(1):14-20. doi:10.1016/0006-291X(92)91518-U

179. Gerl MJ, Bittl V, Kirchner S, et al. Sphingosine-1-phosphate lyase deficient cells as a tool to study protein lipid interactions. *PLoS One*. 2016;11. doi:10.1371/journal.pone.0153009

180. Budelier MM, Cheng WWL, Bergdoll L, et al. Photoaffinity labeling with cholesterol analogues precisely maps a cholesterol-binding site in voltage-dependent anion channel-1. *J Biol Chem*. 2017;292(22):9294. doi:10.1074/JBC.M116.773069

181. Wagner N, Stephan M, Höglinger D, Nadler A. A click cage: Organelle-specific uncaging of lipid messengers. *Angew Chemie Int Ed*. 2018. doi:10.1002/anie.201807497

182. Haberkant P, Stein F, Höglinger D, et al. Bifunctional Sphingosine for Cell-Based Analysis of Protein-Sphingolipid Interactions. *ACS Chem Biol*. 2016;11(1):222-230. doi:10.1021/ACSCHEMBIO.5B00810/SUPPL_FILE/CB5B00810_SI_002.XLSX

183. Gillard BK, Clement RG, Marcus DM. Variations among cell lines in the synthesis of sphingolipids in de novo and recycling pathways. *Glycobiology*. 1998;8(9):885-890. doi:10.1093/GLYCOB/8.9.885

184. Tettamanti G, Bassi R, Viani P, Riboni L. Salvage pathways in glycosphingolipid metabolism. *Biochimie*. 2003;85(3-4):423-437. doi:10.1016/S0300-9084(03)00047-6

185. Höglinger D, Nadler A, Haberkant P, et al. Trifunctional lipid probes for

comprehensive studies of single lipid species in living cells. *Proc Natl Acad Sci U S A*. 2017;114. doi:10.1073/pnas.1611096114

186. Mesmin B, Bigay J, Polidori J, Jamecna D, Lacas-Gervais S, Antonny B. Sterol transfer, PI4P consumption, and control of membrane lipid order by endogenous OSBP. *EMBO J*. 2017;36(21):3156. doi:10.15252/EMBJ.201796687
187. D'Ambrosio JM, Albanese V, Lipp NF, et al. Osh6 requires Ist2 for localization to ER-PM contacts and efficient phosphatidylserine transport in budding yeast. *J Cell Sci*. 2020;133(11). doi:10.1242/JCS.243733/266339/AM/OSH6-REQUIRES-IST2-FOR-LOCALIZATION-TO-THE-ER-PM
188. Zitomer NC, Mitchell T, Voss KA, et al. Ceramide Synthase Inhibition by Fumonisin B1 Causes Accumulation of 1-Deoxysphinganine: A NOVEL CATEGORY OF BIOACTIVE 1-DEOXYSPHINGOID BASES AND 1-DEOXYDIHYDROCERAMIDES BIOSYNTHESIZED BY MAMMALIAN CELL LINES AND ANIMALS*. *J Biol Chem*. 2009;284(8):4786. doi:10.1074/JBC.M808798200
189. Wang E, Norred WP, Bacon CW, Riley RT, Merrill AH. Inhibition of sphingolipid biosynthesis by fumonisins. Implications for diseases associated with Fusarium moniliforme. *J Biol Chem*. 1991;266(22):14486-14490. doi:10.1016/S0021-9258(18)98712-0
190. Gomez-Larrauri A, Presa N, Dominguez-Herrera A, Ouro A, Trueba M, Gomez-Munoz A. Role of bioactive sphingolipids in physiology and pathology. *Essays Biochem*. 2020;64(3):579-589. doi:10.1042/EBC20190091
191. Cartier A, Hla T. Sphingosine 1-phosphate: lipid signaling in pathology and therapy. *Science*. 2019;366(6463). doi:10.1126/SCIENCE.AAR5551
192. Hannun YA, Bell RM. Lysosphingolipids inhibit protein kinase C: Implications for the sphingolipidoses. *Science (80-)*. 1987;235(4789):670-674. doi:10.1126/SCIENCE.3101176
193. Phillips DC, Martin S, Doyle BT, Houghton JA. Sphingosine-Induced Apoptosis in Rhabdomyosarcoma Cell Lines Is Dependent on Pre-Mitochondrial Bax Activation and Post-Mitochondrial Caspases. *Cancer Res*. 2007;67(2):756-764.

doi:10.1158/0008-5472.CAN-06-2374

194. Hussain MM, Jin W, Jiang XC. Mechanisms involved in cellular ceramide homeostasis. *Nutr Metab (Lond)*. 2012;9:71. doi:10.1186/1743-7075-9-71

195. Luberto C, Kraveka JM, Hannun YA. Ceramide regulation of apoptosis versus differentiation: a walk on a fine line. Lessons from neurobiology. *Neurochem Res*. 2002;27(7-8):609-617. doi:10.1023/A:1020267831851

196. Wilhelm LP, Wendling C, Védie B, et al. STARD3 mediates endoplasmic reticulum-to-endosome cholesterol transport at membrane contact sites. *EMBO J*. 2017;36(10):1412. doi:10.15252/EMBJ.201695917

197. Uhlén M, Fagerberg L, Hallström BM, et al. Tissue-based map of the human proteome. *Science (80-)*. 2015;347(6220). doi:10.1126/SCIENCE.1260419/SUPPL_FILE/1260419_UHLEN.SM.PDF

198. Wijdeven RH, Janssen H, Nahidiazar L, et al. Cholesterol and ORP1L-mediated ER contact sites control autophagosome transport and fusion with the endocytic pathway. *Nat Commun*. 2016;7:11808. doi:10.1038/ncomms11808

199. Kaiser SE, Brickner JH, Reilein AR, Fenn TD, Walter P, Brunger AT. Structural Basis of FFAT Motif-Mediated ER Targeting. *Structure*. 2005;13(7):1035-1045. doi:10.1016/J.STR.2005.04.010

200. Slee JA, Levine TP. Systematic prediction of FFAT motifs across eukaryote proteomesidentifies nucleolar and eisosome proteins with the predicted capacity to formbridges to the endoplasmic reticulum. *Contact (Thousand Oaks (Ventura County, Calif))*. 2019;2:1. doi:10.1177/2515256419883136

201. Neefjes J, Cabukusta B. What the VAP: The Expanded VAP Family of Proteins Interacting With FFAT and FFAT-Related Motifs for Interorganellar Contact. *Contact (Thousand Oaks (Ventura County, Calif))*. 2021;4:251525642110122. doi:10.1177/25152564211012246

202. Mikitova V, Levine TP. Analysis of the key elements of FFAT-like motifs identifies new proteins that potentially bind VAP on the ER, including two AKAPs and FAPP2. *PLoS One*. 2012;7(1). doi:10.1371/JOURNAL.PONE.0030455

203. Young MM, Takahashi Y, Fox TE, Yun JK, Kester M, Wang HG. Sphingosine kinase 1 cooperates with autophagy to maintain endocytic membrane trafficking. *Cell Rep*. 2016;17(6):1532. doi:10.1016/J.CELREP.2016.10.019

204. Aguilar A, Saba JD. Truth and consequences of sphingosine-1-phosphate lyase. *Adv Biol Regul*. 2012;52(1):17-30. doi:10.1016/J.ADVENZREG.2011.09.015

205. Nakahara K, Ohkuni A, Kitamura T, et al. The Sjögren-Larsson syndrome gene encodes a hexadecenal dehydrogenase of the sphingosine 1-phosphate degradation pathway. *Mol Cell*. 2012;46(4):461-471. doi:10.1016/J.MOLCEL.2012.04.033

206. Encarnação M, Espada L, Escrevente C, et al. A Rab3a-dependent complex essential for lysosome positioning and plasma membrane repair. *J Cell Biol*. 2016;213(6):631-640. doi:10.1083/JCB.201511093

207. Nakamura S, Yoshimori T. New insights into autophagosome-lysosome fusion. *J Cell Sci*. 2017;130(7):1209-1216. doi:10.1242/JCS.196352/265307/AM/NEW-INSIGHTS-INTO-AUTOPHAGOSOME-LYSOSOME-FUSION

208. Hempelmann P. Supplementary data to the Dissertation “STARD3: A Sphingolipid Transporter at Lysosome-ER Contact Sites” - Mendeley Data. https://data.mendeley.com/drafts/768hbxwt9j. Accessed May 8, 2022.

209. Newton J, Palladino END, Weigel C, et al. Targeting defective sphingosine kinase 1 in Niemann–Pick type C disease with an activator mitigates cholesterol accumulation. *J Biol Chem*. 2020;295(27):9121-9133. doi:10.1074/JBC.RA120.012659

210. Wilhelm LP, Wendling C, Védie B, et al. STARD3 mediates endoplasmic reticulum-to-endosome cholesterol transport at membrane contact sites. *EMBO J*. 2017. doi:10.15252/embj.201695917

211. Hao F, Kondo K, Itoh T, et al. Rheb localized on the Golgi membrane activates lysosomelocalized mTORC1 at the Golgi-lysosome contact site. *J Cell Sci*. 2018;131(3). doi:10.1242/JCS.208017/265484/AM/RHEB-LOCALIZED-ON-THE-GOLGI-MEMBRANE-ACTIVATES

212. Chen Q, Hao M, Wang L, et al. Prefused lysosomes cluster on autophagosomes regulated by VAMP8. *Cell Death Dis 2021 1210*. 2021;12(10):1-10. doi:10.1038/s41419-021-04243-0

213. Elustondo P, Martin LA, Karten B. Mitochondrial cholesterol import. *Biochim Biophys Acta - Mol Cell Biol Lipids*. 2017;1862(1):90-101. doi:10.1016/j.bbalip.2016.08.012

214. Levy M, Futerman AH. Mammalian Ceramide Synthases. *IUBMB Life*. 2010;62(5):347. doi:10.1002/IUB.319

215. Alpy F, Tomasetto C. MLN64 and MENTHO, two mediators of endosomal cholesterol transport. *Biochem Soc Trans*. 2006;34(3):343-345. doi:10.1042/BST0340343

216. Emsley P, Lohkamp B, Scott WG, Cowtan K. Biological Crystallography Features and development of Coot. doi:10.1107/S0907444910007493

217. Pettersen EF, Goddard TD, Huang CC, et al. UCSF Chimera--a visualization system for exploratory research and analysis. *J Comput Chem*. 2004;25(13):1605-1612. doi:10.1002/JCC.20084

218. Alpy F, Tomasetto C, Schwab Y, et al. Give lipids a START: the StAR-related lipid transfer (START) domain in mammals. *J Cell Sci*. 2005;118(Pt 13):2791-2801. doi:10.1242/jcs.02485

219. Maxfield FR, Menon AK. Intracellular sterol transport and distribution. *Curr Opin Cell Biol*. 2006;18(4):379-385. doi:10.1016/J.CEB.2006.06.012

220. Rosen H, Goetzl EJ. Sphingosine 1-phosphate and its receptors: an autocrine and paracrine network. *Nat Rev Immunol*. 2005;5(7):560-570. doi:10.1038/NRI1650

221. Hanada K, Kumagai K, Yasuda S, et al. Molecular machinery for non-vesicular trafficking of ceramide. *Nat 2004 4266968*. 2003;426(6968):803-809. doi:10.1038/nature02188

222. Serra M, Saba JD. Sphingosine 1-phosphate lyase, a key regulator of sphingosine 1-phosphate signaling and function. *Adv Enzyme Regul*.

2010;50(1):349. doi:10.1016/J.ADVENZREG.2009.10.024

223. Lee H, Lee JK, Park MH, et al. Pathological roles of the VEGF/SphK pathway in Niemann-Pick type C neurons. *Nat Commun*. 2014;5. doi:10.1038/NCOMMS6514

224. Schopp IM, Amaya Ramirez CC, Debeljak J, et al. Split-BioID a conditional proteomics approach to monitor the composition of spatiotemporally defined protein complexes. *Nat Commun*. 2017;8. doi:10.1038/NCOMMS15690

225. Weidenfeld I, Gossen M, Löw R, et al. Inducible expression of coding and inhibitory RNAs from retargetable genomic loci. *Nucleic Acids Res*. 2009;37(7):e50. doi:10.1093/NAR/GKP108

226. Harayama T, Hashidate-Yoshida T, Aguilera-Romero A, et al. Establishment of a highly efficient gene disruption strategy to analyze and manipulate lipid co-regulatory networks. *bioRxiv*. November 2020:2020.11.24.395632. doi:10.1101/2020.11.24.395632

227. Thiele C, Wunderling K, Leyendecker P. Multiplexed and single cell tracing of lipid metabolism. *Nat Methods 2019 1611*. 2019;16(11):1123-1130. doi:10.1038/s41592-019-0593-6

List of Abbreviations

ACAT	Acyl-CoA-Acetyltransferase
Ala (A)	alanine
ANK	ankyrin repeat
Arg (R)	arginine
BZH	Biochemistry Center Heidelberg
C1PP	ceramide-1-phosphate phosphatase
Cab45	calcium-binding protein 45
Cer	ceramide
CERK	ceramide kinase
CerS	ceramide synthase
CERT	ceramide transfer protein
CMT	cell-mediated therapy
CoA	coenzyme A
COPI	coat protein complex I
COPII	coat protein complex II
CRAL-TRIO	cellular retinaldehyde-binding domain triple functional domain protein
ctrl	control
CCV	clathrin coated vesicle
DAG	diacylglycerol

DES	sphingolipid desaturase
DHS1P	dihyro-sphingosine-1-phosphate
DHSph	dihydro-sphingosine
DiGalCer	digalactosylceramide
E	eluate
EDTA	ethylene diamine tetraacetic acid
EE	early endosome
EGTA	ethylene glycol tetraacetic acid
ER	endoplasmic reticulum
ERGIC	ER-Golgi intermediate compartment
ERT	enzyme replacement therapy
FB1	Fumonisin B1
FFAT	two phenylalanines in an acidic tract
FFNT	two phenylalanines in a neutral tract
FT	flow-through
GalCer	galactosylceramide
GlcCer	glucosylceramide
GSL	glycosphingolipid
GTPase	guanosine triphosphatase
HeLa	Henrietta Lacks
HEPES	N-2-hydroxyethylpiperazine-N'-2-ethanesulfonic acid
His (H)	histidine
I	input

IP	immunoprecipitation
KO	knock-out
KDHSph	ketodihydrosphingosine
KDSR	ketodihydrosphingosine reductase
LE	late endosome
Leu (L)	leucine
LMP	lysosomal membrane proteins
LTP	lipid-transfer protein
LY	lysosome
Lys (K)	lysine
Lyso-pacSph	lysosome-targeted photocrosslinkable and clickable sphingosine
MCS	membrane contact site
MENTAL	MLN64-N-terminal domain
ML	MD-2-related lipid recognition
MOPS	3-(N-morpholino)propanesulfonic acid
MOSPD	motile sperm domain-containing protein
MSP	motile sperm protein
MTOC	microtuble-organizing center
mTOR	mechanistic target of rapamycin
mTORC1	mechanistic target of rapamycin complex 1
NPC	Niemann-Pick type C
n.s.	not significant
ORD	OSBP-related ligand-binding domain

ORP1L	oxysterol-binding protein-related protein 1
OSBP	oxysterol-binding protein
OX	overexpression
pacFA	photocrosslinkable and clickable fatty acid
pacSph	photocrosslinkable and clickable sphingosine
PBS	phosphate buffer saline
PC	phosphatidylcholine
PDB	protein data bank
PEI	polycation polyethylenimine
PFA	paraformaldehyd
PH	pleckstrin homology domain
PIPs	phosphatidylinositol phosphates
Phe (F)	phenylalanine
PVDF	polyvinylidene fluoride
S1P	sphingosine-1-phosphate
S1PL	sphingosine-1-phosphate lyase (protein)
SDS	sodium dodecyl sulfate
SGPL1	sphingosine-1-phosphate lyase (gene)
SNARE	soluble NSF-attachment protein receptor
SM	sphingomyelin
SMase	sphingomyelinase
SMS	sphingomyelin synthase
SPCA1	secretory pathway calcium ATPase 1

Sph	sphingosine
SphK	sphingosine kinase
SPT	serine palmitoyltransferase
SRT	substrate reduction therapy
STARD3	StAR-related lipid transfer domain containing protein 3
START	StAR-related lipid transfer domain
TAG	triacylglycerol
TFS	trifunctionalsphingosine
TFEB	transcription factor EB
TGN	*trans*-Golgi network
TLC	Thin-layer chromatography
UV	ultraviolet
VAP	vesicle-associated membrane protein (VAMP)-associated protein
VCU	Virginia Commonwealth University
v/v	volume per volume percent
WT	wild type
w/v	weight per volume percent

Appendix

Supplementary data can be found under the digital object identifier (DOI) 10.17632/768hbxwt9j.1[208].

Digitally provided data includes:

- Raw data of microscopy, TLC, immunoprecipitation, and western blot experiments
- Molecular dynamic simulation of START and Sph
- Video of ctrl, STARD3 OX, and FFAT mutant lysosomes (LysoTracker) in Sec61-GFP HeLa cells
- DNA-maps of all plasmids mentioned in this thesis
- File with all gRNAs used for this study

Acknowledgements

This doctoral thesis was conducted between January 2019 and May 2022. Many people supported me throughout this time.

First of all, I am very thankful to Doris Höglinger for giving me the opportunity to carry out my PhD in her laboratory, for creating a supportive working environment, and for giving me the freedom to pursue my own ideas during this time.

I thank my thesis advisory committee, Britta Brügger and Sebastian Schuck, for their scientific input and support over the years. Additionally, I want to thank Carmen Nussbaum-Krammer for examining this thesis.

I would also like to thank all past and present members of the Höglinger lab: Janathan and Valle for all the nice discussions, Denisa for always supporting my cell biology studies with *in vitro* data, and especially Jutta for her help with almost everything in the lab. Additionally, I thank all bachelor and master students who have contributed to this work.

Many parts of this work would not have been possible without the contribution of our collaboration partners. In particular, I want to thank Sarah Spiegel and Ryan Brown for performing lipid mass spectrometry, Walter Nickel and Fabio Lolicato for molecular dynamic simulations, and Emily Eden for performing electron microscopy.

I am happy to have made such good friends during the time of my PhD. Especially big thanks to Elisa and Larissa for all the lovely lunch and coffee breaks, and Annalena and Tamara for all the fun times outside the lab.

A huge thank you belongs to my family, especially to my parents. Thank you for always supporting me!

And finally, I am endlessly grateful to my husband, Alex, for his constant support and love. You always pushed me to give my best, but at the same time, you gave me your hand when I needed it. Lucky me!